

KP SOLITONS IN SHALLOW WATER

YUJI KODAMA

ABSTRACT. The main purpose of the paper is to provide a survey of our recent studies on soliton solutions of the Kadomtsev-Petviashvili (KP) equation. The KP equation describes weakly dispersive and small amplitude wave propagation in a quasi-two dimensional framework. Recently a large variety of exact soliton solutions of the KP equation has been found and classified. These solutions are localized along certain lines in a two-dimensional plane and decay exponentially everywhere else, and are called line-solitons. The classification is based on the far-field patterns of the solutions which consist of a finite number of line-solitons. Each soliton solution is then defined by a point of the totally non-negative Grassmann variety which can be parametrized by a unique derangement of the symmetric group of permutations. Our study also includes certain numerical stability problems of those soliton solutions. Numerical simulations of the initial value problems indicate that certain class of initial waves asymptotically approach to these exact solutions of the KP equation. We then discuss an application of our theory to the Mach reflection problem in shallow water. This problem describes the resonant interaction of solitary waves appearing in the reflection of an obliquely incident wave onto a vertical wall, and it predicts an extra-ordinary four-fold amplification of the wave at the wall. There are several numerical studies confirming the prediction, but all indicate disagreements with the KP theory. Contrary to those previous numerical studies, we find that the KP theory actually provides an excellent model to describe the Mach reflection phenomena when the higher order corrections are included to the quasi-two dimensional approximation. We also present laboratory experiments of the Mach reflection recently carried out by Yeh and his colleagues, and show how precisely the KP theory predicts this wave behavior.

CONTENTS

1. Introduction	1
2. Shallow water waves: Basic equations	3
3. The KP equation	5
3.1. Quasi-two dimensional approximation and one soliton solution	6
3.2. Soliton solutions in the Wronskian determinant	7
4. Totally nonnegative Grassmannian $\text{Gr}^+(N, M)$	10
4.1. The Grassmannian $\text{Gr}(N, M)$	10
4.2. The Plücker coordinates and total non-negativity	13
4.3. The τ -function as a point on $\text{Gr}^+(N, M)$	14
5. Classification of soliton solutions	15
5.1. Asymptotic line-solitons	16
5.2. Characterization of the line-solitons	22
6. (2,2)-soliton solutions	25
6.1. O-type soliton solutions	28
6.2. (3142)-type soliton solutions	30
6.3. T-type soliton solutions	33
7. Numerical simulation and the stability of the soliton solutions	35
7.1. Regular reflection: $\kappa > 1$	37
7.2. The Mach reflection: $\kappa < 1$	39
7.3. T-type interaction with X-shape initial wave	40
8. Shallow water waves: The Mach reflection	41
8.1. Previous numerical results of the Boussinesq-type equations	42

8.2. Experiments	44
References	47

1. INTRODUCTION

It is a quite well-known story that in August 1834 Sir John Scott Russel observed a large solitary wave in a shallow water channel in Scotland. He noted in his first paper (1838) on the subject that

I was observing the motion of a boat which was rapidly drawn along a narrow channel by a pair of horses, when the boat suddenly stopped - not so the mass of water in the channel which it had put in motion; it accumulated round the prow of the vessel in a state of violent agitation, then suddenly leaving it behind, rolled forward with great velocity, assuming the form of a large solitary elevation, a rounded, smooth and well defined heap of water, which continued its course along the channel apparently without change of form or diminution of speed

This solitary wave is now known as an example of a *soliton*, and is described by a solution of the Korteweg-de Vries (KdV) equation. The KdV equation describes one-dimensional wave propagation such as beach waves parallel to the coast line or waves in narrow canal, and is obtained in the leading order approximation of an asymptotic perturbation theory under the assumptions of weak nonlinearity (small amplitude) and weak dispersion (long waves). The KdV equation has rich mathematical structure including the existence of N -soliton solutions and the Lax pair for the inverse scattering method, and it is a prototype equation of the $1 + 1$ dimensional integrable systems. In particular, the initial value problem of the KdV equation has been extensively studied by means of the method of inverse scattering transform (IST). It is well known that a general initial data decaying rapidly in the spatial variable evolves to a number of individual solitons and weakly dispersive wave trains separate from the solitons (see for examples, [1, 31, 34, 44]).

In 1970, Kadomtsev and Petviashvili [17] proposed a $2 + 1$ dimensional dispersive wave equation to study the stability of the one-soliton solution of the KdV equation under the influence of weak transverse perturbations. This equation is now referred to as the KP equation. It turns out that the KP equation has much richer structure than the KdV equation, and might be considered as the most fundamental integrable system in the sense that many known integrable systems can be derived as special reductions of the so-called KP hierarchy which consists of the KP equation together with its infinitely many symmetries. The KP equation can be also represented in the Lax form, that is, there exists a pair of linear equations associated with an eigenvalue problem and an evolution of the eigenfunction, which enables the method of IST. However, unlike the case of the KdV equation, the IST for the KP equation does not seem to provide a practical method of solving the initial value problem for initial waves consisting of line-solitons in the far field.

It is quite important to recognize that the resonant interaction plays a fundamental role in multi-dimensional wave phenomenon. The original description of the soliton interaction for the KP equation was based on a two-soliton solution found in Hirota bilinear form, which has the shape of “X”, describing the intersection of two lines with oblique angle and a phase shift at the intersection point. This X-shape solution is referred to as the “O”-type soliton, where “O” stands for *original*. In his study of 1977 on an oblique interaction of two line-solitons, Miles [28] pointed out that the O-type solution becomes singular if the angle of the intersection is smaller than certain critical value depending on the amplitudes of the solitons. Miles then found that at the critical angle, the two line-solitons of the O-type solution interact resonantly, and a third wave is created to make a “Y-shaped” wave form. Indeed, it turns out that such Y-shaped resonant wave forms are exact solutions of the KP equation (see also [32]). Miles applied his theory to study the Mach reflection of an incident wave onto a vertical wall, and predicted that the third wave, called the *Mach stem*, created by the resonant interaction can reach four-fold amplification of the incidence wave. Several laboratory

and numerical experiments attempted to validate his prediction of four-fold amplification, but with no definitive success (see for examples [15, 21, 41] for numerical experiments, and [36, 27, 46] for laboratory experiments).

After the discovery of the resonant phenomena in the KP equation, several numerical and experimental studies were performed to investigate resonant interactions in other physical two-dimensional equations such as the ion-acoustic and shallow water wave equations under the Boussinesq approximation (see for examples [18, 19, 13, 33, 15, 41, 29, 35, 43]). However, apart from these activities, no significant progress has been made in the study of the solution space or real applications of the KP equation. It would appear that the general perception was that there were not many new and significant results left to be uncovered in the soliton solutions of the KP theory.

Over the past several years, we have been working on the classification problem of the soliton solutions of the KP equation and their applications to shallow water waves. Our studies have revealed a large variety of solutions that were totally overlooked in the past [4, 22, 6, 7, 8, 9]¹, and we found that some of those exact solutions can be applied to study the Mach reflection problem [8, 23, 47, 46]. Our numerical study [20] indicates that the solution to the initial value problem of the KP equation with certain class of initial waves associated with the Mach reflection problem converges asymptotically to some of these new exact solutions, that is, a separation of dispersive radiations from the soliton solution similar to the case of the KdV soliton.

The main purpose of this paper is to present a survey of our studies on the soliton solutions of the KP equation. The paper also presents several results for recent laboratory experiments done by Harry Yeh and his colleagues at Oregon State University.

The paper is organized as follows:

In Section 2, we present the derivation of the Boussinesq-type equation from the three-dimensional Euler equation for the irrotational and incompressible fluid under the assumptions of weak nonlinearity and weak dispersion. The purpose of this section is to give a precise physical meaning to those assumptions and to explain the existence of a solitary wave solution in the form of the KdV soliton.

In Section 3, we explain the quasi-two dimensional approximation to derive the KP equation, and discuss physical interpretation of the KP soliton in terms of the KdV soliton. In order to describe the general soliton solutions, we here introduce the τ -function which is expressed by a Wronskian determinant for a set of N linearly independent functions $\{f_i : i = 1, \dots, N\}$. Each function f_i is a linear combination of the exponential functions $\{E_j : j = 1, \dots, M\}$, where $E_j = e^{\theta_j}$ with $\theta_j = k_j x + k_j^2 y - k_j^3 t$ for some $k_j \in \mathbb{R}$. The τ -function in the Wronskian form was found in

[25, 40, 14] (see also [16]). Setting $f_i = \sum_{j=1}^M a_{ij} E_j$, each solution is parametrized by the $N \times M$ coefficient matrix $A = (a_{ij})$ of rank N . This representation naturally leads to the notion of the Grassmann variety $\text{Gr}(N, M)$, the set of N -dimensional subspaces given by $\text{Span}_{\mathbb{R}}\{f_i : i = 1, \dots, N\}$ of $\mathbb{R}^M = \text{Span}_{\mathbb{R}}\{E_j : j = 1, \dots, M\}$, and each point of $\text{Gr}(N, M)$ is marked by this A -matrix [39, 22, 8].

In Section 4, we provide a brief summary of the totally nonnegative (TNN) Grassmann variety, denoted by $\text{Gr}^+(N, M)$, which provides the foundation of the classification theorem for the *regular* soliton solutions of the KP equation discussed in the next Section. The main purpose of this section is to show that the τ -function in the Wronskian determinant form described in Section 3 can be identified as a point of the TNN Grassmannian cell. That is, a classification of the regular soliton solutions of the KP equation is equivalent to a parametrization of TNN Grassmannian cells [6, 8, 9].

In Section 5, we present a classification theorem which states that the τ -function identified as a point of $\text{Gr}^+(N, M)$ generates a soliton solution of the KP equation that has asymptotically $M - N$ line-solitons for $y \ll 0$ and N line-solitons for $y \gg 0$. Moreover, these solutions can be parametrized

¹The lower dimensional solutions, called (2, 2)-soliton solutions, have been found by the binary Darboux transformation in [5].

by the derangements (the permutations without fixed points) of the symmetric group S_M . This type of solutions is called $(M - N, N)$ -soliton solution. The derangements then give a parametrization of the TNN Grassmannian cells, and each derangement is expressed by a unique *chord diagram*. The chord diagram is particularly useful to describe the far-field structure of the corresponding soliton solution. (See [6, 8, 9].)

In Section 6, we explain all the soliton solutions generated by the τ -functions on $\text{Gr}^+(2, 4)$ (see also [5]). Some of these solutions are useful to describe the Mach reflection problem in shallow water. We show that the A -matrix determine the detailed structure of those solutions, such as the asymptotic locations of solitons and local interaction patterns. (See [8, 20, 9].)

In Section 7, we present the numerical study of the KP equation for certain types of initial waves. In particular, we consider an initial value problem where the initial wave consists of two semi-infinite line-solitons forming a V-shape pattern. Those initial waves were considered in the study of the generation of large amplitude waves in shallow water [37, 43]. The main result of this section is to show that the solutions of this particular initial value problem *converge* asymptotically to some of the exact (2,2)-soliton solutions. These results demonstrate a separation of the (exact) soliton solution from dispersive radiation in the manner similar to the KdV case. (See [8, 23, 20].)

In Section 8, we discuss the Mach reflection problem in terms of the KP solitons which is equivalent to Miles' theory (assuming quasi-two dimensionality). We first show that the previous numerical results (see for examples [15, 41]), which reported a large discrepancy with the theory, are actually in a good agreement with the predictions given by the KP theory. However, here one needs to give a proper physical interpretation of the theory when one compares it with the numerical results. We also present some laboratory experiments of shallow water waves [46, 47]. We show that the experimental results are all in good agreement with the predictions of the KP theory which can describe the evolution of the wave-profile. Finally we demonstrate that the most complex (2,2)-soliton solution associated with the τ -function on $\text{Gr}^+(2, 4)$, referred to as T-type solution, can be realized in an experiment.

Sir John Scott Russel continued on to say in his book (1865) that

This is a most beautiful and extraordinary phenomenon: the first day I saw it was the happiest day of my life. Nobody has ever had the good fortune to see it before or, at all events, to know what it meant. It is now known as the solitary wave of translation. No one before had fancied a solitary wave as a possible thing.

I hope this survey is successful to convince the readers that the two-dimensional wave pattern generated by the soliton solutions of the KP equation *is a most beautiful and extraordinary phenomena* of two-dimensional shallow water waves, and one should have no doubt that observing these patterns at a beach will bring the *happiest* moment of one's life.

2. SHALLOW WATER WAVES: BASIC EQUATIONS

Let us start with the physical background of the KP equation: We consider a surface wave on water which is assumed to be irrotational and incompressible (see for examples [44, 1]). Then the surface wave may be described by the three-dimensional Euler equation,

$$(2.1) \quad \left. \begin{aligned} \tilde{\Delta} \tilde{\phi} &= 0, & \text{for } 0 < \tilde{z} < h_0 + \tilde{\eta}, \\ \tilde{\phi}_{\tilde{z}} &= 0, & \text{at } \tilde{z} = 0, \\ \tilde{\phi}_{\tilde{t}} + \frac{1}{2} \left| \tilde{\nabla} \tilde{\phi} \right|^2 + g \tilde{\eta} &= 0, \\ \tilde{\eta}_{\tilde{t}} + \tilde{\nabla}_{\perp} \tilde{\phi} \cdot \tilde{\nabla}_{\perp} \tilde{\eta} &= \tilde{\phi}_{\tilde{z}}, \end{aligned} \right\} \text{at } \tilde{z} = \tilde{\eta} + h_0,$$

where $\tilde{\phi}$ is the velocity potential with the Laplacian $\tilde{\Delta} = \partial_{\tilde{x}}^2 + \partial_{\tilde{y}}^2 + \partial_{\tilde{z}}^2$, $g = 980 \text{ cm/sec}^2$ the gravitational constant, and h_0 the average depth. The first two equations of (2.1) implies,

$$\tilde{\phi}(\tilde{x}, \tilde{y}, \tilde{z}, \tilde{t}) = \cos(\tilde{z}\sqrt{\tilde{\Delta}_\perp}) \tilde{\psi}(\tilde{x}, \tilde{y}, \tilde{t}) \quad \text{with} \quad \tilde{\Delta}_\perp = \partial_{\tilde{x}}^2 + \partial_{\tilde{y}}^2,$$

where $\psi(\tilde{x}, \tilde{y}, \tilde{t}) = \phi(\tilde{x}, \tilde{y}, 0, \tilde{t})$. In the linear limit, the system can be written in the form,

$$\begin{cases} \cos(h_0\sqrt{\tilde{\Delta}_\perp}) \tilde{\psi}_{\tilde{t}} + g\tilde{\eta} = 0 \\ \tilde{\eta}_{\tilde{t}} = \sqrt{\tilde{\Delta}_\perp} \sin(h_0\sqrt{\tilde{\Delta}_\perp}) \tilde{\psi}. \end{cases}$$

This then gives the dispersion relation,

$$(2.2) \quad \omega^2 = gk \tanh h_0 k = c_0^2 k^2 \left(1 - \frac{1}{3} h_0^2 k^2 + \dots \right),$$

where $k := \sqrt{k_x^2 + k_y^2}$ and the speed of the surface wave $c_0 = \sqrt{gh_0}$ (e.g. $c_0 = 70 \text{ cm/sec}$ when $h_0 = 5 \text{ cm}$).

Let us denote the following scales:

$$\begin{aligned} \lambda_0 &\sim \text{horizontal length scale} \\ h_0 &\sim \text{vertical length scale} = \text{water depth} \\ a_0 &\sim \text{amplitude scale} \end{aligned}$$

The non-dimensional variables $\{x, y, z, t, \eta, \phi\}$ are defined as

$$(2.3) \quad \begin{cases} \tilde{x} = \lambda_0 x, & \tilde{y} = \lambda_0 y, & \tilde{z} = h_0 z, & \tilde{t} = \frac{\lambda_0}{c_0} t, \\ \tilde{\eta} = a_0 \eta, & \tilde{\phi} = \frac{a_0}{h_0} \lambda_0 c_0 \phi. \end{cases}$$

Then the shallow water equation in the non-dimensional form is given by

$$\begin{aligned} \phi_{zz} + \beta \Delta_\perp \phi &= 0, & \text{for } 0 < z < 1 + \alpha \eta, \\ \phi_z &= 0, & \text{at } z = 0, \\ \left. \begin{aligned} \phi_t + \frac{1}{2} \alpha |\nabla_\perp \phi|^2 + \frac{1}{2} \frac{\alpha}{\beta} \phi_z^2 + \eta &= 0, \\ \eta_t + \alpha \nabla_\perp \phi \cdot \nabla_\perp \eta &= \frac{1}{\beta} \phi_z, \end{aligned} \right\} & \text{at } z = 1 + \alpha \eta, \end{aligned}$$

where the parameters α and β are given by

$$\alpha = \frac{a_0}{h_0} \quad \text{and} \quad \beta = \left(\frac{h_0}{\lambda_0} \right)^2.$$

The weak nonlinearity implies $\alpha \ll 1$, and the weak dispersion (or long wave assumption) implies $\beta \ll 1$. With a small parameter $\epsilon \ll 1$, we assume

$$\alpha \sim \beta = \mathcal{O}(\epsilon).$$

As in the previous manner, ϕ can be written formally in the form,

$$\phi(x, y, z, t) = \cos\left(z\sqrt{\beta\Delta_\perp}\right) \psi(x, y, t),$$

which leads to the expansion,

$$\phi = \psi - \beta \frac{z^2}{2} \Delta_\perp \psi + \mathcal{O}(\epsilon^2).$$

Then the equations at the surface gives the following system of equations, sometimes called the Boussinesq-type equation,

$$(2.4) \quad \begin{cases} \eta + \psi_t + \frac{\alpha}{2} |\nabla\psi|^2 - \frac{\beta}{2} \Delta\psi_t = \mathcal{O}(\epsilon^2) \\ \eta_t + \Delta\psi - \alpha \nabla \cdot (\psi_t \nabla\psi) - \frac{\beta}{6} \Delta^2\psi = \mathcal{O}(\epsilon^2). \end{cases}$$

Here we have omitted \perp sign. Eliminating η in (2.4), we obtain the so-called isotropic Benney-Luke equation [2],

$$\psi_{tt} - \Delta\psi + \alpha (\nabla\psi \cdot \nabla\psi_t + \nabla \cdot (\psi_t \nabla\psi)) - \frac{\beta}{2} \left(\Delta\psi_{tt} - \frac{1}{3} \Delta^2\psi \right) = \mathcal{O}(\epsilon^2).$$

One can then write this equation in the following form up to the same order,

$$(2.5) \quad \left(1 - \frac{\beta}{3} \Delta \right) \psi_{tt} - \Delta\psi + \alpha (\nabla\psi \cdot \nabla\psi_t + \nabla \cdot (\psi_t \nabla\psi)) = \mathcal{O}(\epsilon^2).$$

This is a regularized form of the two-dimensional Boussinesq-type equation for the shallow water waves. Note here that the dispersion relation of this equation is given by

$$\omega^2 = \frac{k^2}{1 + \frac{\beta}{3}k^2} = k^2 \left(1 - \frac{\beta}{3}k^2 + \dots \right).$$

which agrees with (2.2) up to $\mathcal{O}(\epsilon^2)$.

It is also well-known that the Boussinesq-type equation can be reduced to the KdV equation for a far field with a unidirectional approximation: Let χ be the coordinate which is perpendicular to the wave crest of a linear shape solitary wave, i.e.

$$\chi = \tilde{x} \cos \Psi_0 + \tilde{y} \sin \Psi_0,$$

where $(\cos \Psi_0, \sin \Psi_0)$ is the unit vector in the propagation direction. Then using the far-field coordinates in the propagation direction, i.e.

$$\xi := \chi - t, \quad \tau = \epsilon t,$$

the Boussinesq-type equation (2.5) becomes the KdV equation,

$$\epsilon\psi_{\tau\xi} + \frac{3\alpha}{2} \psi_\xi \psi_{\xi\xi} + \frac{\beta}{6} \psi_{\xi\xi\xi} = 0.$$

From the first equation of (2.4), we have $\eta = \psi_\chi + \mathcal{O}(\epsilon)$. Then the KdV equation can be expressed in the form with physical coordinates,

$$(2.6) \quad \tilde{\eta}_{\tilde{t}} + c_0 \tilde{\eta}_\chi + \frac{3c_0}{2h_0} \tilde{\eta} \tilde{\eta}_\chi + \frac{c_0 h_0^2}{6} \tilde{\eta}_{\chi\chi\chi} = 0.$$

The one-soliton solution of the KdV equation is then given by

$$(2.7) \quad \tilde{\eta} = \hat{a}_0 \operatorname{sech}^2 \sqrt{\frac{3\hat{a}_0}{4h_0^3}} \left[\chi - c_0 \left(1 + \frac{\hat{a}_0}{2h_0} \right) \tilde{t} - \chi_0 \right],$$

where $\hat{a}_0 > 0$ and χ_0 are arbitrary constants. One should note that any line-solitary wave in the Euler equation (2.1) can be (at least locally) approximated by this soliton under the assumption of weak dispersion and weak nonlinearity. This remark will be important when we compare any numerical results of the Euler equation or the Boussinesq-type equation with those of the KP equation.

3. THE KP EQUATION

In this section, we give some basic property of the KP equation, and introduce the soliton solutions relevant to shallow water wave problem. In particular, we discuss the physical aspect of the KP equation which is derived by a further assumption called *quasi*-two dimensional approximation (see for examples [17, 1]).

3.1. Quasi-two dimensional approximation and one soliton solution. Let us now assume a quasi-two dimensionality with a weak dependence in the y -direction, and we introduce a small parameter γ so that the y -coordinate is scaled as

$$(3.1) \quad \zeta := \sqrt{\gamma}y, \quad \text{with } \gamma = \mathcal{O}(\epsilon).$$

Then the system of equations (2.4) becomes

$$\begin{cases} \eta + \psi_t + \frac{\alpha}{2}\psi_x^2 - \frac{\beta}{2}\psi_{xxt} = \mathcal{O}(\epsilon^2) \\ \eta_t + \psi_{xx} - \alpha(\psi_t\psi_x)_x - \frac{\beta}{6}\psi_{xxxx} + \gamma\psi_{\zeta\zeta} = \mathcal{O}(\epsilon^3). \end{cases}$$

Now we consider a far field expressed with the scaling,

$$(3.2) \quad \xi = x - t \quad \text{and} \quad \tau = \epsilon t.$$

Then the above equations have the expansions,

$$\begin{cases} \eta - \psi_\xi + \epsilon\psi_\tau + \frac{\alpha}{2}\psi_\xi^2 + \frac{\beta}{2}\psi_{\xi\xi\xi} = \mathcal{O}(\epsilon^2) \\ -\eta_\xi + \psi_{\xi\xi} + \epsilon\eta_\tau + \alpha(\psi_\xi^2)_\xi - \frac{\beta}{6}\psi_{\xi\xi\xi\xi} + \gamma\psi_{\zeta\zeta} = \mathcal{O}(\epsilon^2). \end{cases}$$

Eliminating η , we obtain

$$2\epsilon\psi_{\tau\xi} + 3\alpha\psi_\xi\psi_{\xi\xi} + \frac{\beta}{3}\psi_{\xi\xi\xi\xi} + \gamma\psi_{\zeta\zeta} = \mathcal{O}(\epsilon^2)$$

Noting $\eta = \psi_\xi + \mathcal{O}(\epsilon)$, we have the KP equation for η at the leading order,

$$(3.3) \quad \left(2\epsilon\eta_\tau + 3\alpha\eta\eta_\xi + \frac{\beta}{3}\eta_{\xi\xi\xi} \right)_\xi + \gamma\eta_{\zeta\zeta} = \mathcal{O}(\epsilon^2)$$

In terms of physical coordinates, the KP equation is given by

$$\left(\tilde{\eta}_{\tilde{t}} + c_0\tilde{\eta}_{\tilde{x}} + \frac{3c_0}{2h_0}\tilde{\eta}\tilde{\eta}_{\tilde{x}} + \frac{c_0h_0^2}{6}\tilde{\eta}_{\tilde{x}\tilde{x}\tilde{x}} \right)_{\tilde{x}} + \frac{c_0}{2}\tilde{\eta}_{\tilde{y}\tilde{y}} = 0.$$

As a particular solution, we have one line-soliton solution in the form,

$$(3.4) \quad \tilde{\eta} = a_0 \operatorname{sech}^2 \sqrt{\frac{3a_0}{4h_0^3}} \left[\tilde{x} + \tilde{y} \tan \Psi_0 - c_0 \left(1 + \frac{a_0}{2h_0} + \frac{1}{2} \tan^2 \Psi_0 \right) \tilde{t} - \tilde{x}_0 \right],$$

where $a_0 > 0$, Ψ_0 and \tilde{x}_0 are arbitrary constants. One should note that the KP equation is derived under the assumption of quasi-two dimensionality, that is, the angle Ψ_0 should be small of order $\mathcal{O}(\epsilon)$, and the solution (3.4) becomes unphysical for the case with a large angle. This can be seen explicitly by writing it in the following form in the coordinate perpendicular to the wave crest, i.e. $\chi = \tilde{x} \cos \Psi_0 + \tilde{y} \sin \Psi_0$,

$$(3.5) \quad \tilde{\eta} = a_0 \operatorname{sech}^2 \sqrt{\frac{3a_0}{4h_0^3 \cos^2 \Psi_0}} \left[\chi - c_0 \cos \Psi_0 \left(1 + \frac{a_0}{2h_0} + \frac{1}{2} \tan^2 \Psi_0 \right) \tilde{t} - \chi_0 \right].$$

Noting that $\cos \Psi_0 = 1 - \frac{1}{2} \tan^2 \Psi_0 + \mathcal{O}(\epsilon^4)$ with $\Psi_0 = \mathcal{O}(\epsilon)$, the velocity of the soliton has the corrected form up to $\mathcal{O}(\epsilon^2)$, i.e.

$$\cos \Psi_0 \left(1 + \frac{a_0}{2h_0} + \frac{1}{2} \tan^2 \Psi_0 \right) = 1 + \frac{a_0}{2h_0} + \mathcal{O}(\epsilon^3),$$

which does not depend on the angle up to $\mathcal{O}(\epsilon^2)$. This is consistent with the assumption of the quasi-two dimensionality.

We also note that the line-soliton of (3.4) does not satisfy the KdV equation (2.6) except the case with $\Psi_0 = 0$. Now comparing the KP soliton (3.4) with the KdV soliton (2.7), one can find

the correction to the quasi-two dimensional approximation, that is, the amplitude a_0 in (3.4) is now corrected to

$$(3.6) \quad \hat{a}_0 = \frac{a_0}{\cos^2 \Psi_0}.$$

With this correction, the KP soliton (3.4) now satisfies the KdV equation (2.6) up to $\mathcal{O}(\epsilon^2)$. This correction becomes quite important when we compare our KP results with numerical results of the Euler or Boussinesq-type equations, that is, (3.6) gives the relation between the amplitudes of the KP soliton and the KdV soliton (see Section 8 for the details).

3.2. Soliton solutions in the Wronskian determinant. In order to give a general scheme to discuss the soliton solutions, we first put the KP equation (3.3) in the standard form,

$$(3.7) \quad (4u_T + 6uu_X + u_{XXX})_X + 3u_{YY} = 0,$$

where the new variables (X, Y, T) and u are related to the physical ones with

$$(3.8) \quad \tilde{\eta} = \frac{2h_0}{3} u, \quad \tilde{x} - c_0 \tilde{t} = h_0 X, \quad \tilde{y} = h_0 Y, \quad \tilde{t} = \frac{3h_0}{2c_0} T.$$

Hereafter we use the lower case letters (x, y, t) for (X, Y, T) (we do not use the non-dimensional variables in (2.3), and the KP variables can be converted to the physical variables directly through the relations (3.8)). We write the solution of the KP equation (3.7) in the τ -function form,

$$(3.9) \quad u(x, y, t) = 2\partial_x^2 \ln \tau(x, y, t).$$

where the τ -function is assumed to be the Wronskian determinant with N functions f_i 's (see for examples [40, 25, 14, 16]),

$$(3.10) \quad \tau = \text{Wr}(f_1, f_2, \dots, f_N) := \begin{vmatrix} f_1 & f_1^{(1)} & \cdots & f_1^{(N-1)} \\ f_2 & f_2^{(1)} & \cdots & f_2^{(N-1)} \\ \vdots & \vdots & \ddots & \vdots \\ f_N & f_N^{(1)} & \cdots & f_N^{(N-1)} \end{vmatrix},$$

with $f_i^{(n)} = \partial_x^n f_i$. The functions $\{f_i : i = 1, \dots, N\}$ satisfy the linear equations $\partial_y f_i = \partial_x^2 f_i$ and $\partial_t f_i = -\partial_x^3 f_i$, and for the soliton solution, we take

$$(3.11) \quad f_i = \sum_{j=1}^M a_{ij} E_j, \quad \text{with} \quad E_j = e^{\theta_j} := \exp(k_j x + k_j^2 y - k_j^3 t).$$

Here $A := (a_{ij})$ defines an $N \times M$ matrix $A = (a_{ij})$ of rank N , and we assume the real parameters $\{k_j : j = 1, \dots, M\}$ to be ordered,

$$k_1 < k_2 < \cdots < k_M.$$

One should emphasize here that we have a parametrization of each soliton solution of the KP equation in terms of the k -parameters and the A -matrix. Then the classification of the soliton solutions is to give a complete characterization of the τ -function (3.10) with the exponential functions in (3.11). This is the main theme in [22, 3, 8, 9] and will be discussed in the following sections.

In terms of the τ -function, the KP equation (3.7) is written in the bilinear form,

$$(3.12) \quad 4(\tau\tau_{xt} - \tau_x\tau_t) + \tau\tau_{xxxx} - 4\tau_x\tau_{xxx} + 3\tau_{xx}^2 + 3(\tau\tau_{yy} - \tau_{xx}^2) = 0.$$

To show that the τ -function (3.10) satisfies this equation, we express the derivatives of the τ -function using the Young diagram. Let Y be given by the partition $Y = (\lambda_1 \geq \dots \geq \lambda_n)$ where λ_j 's represent the numbers of boxes in Y , and $|Y|$ denote the total number of boxes, i.e. $|Y| = \sum_{i=1}^n \lambda_i$. Denote τ in the N -tablet,

$$\tau = \tau_\emptyset = (0, 1, 2, \dots, N-1),$$

where the numbers describe the orders of the derivative of the column vector $(f_1, \dots, f_N)^T$ in the τ -function (3.10). Then the number of boxes in each row of Y can be found by counting the missing numbers which are less than the corresponding number in τ_Y . For example, τ_{\square} represents

$$\tau_{\square} = (0, 1, 2, \dots, N-3, N-1, N+1).$$

For the number $N+1$, two numbers $N-2$ and N are missing, and this gives \square . For the number $N-1$, one number $N-2$ is missing and this gives \square . In terms of the determinant, τ_{\square} represents,

$$\tau_{\square} = \begin{vmatrix} f_1 & \cdots & f_1^{(N-3)} & f_1^{(N-1)} & f_1^{(N+1)} \\ f_2 & \cdots & f_2^{(N-3)} & f_2^{(N-1)} & f_2^{(N+1)} \\ \vdots & & \vdots & \vdots & \vdots \\ f_N & \cdots & f_N^{(N-3)} & f_N^{(N-1)} & f_N^{(N+1)} \end{vmatrix}$$

With this notation and using the equations for f_i , i.e. $\partial_y f_i = f_i^{(2)}$, $\partial_t f_i = -f_i^{(3)}$, the derivatives of the τ -function (3.10) are given by

$$\begin{aligned} \tau_{\square} &= \tau_x, & \tau_{\square} &= \frac{1}{2}(\tau_{xx} + \tau_y), & \tau_{\square} &= \frac{1}{2}(\tau_{xx} - \tau_y) \\ \tau_{\square} &= \frac{1}{12}(\tau_{xxxx} + 3\tau_{yy} - 4\tau_{xt}), & \tau_{\square} &= \frac{1}{3}(\tau_{xxx} - \tau_t) \end{aligned}$$

Then the bilinear equation (3.12) can be written in the form,

$$(3.13) \quad \tau_{\phi} \tau_{\square} - \tau_{\square} \tau_{\square} + \tau_{\square} \tau_{\square} = 0.$$

This equation is nothing but the Laplace expansion of the following $2N \times 2N$ determinant identity,

$$\begin{vmatrix} f_1 & \cdots & f_1^{(N-2)} & f_1 & \cdots & f_1^{(N-3)} & f_1^{(N-1)} & f_1^{(N)} & f_1^{(N+1)} \\ \vdots & \ddots & \vdots & \vdots & \ddots & \vdots & \vdots & \vdots & \vdots \\ f_N & \cdots & f_N^{(N-2)} & f_N & \cdots & f_N^{(N-3)} & f_N^{(N-1)} & f_N^{(N)} & f_N^{(N+1)} \\ 0 & \cdots & 0 & f_1 & \cdots & f_1^{(N-3)} & f_1^{(N-1)} & f_1^{(N)} & f_1^{(N+1)} \\ \vdots & \ddots & \vdots & \vdots & \ddots & \vdots & \vdots & \vdots & \vdots \\ 0 & \cdots & 0 & f_N & \cdots & f_N^{(N-3)} & f_N^{(N-1)} & f_N^{(N)} & f_N^{(N+1)} \end{vmatrix} \equiv 0,$$

so that (3.13) is identically satisfied. The relation (3.13) is the simplest example of the Plücker relations (see below), and it can be symbolically written by

$$(3.14) \quad \xi(1, 2)\xi(3, 4) - \xi(1, 3)\xi(2, 4) + \xi(1, 4)\xi(2, 3) = 0,$$

where the Young diagrams are expressed by $Y = (j-2, i-1)$ for the symbol $\xi(i, j)$. These symbols $\xi(j_1, \dots, j_N)$ are the so-called Plücker coordinates of the Grassmann manifold $\text{Gr}(N, M)$. In the next section, we outline the basic information for the Grassmannian $\text{Gr}(N, M)$ which will provide the foundation of the classification theory for the soliton solutions of the KP equation [22, 8].

Example 3.1. Let us express one line-soliton solution (3.4) in our setting. Here we also introduce some notations to describe the soliton solutions. The soliton solution (3.4) is obtained by the τ -function with $M = 2$ and $N = 1$, i.e.

$$\tau = f_1 = a_{11}E_1 + a_{12}E_2.$$

Since the solution u is given by (3.9), one can assume $a_{11} = 1$ and denote $a_{12} = a > 0$. Then

$$\tau = E_1 + aE_2 = 2\sqrt{ae}^{\frac{1}{2}(\theta_1 + \theta_2)} \cosh \frac{1}{2}(\theta_1 - \theta_2 - \ln a),$$

with the 1×2 A -matrix of the form $A = (1 \ a)$. The parameter a in the A -matrix must be $a \geq 0$ for a *non-singular* solution and it determines the location of the soliton solution. Since $a = 0$ leads to a trivial solution, we consider only $a > 0$. Then the solution $u = 2\partial_x^2(\ln \tau)$ gives

$$u = \frac{1}{2}(k_1 - k_2)^2 \operatorname{sech}^2 \frac{1}{2}(\theta_1 - \theta_2 - \ln a).$$

Thus the solution is localized along the line $\theta_1 - \theta_2 = \ln a$, hence we call it *line-soliton* solution. We emphasize here that the line-soliton appears at the boundary of two regions where either E_1 or E_2 is the dominant exponential term, and because of this we also call this soliton a $[1, 2]$ -soliton solution. In Section 5, we will construct more general line-soliton solutions which separates into a number of one-soliton solutions asymptotically as $|y| \rightarrow \infty$. We refer to each of these asymptotic line-solitons as the $[i, j]$ -soliton. The $[i, j]$ -soliton solution with $i < j$ has the same (local) structure as the one-soliton solution, and can be described as follows

$$u = A_{[i,j]} \operatorname{sech}^2 \frac{1}{2} \left(\mathbf{K}_{[i,j]} \cdot \mathbf{x} - \Omega_{[i,j]} t + \Theta_{[i,j]}^0 \right)$$

with some constant $\Theta_{[i,j]}^0$. The amplitude $A_{[i,j]}$, the wave-vector $\mathbf{K}_{[i,j]}$ and the frequency $\Omega_{[i,j]}$ are defined by

$$\begin{cases} A_{[i,j]} = \frac{1}{2}(k_j - k_i)^2 \\ \mathbf{K}_{[i,j]} = (k_j - k_i, k_j^2 - k_i^2) = (k_j - k_i)(1, k_i + k_j), \\ \Omega_{[i,j]} = k_j^3 - k_i^3 = (k_j - k_i)(k_i^2 + k_i k_j + k_j^2). \end{cases}$$

The direction of the wave-vector $\mathbf{K}_{[i,j]} = (K_{[i,j]}^x, K_{[i,j]}^y)$ is measured in the counterclockwise sense from the y -axis, and it is given by

$$\frac{K_{[i,j]}^y}{K_{[i,j]}^x} = \tan \Psi_{[i,j]} = k_i + k_j,$$

that is, $\Psi_{[i,j]}$ gives the angle between the line $\mathbf{K}_{[i,j]} \cdot \mathbf{x} = \text{const}$ and the y -axis. Then one line-soliton can be written in the form with three parameters $A_{[i,j]}$, $\Psi_{[i,j]}$ and $x_{[i,j]}^0$,

$$(3.15) \quad u = A_{[i,j]} \operatorname{sech}^2 \sqrt{\frac{A_{[i,j]}}{2}} \left(x + y \tan \Psi_{[i,j]} - C_{[i,j]} t - x_{[i,j]}^0 \right),$$

with $C_{[i,j]} = k_i^2 + k_i k_j + k_j^2 = \frac{1}{2} A_{[i,j]} + \frac{3}{4} \tan^2 \Psi_{[i,j]}$. In Figure 3.1, we illustrate one line-soliton solution of $[i, j]$ -type. In the right panel of this figure, we show a *chord diagram* which represents this soliton solution. Here the chord diagram indicates the permutation of the dominant exponential terms E_i and E_j in the τ -function, that is, with the ordering $k_i < k_j$, E_i dominates in $x \ll 0$, while E_j dominates in $x \gg 0$ (see Section 4 for the precise definition of the chord diagram).

For each soliton solution of (3.15), the wave vector $\mathbf{K}_{[i,j]}$ and the frequency $\Omega_{[i,j]}$ satisfy the soliton-dispersion relation (see (2.2)),

$$(3.16) \quad 4\Omega_{[i,j]} K_{[i,j]}^x = (K_{[i,j]}^x)^4 + 3(K_{[i,j]}^y)^2.$$

The soliton velocity $\mathbf{V}_{[i,j]}$ is along the direction of the wave-vector $\mathbf{K}_{[i,j]}$, and is defined by $\mathbf{K}_{[i,j]} \cdot \mathbf{V}_{[i,j]} = \Omega_{[i,j]}$, which yields

$$\mathbf{V}_{[i,j]} = \frac{\Omega_{[i,j]}}{|\mathbf{K}_{[i,j]}|^2} \mathbf{K}_{[i,j]} = \frac{k_i^2 + k_i k_j + k_j^2}{1 + (k_i + k_j)^2} (1, k_i + k_j).$$

Note in particular that since $C_{[i,j]} = k_i^2 + k_i k_j + k_j^2 > 0$, the x -component of the soliton velocity is *always* positive, i.e., any soliton propagates in the positive x -direction. In the physical coordinates (see (3.8)), this implies that soliton propagates in super-sonic (i.e. the speed of soliton is faster than $c_0 = \sqrt{gh_0}$, because of its nonlinear effect with $\tilde{\eta} > 0$, see Section 2). On the other hand, one should note that any small perturbation propagates in the negative x -direction, i.e., the x -component of the

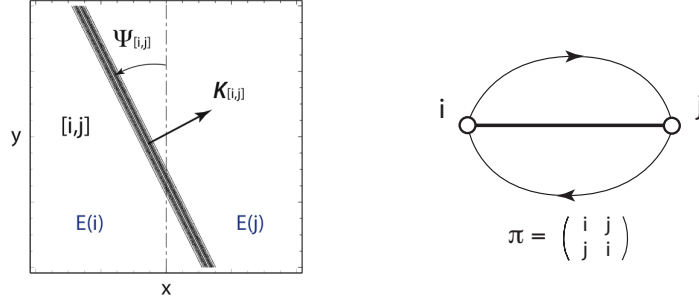


FIGURE 3.1. One line-soliton solution of $[i, j]$ -type and the corresponding chord diagram. The amplitude $A_{[i,j]}$ and the angle $\Psi_{[i,j]}$ are given by $A_{[i,j]} = \frac{1}{2}(k_i - k_j)^2$ and $\tan \Psi_{[i,j]} = k_i + k_j$. The upper oriented chord represents the part of $[i, j]$ -soliton for $y \gg 0$ and the lower one for $y \ll 0$.

group velocity is always negative. This can be seen from the dispersion relation of the *linearized* KP equation for a plane wave $\phi = \exp(i\mathbf{k} \cdot \mathbf{x} - i\omega t)$ with the wave-vector $\mathbf{k} = (k_x, k_y)$ and the frequency ω ,

$$\omega = -\frac{1}{4}k_x^3 + \frac{3}{4}\frac{k_y^2}{k_x},$$

from which the group velocity of the wave is given by

$$\mathbf{v} = \nabla\omega = \left(\frac{\partial\omega}{\partial k_x}, \frac{\partial\omega}{\partial k_y} \right) = \left(-\frac{3}{4}\left(k_x^2 + \frac{k_y^2}{k_x}\right), \frac{3}{2}\frac{k_y}{k_x} \right).$$

Physically, this means that the radiations disperse with sub-sonic speeds. This is similar to the case of the KdV equation, and we expect that asymptotically, the soliton separates from small radiations. We further discuss this issue in Section 7 where we numerically observe the separation.

Remark 3.2. In the formulas (3.11), if we include the higher times t_n in the exponential functions, i.e.

$$E_j = \exp\left(\sum_{n=1}^{\infty} k_j^n t_n\right),$$

then the τ -function (3.10) gives a solution of the KP hierarchy. The equation for the t_n -flow is a symmetry of the KP equation, and the τ -function with those higher times also satisfies the other Plücker relations which are expressed with the Young diagrams having larger numbers of boxes [30].

4. TOTALLY NONNEGATIVE GRASSMANNIAN $\text{Gr}^+(N, M)$

In the previous section, we considered a class of solutions which are expressed by the τ -functions (3.10) with the exponential functions (3.11). Those solutions are determined by the k -parameters and the A -matrix. Fixing the k -parameters, we have a set of M exponentials $\{E_j = e^{\theta_j} : j = 1, \dots, M\}$ which spans \mathbb{R}^M . Then the set of functions $\{f_i : i = 1, \dots, N\}$ of (3.11) defines an N -dimensional subspace of \mathbb{R}^M . This leads naturally to the notion of Grassmannian $\text{Gr}(N, M)$, the set of all N -dimensional subspaces in \mathbb{R}^M , and each point of $\text{Gr}(N, M)$ can be parametrized by the A -matrix in (3.11). Here we give a brief review of the Grassmann manifold $\text{Gr}(N, M)$, in particular, we describe the totally non-negative part of $\text{Gr}(N, M)$. The main purpose of this section is to explain a mathematical background of *regular* soliton solutions of the KP equation.

4.1. The Grassmannian $\text{Gr}(N, M)$. Recall that the set of the functions f_i spans an N -dimensional subspace which is parametrized by an $N \times M$ matrix A of rank N , i.e.

$$(f_1, f_2, \dots, f_N) = (E_1, E_2, \dots, E_M) A^T.$$

Since other set of functions $(g_1, \dots, g_N) = (f_1, \dots, f_N)H$ for some $H \in \text{GL}_N(\mathbb{R})$ gives the same subspace, the A -matrix can be canonically chosen in the *reduced row echelon form* (RREF). This then gives an explicit definition of the Grassmannian,

$$\text{Gr}(N, M) = \text{GL}_N(\mathbb{R}) \backslash \mathcal{M}_{N \times M}(\mathbb{R}),$$

where $\mathcal{M}_{N \times M}(\mathbb{R})$ denotes the set of $N \times M$ matrices of rank N . The canonical form of A is distinguished by a set of *pivot* columns labeled by $I = \{i_1, i_2, \dots, i_N\}$, $1 \leq i_1 < i_2 < \dots < i_N \leq M$ such that the $N \times N$ sub-matrix A_I formed by the column set I is the identity matrix. Each $N \times M$ matrix A in RREF uniquely determines an N -dimensional subspace, thus providing a coordinate for a point of $\text{Gr}(N, M)$. The set W_I of all points in $\text{Gr}(N, M)$ represented by RREF matrices A which have the same pivot set I is called a Schubert cell which gives the decomposition of the Grassmannian, the Schubert decomposition,

$$(4.1) \quad \text{Gr}(N, M) = \bigsqcup_{1 \leq i_1 < i_2 < \dots < i_N \leq M} W_I, \quad I = \{i_1, i_2, \dots, i_N\}.$$

For example, if $I = \{1, 2, \dots, N\}$, then the Schubert cell W_I contains all A matrices whose RREF is given by

$$\begin{pmatrix} 1 & 0 & \cdots & 0 & * & \cdots & * \\ 0 & 1 & \cdots & 0 & * & \cdots & * \\ \vdots & \vdots & \ddots & \vdots & \vdots & \vdots & \vdots \\ 0 & 0 & \cdots & 1 & * & \cdots & * \end{pmatrix}$$

where the $N(M - N)$ entries of the right-hand block are arbitrary real numbers. This particular Schubert cell is often referred to as the *top* cell which has the maximum number of free parameters marked by $*$. It follows from this that the dimension of $\text{Gr}(N, M)$ is $N(M - N)$. The number of free parameters for an A -matrix in RREF with a given pivot set $I = \{i_1, \dots, i_N\}$ is equal to the the dimension of the cell W_I , and is given by

$$\dim W_I = N(M - N) - \sum_{n=1}^N (i_n - n).$$

Note here that the index set $I = \{i_1, \dots, i_N\}$ can be expressed by the Young diagram with $Y_I = (i_N - N, \dots, i_2 - 2, i_1 - 1)$, and then $\text{codim } W_I = |Y|$.

Example 4.1. The Schubert decomposition of $\text{Gr}(2, 4)$ has the form,

$$\text{Gr}(2, 4) = \bigsqcup_{1 \leq i < j \leq 4} W_{\{i, j\}}.$$

There are six cells W_I with $\dim W_I = 7 - (i + j)$, and are listed below:

$$\begin{aligned} \text{(a)} \quad W_{\{1,2\}} = W_{\emptyset} &= \left\{ \begin{pmatrix} 1 & 0 & * & * \\ 0 & 1 & * & * \end{pmatrix} \right\}, & \text{(b)} \quad W_{\{1,3\}} = W_{\square} &= \left\{ \begin{pmatrix} 1 & * & 0 & * \\ 0 & 0 & 1 & * \end{pmatrix} \right\}, \\ \text{(c)} \quad W_{\{1,4\}} = W_{\square\square} &= \left\{ \begin{pmatrix} 1 & * & * & 0 \\ 0 & 0 & 0 & 1 \end{pmatrix} \right\}, & \text{(d)} \quad W_{\{2,3\}} = W_{\boxminus} &= \left\{ \begin{pmatrix} 0 & 1 & 0 & * \\ 0 & 0 & 1 & * \end{pmatrix} \right\}, \\ \text{(e)} \quad W_{\{2,4\}} = W_{\boxplus} &= \left\{ \begin{pmatrix} 0 & 1 & * & 0 \\ 0 & 0 & 0 & 1 \end{pmatrix} \right\}, & \text{(f)} \quad W_{\{3,4\}} = W_{\boxtimes} &= \left\{ \begin{pmatrix} 0 & 0 & 1 & 0 \\ 0 & 0 & 0 & 1 \end{pmatrix} \right\}. \end{aligned}$$

The top cell $W_{\{1,2\}}$ has four free parameters which gives $\dim \text{Gr}(2, 4)$, while the bottom cell $W_{\{3,4\}}$ is 0-dimensional and corresponds to a single point of the Grassmannian.

We also note that each cell in the Schubert decomposition can be parametrized by a unique element of S_M , the symmetric group of permutations for M letters. The group S_M is generated by the adjacent transpositions $s_j := (j, j + 1)$, i.e.

$$S_M = \langle s_1, s_2, \dots, s_{M-1} \rangle,$$

with $s_i^2 = e$, the identity element, $s_i s_j = s_j s_i$ if $|i - j| > 1$ and $(s_i s_{i+1})^3 = e$. Let P_N be a maximal parabolic subgroup of S_M generated by s_j 's without the element s_{M-N} , i.e.

$$P_N := \langle s_1, \dots, s_{M-N-1}, s_{M-N+1}, \dots, s_{M-1} \rangle \cong S_{M-N} \times S_N.$$

Then the pivot set $I = \{i_1, i_2, \dots, i_N\}$ parametrizing the Schubert cell W_I can be uniquely labeled by a minimal length representative of the coset ,

$$S_M^{(N)} := \frac{S_M}{P_N} = \{ \text{the reduced words ending with } s_{M-N} \}.$$

Namely, we have the Schubert decomposition of $\text{Gr}(N, M)$ in terms of the coset $S_M^{(N)}$,

$$\text{Gr}(N, M) = \bigsqcup_{\pi \in S_M^{(N)}} W_\pi.$$

where the dimension of the cell W_π is given by the length of the permutation, i.e. $\dim W_\pi = \ell(\pi)$. For example, in the case of $\text{Gr}(1, 3)$, we have $S_3^{(1)} = \langle s_1, s_2 \rangle / \langle s_1 \rangle = \{e, s_2, s_1 s_2\}$,

$$e = \begin{pmatrix} 1 & 2 & \boxed{3} \\ 1 & 2 & 3 \end{pmatrix} \xrightarrow{s_2} \begin{pmatrix} 1 & \boxed{2} & 3 \\ 1 & 3 & 2 \end{pmatrix} \xrightarrow{s_1} \begin{pmatrix} \boxed{1} & 2 & 3 \\ 3 & 1 & 2 \end{pmatrix}$$

Here \boxed{i} represents a pivot, so that we have

$$W_e = \{(0, 0, 1)\}, \quad W_{s_2} = \{(0, 1, *)\}, \quad W_{s_1 s_2} = \{(1, *, *)\}.$$

Also in the case of $\text{Gr}(2, 3)$, we have $S_3^{(2)} = \langle s_1, s_2 \rangle / \langle s_2 \rangle = \{e, s_1, s_2 s_1\}$,

$$e = \begin{pmatrix} 1 & \boxed{2} & \boxed{3} \\ 1 & 2 & 3 \end{pmatrix} \xrightarrow{s_1} \begin{pmatrix} \boxed{1} & 2 & \boxed{3} \\ 2 & 1 & 3 \end{pmatrix} \xrightarrow{s_2} \begin{pmatrix} \boxed{1} & \boxed{2} & 3 \\ 2 & 3 & 1 \end{pmatrix},$$

and the Schubert cells W_π are given by

$$W_e = \left\{ \begin{pmatrix} 0 & 1 & 0 \\ 0 & 0 & 1 \end{pmatrix} \right\}, \quad W_{s_1} = \left\{ \begin{pmatrix} 1 & * & 0 \\ 0 & 0 & 1 \end{pmatrix} \right\}, \quad W_{s_2 s_1} = \left\{ \begin{pmatrix} 1 & 0 & * \\ 0 & 1 & * \end{pmatrix} \right\}.$$

Note in particular that the last elements in the above examples have no fixed points, and they are called derangements. As we will show that each derangement of S_M parametrizes a unique line-soliton solution generated by the τ -function of the form (3.10). It is important for our purposes to remark that each permutation $\pi \in S_M$ with marked pivot positions can be uniquely expressed by the *chord diagram*. This permutation is the decorated permutation defined in [38] for a parametrization of the totally non-negative Grassmann cells.

Definition 4.2. A chord diagram associated with $\pi \in S_M$ is defined as follows: Consider a line segment with M marked points by the numbers $\{1, 2, \dots, M\}$ in the increasing order from the left.

- (a) If $i < \pi(i)$ (excedance), then draw a chord joining i and $\pi(i)$ on the upper part of the line.
- (b) If $j < \pi(j)$ (deficiency), then draw a chord joining j and $\pi(j)$ on the lower part of the line.
- (c) If $l = \pi(l)$ (fixed point), then
 - (i) if l is a pivot, then draw a loop on the upper part of the line at this point.
 - (ii) if l is a non-pivot, then draw a loop on the lower part of the line at this point.

The dimension of each Schubert cell of $\text{Gr}(N, M)$ can be also found from the chord diagram, and it is given by

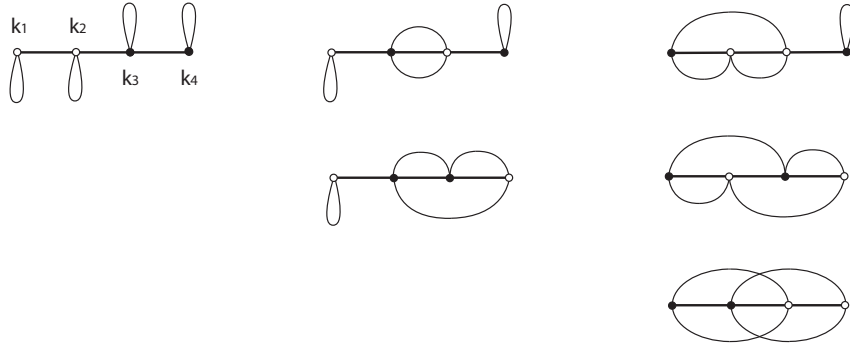
$$\dim W_\pi = N + \{ \# \text{ of crossings} \} + \{ \# \text{ of cusps in the lower part} \} \\ - \{ \# \text{ of loops in the upper part} \}.$$

Here we say that the point marked by j is a ‘‘cusp’’, if $\pi(j) < j = \pi(k) < k$ or $k < \pi(k) = j < \pi(j)$ for some k . In particular, the point j is a cusp in the lower part of the diagram, if $\pi(j) < j = \pi(k) < k$ (see [10, 45]).

Example 4.3. Consider the case of $\text{Gr}(2,4)$. The Schubert cells $W_{\{i,j\}}$ are marked by the pivots $\{i,j\}$ with $1 \leq i < j \leq 4$, and the permutation representations are given by

$$\begin{array}{ccccc}
 \begin{pmatrix} 1 & 2 & \boxed{3} & \boxed{4} \\ 1 & 2 & 3 & 4 \end{pmatrix} & \xrightarrow{s_2} & \begin{pmatrix} 1 & \boxed{2} & 3 & \boxed{4} \\ 1 & 3 & 2 & 4 \end{pmatrix} & \xrightarrow{s_1} & \begin{pmatrix} \boxed{1} & 2 & 3 & \boxed{4} \\ 3 & 1 & 2 & 4 \end{pmatrix} \\
 & & s_3 \downarrow & & s_3 \downarrow \\
 & & \begin{pmatrix} 1 & \boxed{2} & \boxed{3} & 4 \\ 1 & 3 & 4 & 2 \end{pmatrix} & \xrightarrow{s_1} & \begin{pmatrix} \boxed{1} & 2 & \boxed{3} & 4 \\ 3 & 1 & 4 & 2 \end{pmatrix} \\
 & & & & s_2 \downarrow \\
 & & & & \begin{pmatrix} \boxed{1} & \boxed{2} & 3 & 4 \\ 3 & 4 & 1 & 2 \end{pmatrix}
 \end{array}$$

The chord diagrams are shown below, and the points with filled circle indicate the pivots for those cells: One should note here that each fixed point corresponds to a loop of the diagrams, and the



diagrams without loops are associated with the derangements of the permutation group.

As we will show, each chord (not loop) identifies a line-soliton for $y \gg 0$ (or $y \ll 0$) corresponding to the location of the chord in the upper (or lower) part of the chord diagram. For example, in the case $\pi = \begin{pmatrix} 1 & 2 & 3 & 4 \\ 3 & 1 & 4 & 2 \end{pmatrix}$, we have $[1, 3]$ - and $[3, 4]$ -solitons in $y \gg 0$ and $[1, 2]$ - and $[2, 4]$ -solitons in $y \ll 0$.

4.2. The Plücker coordinates and total non-negativity. We here describe the totally non-negative (TNN) Grassmannian $\text{Gr}^+(N, M)$ as a subspace of $\text{Gr}(N, M)$. Then we will show that the τ -function associated with $\text{Gr}^+(N, M)$ is necessary and sufficient conditions for the solution generated by the τ -function to be regular.

We first note that the coordinates of $\text{Gr}(N, M)$ is given by the Plücker embedding into the projectivization of the wedge product space $\wedge^N \mathbb{R}^M$, i.e.

$$\text{Gr}(N, M) \hookrightarrow \mathbb{P}(\wedge^N \mathbb{R}^M),$$

which maps each frame given by $[f_1, \dots, f_N] \in \text{Gr}(N, M)$ to the point on $\mathbb{P}(\wedge^N \mathbb{R}^M)$, i.e.

$$(4.2) \quad f_1 \wedge \dots \wedge f_N = \sum_{1 \leq j_1 < \dots < j_N \leq M} \xi(j_1, \dots, j_N) E_{j_1} \wedge \dots \wedge E_{j_N}.$$

Here the coefficients $\xi(j_1, \dots, j_N)$ are the $N \times N$ minors of the A -matrix defined by

$$\xi(j_1, \dots, j_N) := \det|(a_{n, j_n})_{1 \leq n \leq N}|.$$

Note here that $\xi(j_1, \dots, j_N) = 1$ where the set $\{j_1, \dots, j_N\}$ is the pivot set. Those minors $\xi(j_1, \dots, j_N)$ are called the *Plücker coordinates*, which give a coordinate system for the linear space $\wedge^N \mathbb{R}^M$ with the basis,

$$\{E_{j_1} \wedge \dots \wedge E_{j_N} : 1 \leq j_1 < \dots < j_N \leq M\}.$$

Then the Grassmannian structure is determined by certain relations on the Plücker coordinates, called the *Plücker relations*: for any two index sets $\{\alpha_1, \dots, \alpha_{N-1}\}$ and $\{\beta_1, \dots, \beta_{N+1}\}$ with $1 \leq \alpha_i, \beta_j \leq M$, they are given by

$$(4.3) \quad \sum_{j=1}^{N+1} \xi(\alpha_1, \dots, \alpha_{N-1}, \beta_j) \xi(\beta_1, \dots, \check{\beta}_j, \dots, \beta_{N+1}) = 0,$$

where $\check{\beta}_j$ implies the deletion of β_j . The Plücker relations can be derived using elementary linear algebra from the Laplace expansion of the following $2N \times 2N$ determinant formed by the columns A_i of the matrix A , i.e.

$$\begin{vmatrix} A_{\alpha_1} & \cdots & A_{\alpha_{N-1}} & A_{\beta_1} & \cdots & A_{\beta_{N+1}} \\ 0 & \cdots & 0 & A_{\beta_1} & \cdots & A_{\beta_{N+1}} \end{vmatrix} = 0.$$

The Plücker coordinates, modulo the Plücker relations, give the correct dimension of $\text{Gr}(N, M)$ which is typically less than the dimension of $\mathbb{P}(\bigwedge^N \mathbb{R}^M)$.

Example 4.4. For $\text{Gr}(2, 4)$, the Plücker coordinates are given by the maximal minors,

$$\xi(1, 2), \quad \xi(1, 3), \quad \xi(1, 4), \quad \xi(2, 3), \quad \xi(2, 4), \quad \xi(3, 4).$$

Taking $\{\alpha_1\} = \{1\}$, $\{\beta_1, \beta_2, \beta_3\} = \{2, 3, 4\}$ in (4.3) gives the only Plücker relation in this case,

$$\xi(1, 2)\xi(3, 4) - \xi(1, 3)\xi(2, 4) + \xi(1, 4)\xi(2, 3) = 0,$$

which is the same as (3.14). Since $\dim(\bigwedge^2 \mathbb{R}^4) = 6$, and the projectivization gives $\dim(\mathbb{P}(\bigwedge^2 \mathbb{R}^4)) = 6 - 1 = 5$. Then with one Plücker relation, the dimension of $\text{Gr}(2, 4)$ turns out to be 4, which is consistent with the dimension of the top cell $W_{\{1,2\}}$ as shown in Example 3.2 (case (a)).

Since each point of $\text{Gr}(N, M)$ is expressed by (4.2), the TNN Grassmannian $\text{Gr}^+(N, M)$ is defined by the set of $N \times M$ matrices of rank N whose minors, the Plücker coordinates, are all non-negative, i.e.

$$\text{Gr}^+(N, M) := \{A \in \text{Gr}(N, M) : \xi(j_1, \dots, j_N) \geq 0, \forall 1 \leq j_1 < \dots < j_N \leq M\}.$$

Then the most interesting question is to find a parametrization of all the cells in $\text{Gr}^+(N, M)$. This question has been solved by Postnikov and his colleagues (see [38, 45]), and our classification theorem of the soliton solutions provides an alternative proof based on a simple asymptotic analysis as described in Section 5 (see also [6, 8]).

4.3. The τ -function as a point on $\text{Gr}^+(N, M)$. Expanding the τ -function in the Wronskian determinant (3.10) by Binet-Cauchy formula, we have

$$(4.4) \quad \tau = \text{Wr}(f_1, f_2, \dots, f_N) = \sum_{1 \leq i_1 < \dots < i_N \leq M} \xi(i_1, i_2, \dots, i_N) E(i_1, i_2, \dots, i_N),$$

where $\xi(i_1, i_2, \dots, i_N)$ are the Plücker coordinates given by the maximal minors of the A -matrix, and $E(i_1, i_2, \dots, i_N) = \text{Wr}(E_{i_1}, E_{i_2}, \dots, E_{i_N})$. Here each $E(i_1, i_2, \dots, i_N)$ can be identified with $E_{i_1} \wedge E_{i_2} \wedge \dots \wedge E_{i_N}$ which is the basis element for $\bigwedge^N \mathbb{R}^M$, i.e.

$$\text{Span}_{\mathbb{R}} \{E(i_1, i_2, \dots, i_N) : 1 \leq i_1 < i_2 < \dots < i_N \leq M\} \cong \bigwedge^N \mathbb{R}^M.$$

Note here that the sum $k_{i_1} + k_{i_2} + \dots + k_{i_N}$ should be distinct for distinct sets $\{i_1, i_2, \dots, i_N\}$ in order for the functions $\{E(i_1, i_2, \dots, i_N)\}$ to be linearly independent. It is then clear that the τ -function given by the Wronskian determinant (3.10) can be identified with a point of $\text{Gr}(N, M)$, and the Wronskian map $\text{Wr}: [f_1, \dots, f_N] \mapsto \tau$ gives the Plücker embedding. With the ordering $k_1 < \dots < k_M$, the Wronskian $\text{Wr}(E_{i_1}, \dots, E_{i_N}) > 0$ for $i_1 < \dots < i_N$. Then $\tau \in \text{Gr}^+(N, M)$ implies that τ -function is positive definite and the solution $u(x, y, t) = 2\partial_x^2(\ln \tau)$ is regular for all $(x, y, t) \in \mathbb{R}^3$. In order to prove a converse of this statement, we first show the following: Let (t_1, t_2, \dots, t_M) be the higher times for the KP equation (see Remark 3.2, and here the first three times $t_1 = x, t_2 = y$ and $t_3 = -t$ give the KP variables).

Proposition 4.1. *Suppose that the τ -function is regular for all (t_1, t_2, \dots, t_M) . Then $\tau \in Gr^+(N, M)$.*

Proof. Let us first write the exponential terms,

$$E_j = \exp \left(\sum_{n=1}^M k_j^n t_n + \theta_j^0 \right) =: \hat{E}_j e^{\theta_j^0} \quad \text{for } j = 1, \dots, M,$$

with $\theta_j^0 \in \mathbb{R}$, i.e. the shifts of t_n 's in the exponential functions. Because the k -parameters are all distinct, one can take the coordinates $(\theta_1^0, \dots, \theta_M^0)$ instead of (t_1, \dots, t_M) . The τ -function is then given by

$$\tau = \sum_{1 \leq j_1 < \dots < j_N \leq M} \xi(j_1, \dots, j_N) \hat{E}(j_1, \dots, j_N) \prod_{k=1}^N e^{\theta_{j_k}^0},$$

where $\hat{E}(j_1, \dots, j_N) = \text{Wr}(\hat{E}_{j_1}, \dots, \hat{E}_{j_N})$. Then one can choose the parameters $(\theta_{j_1}^0, \dots, \theta_{j_N}^0)$ so that

$$\sum_{k=1}^N \theta_{j_k}^0 \gg \sum_{k=1}^N \theta_{l_k}^0,$$

for any other choice of the parameters $(\theta_{l_1}^0, \dots, \theta_{l_N}^0)$. This means that the exponential term having this index set $\{j_1, \dots, j_N\}$ is the dominant one in the τ -function, while all other parameters are of $\mathcal{O}(1)$. Suppose the minor $\xi(j_1, \dots, j_N)$ associated with this index set is negative, that is, $\tau \approx \xi(j_1, \dots, j_N) E(j_1, \dots, j_N) < 0$. Now note that for $x \ll 0$, the dominant exponential in the τ -function is $E(e_1, \dots, e_N) > 0$ with the pivot set $\{e_1, \dots, e_N\}$ and the ordering $k_1 < \dots < k_M$, so that $\tau \approx E(e_1, \dots, e_N) > 0$. This implies that the τ -function vanishes at some point in (x, y) -plane, and therefore the solution $u(x, y, t)$ is not regular. \square

It is then clear from the proof that the total non-negativity is not only sufficient but necessary for the regularity of the solution. Namely we have the following.

Corollary 4.1. *The solution of the KP equation generated by the τ -function in the form (3.10) with (3.11) is non-singular for any initial data if and only if $\tau \in Gr^+(N, M)$.*

Thus the classification of the regular soliton solutions is equivalent to a study of the totally non-negative Grassmannian.

Remark 4.5. Since each τ -function can be identified as a point on $\text{Gr}(N, M)$, one can define a moment map, $\mu : \text{Gr}(N, M) \rightarrow \mathfrak{h}_{\mathbb{R}}^*$ [24],

$$\mu(\tau) = \frac{\sum_{1 \leq j_1 < \dots < j_N \leq M} |\xi(j_1, \dots, j_N) E(j_1, \dots, j_N)|^2 (L_{j_1} + \dots + L_{j_N})}{\sum_{1 \leq j_1 < \dots < j_N \leq M} |\xi(j_1, \dots, j_N) E(j_1, \dots, j_N)|^2},$$

where L_j are the weights of the standard representation of $\text{SL}(M)$, and $\mathfrak{h}_{\mathbb{R}}^*$ is the real part of the dual of the Cartan subalgebra of $\mathfrak{sl}(M)$ defined by

$$\mathfrak{h}_{\mathbb{R}}^* = \text{Span}_{\mathbb{R}} \left\{ L_1, \dots, L_M : \sum_{j=1}^M L_j = 0 \right\} \cong \mathbb{R}^{M-1}.$$

Then the closure of the image of the moment map is a convex polytope whose vertices are the fixed points of the S_M orbit, that is, the dominant exponentials.

5. CLASSIFICATION OF SOLITON SOLUTIONS

In this section, we now show the asymptotic behavior of the τ -function in (4.4) and then present a classification scheme for the regular line-soliton solutions of KP based on the τ -function asymptotics (see also [3]).

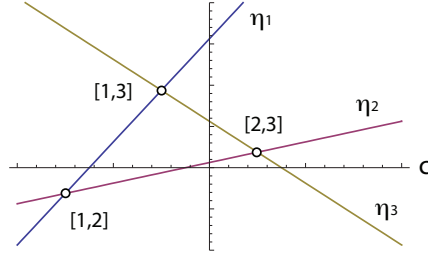


FIGURE 5.1. The graphs of $\eta_j(c) = k_j(k_j - c)$. Each $[i, j]$ represents the exchange of the order between η_i and η_j . The parameters are given by $(k_1, k_2, k_3) = (-\frac{5}{4}, -\frac{1}{4}, \frac{3}{4})$.

5.1. Asymptotic line-solitons. The τ -function of (4.4) is given explicitly by the sum of exponential terms with the Wronskians,

$$(5.1) \quad \tau(x, y, t) = \sum_{1 \leq m_1 < \dots < m_N \leq M} \xi(m_1, \dots, m_N) E(m_1, \dots, m_N),$$

where $E(m_1, \dots, m_N) = \text{Wr}(E_{m_1}, \dots, E_{m_N})$ with $E_m = e^{\theta_m}$, and $\theta_m(x, y, t) = k_m x + k_m^2 y - k_m^3 t$. Since $u = 2\partial_x^2(\ln \tau)$, the regularity condition on the line-soliton solutions requires that the τ -function does not vanish for all values of x, y and t . To ensure that it is sign-definite, the following necessary and sufficient conditions are imposed on the τ -function in (5.1).

- (i) The parameters k_1, k_2, \dots, k_M are ordered as $k_1 < k_2 < \dots < k_M$, and the sums $k_i + k_j$ are all distinct.
- (ii) A is a TNN matrix, that is, all its maximal minors are $\xi(m_1, \dots, m_N) \geq 0$.

The asymptotic spatial structure of the solution $u(x, y, t)$ is determined from the consideration of dominant exponentials $E(m_1, \dots, m_N)$ in the τ -function at different regions of the (x, y) -plane for large $|y|$. The solution $u = 2\partial_x^2(\ln \tau)$ is localized at the *boundaries* of two distinct regions where a balance exists between two dominant exponentials in the τ -function (5.1), whereas the solution is exponentially small in the interior of each of these regions where only one exponential $E(m_1, \dots, m_N)$ with a specific index set $\{m_1, \dots, m_N\}$ is dominant. Before discussing a general theorem, let us first consider the following simple examples which illustrate the resonant interactions among the line-solitons. As discussed in Introduction, the resonant interaction is one of the most important features of the KP equation (see e.g. [28, 32, 18]).

Example 5.1. We consider the case with $N = 1$ and $M = 3$, where the 1×3 coefficient matrix A is given by

$$A = \begin{pmatrix} 1 & a & b \end{pmatrix}.$$

The parameters a, b in the matrix are positive constants; meaning that this A -matrix marks a point on $\text{Gr}^+(1, 3)$, and the positivity implies the regularity of the KP solution. The τ -function is simply given by

$$\tau = f = E_1 + aE_2 + bE_3.$$

Now let us determine the dominant exponentials and analyze the structure of the solution in the xy -plane. First we consider the function f along the line $x = -cy$ with $c = \tan \Psi$ where Ψ is the angle measured counterclockwise from the y -axis (see Figure 3.1). Then along $x = -cy$, we have the exponential function $E_j = \exp[\eta_j(c)y - k_j^3 t]$ with

$$(5.2) \quad \eta_j(c) = k_j(k_j - c).$$

It is then seen from Figure 5.1 that for $y \gg 0$ and a fixed t , the exponential term E_1 dominates when

c is large positive ($\Psi \approx \frac{\pi}{2}$, i.e. $x \rightarrow -\infty$). Decreasing the value of c (rotating the line clockwise), the dominant term changes to E_3 . Thus we have

$$w := \partial_x \ln f \longrightarrow \begin{cases} k_1 & \text{as } x \rightarrow -\infty, \\ k_3 & \text{as } x \rightarrow \infty. \end{cases}$$

The transition of the dominant exponentials $E_1 \rightarrow E_3$ is characterized by the condition $\eta_1 = \eta_3$, which corresponds the direction parameter value $c = \tan \Psi_{[1,3]} = k_1 + k_3$. In the neighborhood of this line, the function f can be approximated as

$$f \approx E_1 + bE_3,$$

which implies that there exists a $[1, 3]$ -soliton for $y \gg 0$. The constant b can be used to choose a specific location of this soliton.

Next consider the case of $y \ll 0$. The dominant exponential corresponds to the *least* value of η_j for any given value of c . For large positive c ($\Psi \approx \frac{\pi}{2}$, i.e. $x \rightarrow \infty$), E_3 is the dominant term. Decreasing the value of c (rotating the line $x = -cy$ clockwise), the dominant term changes to E_2 when $k_2 + k_3 > c > k_1 + k_2$, and E_1 becomes dominant for $c < k_1 + k_2$. Hence, we have for $y \ll 0$

$$w = \partial_x \ln f \longrightarrow \begin{cases} k_1 & \text{as } x \rightarrow -\infty, \\ k_2 & \text{for } -(k_1 + k_2)y < x < -(k_2 + k_3)y, \\ k_3 & \text{as } x \rightarrow \infty. \end{cases}$$

In the neighborhood of the line $x + (k_1 + k_2)y = \text{constant}$,

$$f \approx E_1 + aE_2,$$

which corresponds to a $[1, 2]$ -soliton and its location is fixed by the constant a . The solution in $y \ll 0$ also consists of a $[2, 3]$ -soliton in the neighborhood of the line $x + (k_2 + k_3)y = \text{constant}$, and whose location is determined by the locations of other line-solitons. Therefore, we need only two parameters a, b (besides the k -parameters) to specify the solution uniquely, and those parameters fix the locations of line $x + y \tan \Psi_{[i,j]} - C_{[i,j]}t = x_{[i,j]}^0$ for $[i, j]$ -soliton. For $[i, j] = [1, 3]$ and $[2, 3]$ in $x \gg 0$, we have

$$x_{[1,3]} = -\frac{1}{k_3 - k_1} \ln b, \quad x_{[2,3]} = -\frac{1}{k_3 - k_2} \ln \frac{b}{a}.$$

The shape of solution generated by $f = E_1 + aE_2 + bE_3$ with $a = b = 1$ (i.e. at $t = 0$ three line-solitons meet at the origin) is illustrated via the contour plot in Figure 5.2. In this Figure, one can see that the line-soliton in $y \gg 0$ labeled by $[1, 3]$, is localized along the line $\theta_1 = \theta_3$ with direction parameter $c = k_1 + k_3$; two other line-solitons in $y \ll 0$ labeled by $[1, 2]$ and $[2, 3]$ are localized respectively, along the phase transition lines with $c = k_1 + k_2$ and $c = k_2 + k_3$. This solution represents a resonant solution of three line-solitons. The resonant condition among those three line-solitons is given by

$$\mathbf{K}_{[1,3]} = \mathbf{K}_{[1,2]} + \mathbf{K}_{[2,3]}, \quad \Omega_{[1,3]} = \Omega_{[1,2]} + \Omega_{[2,3]},$$

which are trivially satisfied with $\mathbf{K}_{[i,j]} = (k_j - k_i, k_j^2 - k_i^2)$ and $\Omega_{[i,j]} = k_j^3 - k_i^3$. The resonant condition may be symbolically written as

$$[1, 3] = [1, 2] + [2, 3].$$

One can also represent this line-soliton solution by a permutation of three indices: $\{1, 2, 3\}$ which is illustrated by a (linear) *chord diagram* shown below. Here, the upper chord represents the $[1, 3]$ -soliton in $y \gg 0$ and the lower two chords represent $[1, 2]$ and $[2, 3]$ -solitons in $y \ll 0$. Following the arrows in the chord diagram, one recovers the permutation,

$$\pi = \begin{pmatrix} 1 & 2 & 3 \\ 3 & 1 & 2 \end{pmatrix} \quad \text{or simply } \pi = (312).$$

In general, each line-soliton solution of the KP equation can be parametrized by a *unique* permutation corresponding to a chord diagram (see the next subsection).

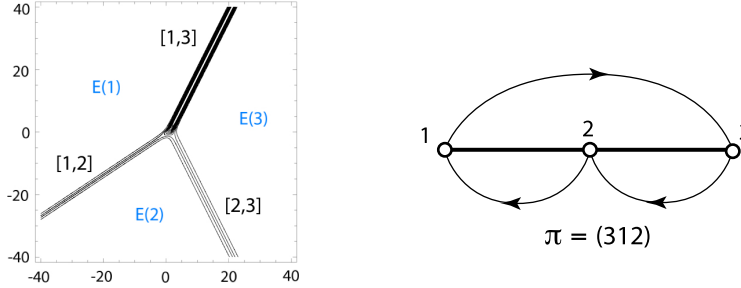


FIGURE 5.2. Example of $(2, 1)$ -soliton solution and the chord diagram. The k -parameters are chosen as $(k_1, k_2, k_3) = (-\frac{5}{4}, -\frac{1}{4}, \frac{3}{4})$. The right panel is the corresponding chord diagrams. We take the A -matrix $A = (1 \ 1 \ 1)$ so that at $t = 0$ three line-solitons meet at the origin. Each $E(j)$ with $j = 1, 2$ or 3 indicates the dominant exponential term E_j in that region. The boundaries of any two adjacent regions give the line-solitons indicating the transition of the dominant terms E_j . The k -parameters are the same as those in Figure 5.1, and the line-solitons are determined from the intersection points of the $\eta_j(c)$'s in Figure 5.1. Here $a = b = 1$ (i.e. $\tau = E_1 + E_2 + E_3$) so that the three solitons meet at the origin at $t = 0$.

The results described in this example can be easily extended to the general case where f has arbitrary number of exponential terms (see also [26, 4]).

Proposition 5.1. *If $f = a_1 E_1 + a_2 E_2 + \dots + a_M E_M$ with $a_j > 0$ for $j = 1, 2, \dots, M$, then the solution u consists of $M - 1$ line-solitons for $y \ll 0$ and one line-soliton for $y \gg 0$.*

Such solutions are referred to as the $(M - 1, 1)$ -soliton solutions; meaning that $(M - 1)$ line-solitons for $y \ll 0$ and one line-soliton for $y \gg 0$. Note that the line-soliton for $y \gg 0$ is labeled by $[1, M]$, whereas the other line-solitons in $y \ll 0$ are labeled by $[k, k + 1]$ for $k = 1, 2, \dots, M - 1$, counterclockwise from the negative to the positive x -axis, i.e. increasing Ψ from $-\frac{\pi}{2}$ to $\frac{\pi}{2}$. As in the previous examples one can set $a_1 = 1$ without any loss of generality, then the remaining $M - 1$ parameters a_2, \dots, a_M determine the locations of the M line-solitons. Also note that the xy -plane is divided into M sectors for the asymptotic region with $x^2 + y^2 \gg 0$, and the boundaries of those sectors are given by the asymptotic line-solitons. This feature is common even for the general case.

Figure 5.3 illustrates the case for a $(3, 1)$ -soliton solution with $f = E_1 + E_2 + E_3 + E_4$. The chord diagram for this solution represents the permutation $\pi = (4123) = s_4 s_3 s_2 \in S_4^{(1)}$.

Example 5.2. Let us now consider the case with $N = 2$ and $M = 3$: We take the A -matrix in (3.11) of the form,

$$A = \begin{pmatrix} 1 & 0 & -b \\ 0 & 1 & a \end{pmatrix}.$$

where a and b are positive constants, that is, A marks a point on $\text{Gr}^+(2, 3)$. Then the τ -function is given by

$$\tau = E(1, 2) + aE(1, 3) + bE(2, 3).$$

In order to carry out the asymptotic analysis in this case one needs to consider the sum of two $\eta_j(c)$, i.e. $\eta_{i,j} = \eta_i + \eta_j$ for $1 \leq i < j \leq 3$. This can still be done using Figure 5.1, but a more effective way is described below (see the graph of $\eta(k, c)$ in Figure 5.5).

For $y \gg 0$, the transitions of the dominant exponentials are given by following scheme:

$$E(1, 2) \longrightarrow E(1, 3) \longrightarrow E(2, 3),$$

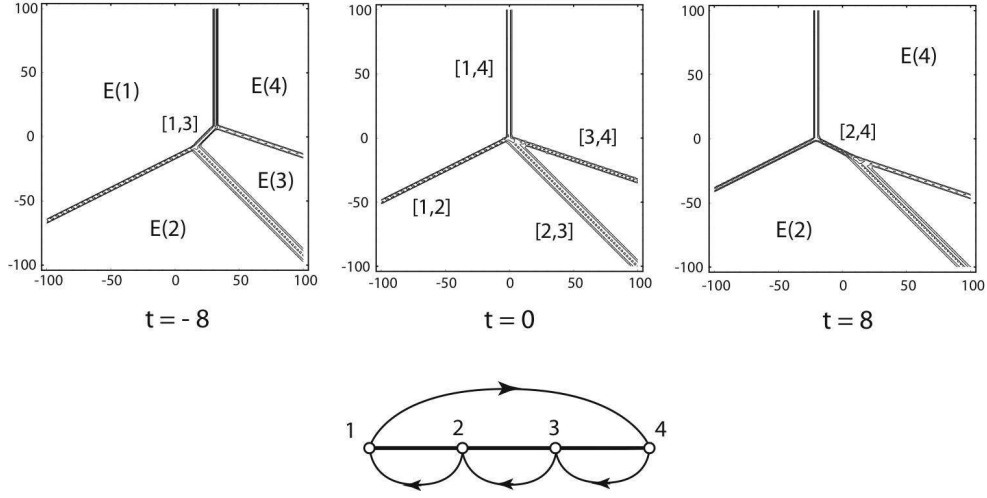


FIGURE 5.3. The time evolution of a $(3, 1)$ -soliton solution and the corresponding chord diagram. The upper chord represents the $[1, 4]$ -soliton, and the lower ones represent $[1, 2]$ -, $[2, 3]$ - and $[3, 4]$ -solitons. The chord diagram shows $\pi = (4123)$. The intermediate solitons are $[1, 3]$ -soliton at $t = -8$ and $[2, 4]$ -soliton at $t = 8$, respectively. These solitons appear as the resonant $(2, 1)$ -type solutions.

as c varies from large positive (i.e. $x \rightarrow -\infty$) to large negative values (i.e. $x \rightarrow \infty$). The boundary between the regions with the dominant exponentials $E(1, 2)$ and $E(1, 3)$ defines the $[2, 3]$ -soliton solution since here the τ -function can be approximated as

$$\tau \approx E(1, 2) + aE(1, 3) = 2(k_2 - k_1)e^{\theta_1 + \frac{1}{2}(\theta_2 + \theta_3 - \theta_{23})} \cosh \frac{1}{2}(\theta_2 - \theta_3 + \theta_{23}),$$

so that we have

$$u = 2\partial_x^2 \ln \tau \approx \frac{1}{2}(k_2 - k_3)^2 \operatorname{sech}^2 \frac{1}{2}(\theta_2 - \theta_3 + \theta_{23}),$$

where θ_{23} is related to the parameter of the A -matrix (see below). A similar computation as above near the transition boundary of the dominant exponentials $E(1, 3)$ and $E(2, 3)$ yields

$$\tau \approx 2(k_3 - k_1)ae^{\theta_3 + \frac{1}{2}(\theta_1 + \theta_2 - \theta_{12})} \cosh \frac{1}{2}(\theta_1 - \theta_2 + \theta_{12}).$$

The phases θ_{12} and θ_{23} are related to the parameters of the A -matrix,

$$a = \frac{k_2 - k_1}{k_3 - k_1} e^{-\theta_{23}}, \quad b = \frac{k_2 - k_1}{k_3 - k_2} e^{-\theta_{12}}.$$

For $y \ll 0$, there is only one transition, namely

$$E(2, 3) \longrightarrow E(1, 2),$$

as c varies from large positive value (i.e. $x \rightarrow \infty$) to large negative value (i.e. $x \rightarrow -\infty$). In this case, a $[1, 3]$ -soliton is formed for $y \ll 0$ at the boundary of the dominant exponentials $E(2, 3)$ and $E(1, 2)$. The contour plot of the line-soliton solution is shown in Figure 5.4. Notice that this figure can be obtained from Figure 5.2 by changing $(x, y) \rightarrow (-x, -y)$. This solution can be represented by the chord diagram corresponding to the permutation $\pi = (231)$ shown below. Note that this diagram is the π -rotation of the chord diagram in Example 5.1 whose permutation $\pi = (312)$ is the inverse of $\pi = (231)$.

As shown in those examples, it is now clear that each line-soliton appears as a boundary of two dominant exponentials, and with the condition that $k_i + k_j$ are all distinct for $i \neq j$, we have the following Proposition:

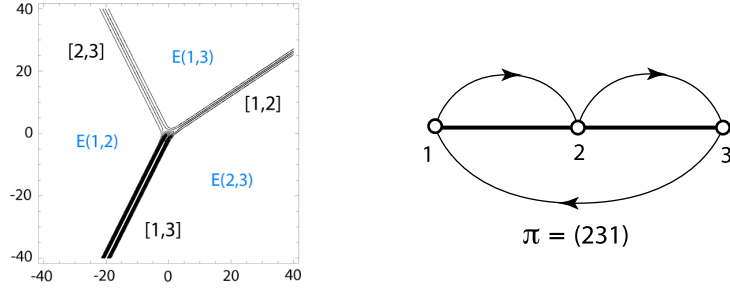


FIGURE 5.4. Example of $(1,2)$ -soliton solution and the chord diagram. The k -parameters are the same as the $(2,1)$ -soliton in the previous figure. The right panels are the corresponding chord diagrams. The parameters in the A -matrices are chosen as $a = \frac{1}{2}$ and $b = 1$ so that at $t = 0$ three line-solitons meet at the origin.

Proposition 5.2. *Two dominant exponentials of the τ -function in adjacent regions of the xy -plane are of the form $E(i, m_2, \dots, m_N)$ and $E(j, m_2, \dots, m_N)$ for some $N-1$ common indices m_2, \dots, m_N .*

As a consequence of Proposition 5.2, the KP solution behaves asymptotically like a single line-soliton

$$(5.3) \quad u(x, y, t) \simeq \frac{1}{2}(k_j - k_i)^2 \operatorname{sech}^2 \frac{1}{2}(\theta_j - \theta_i + \theta_{ij}),$$

in the neighborhood of the line $x + (k_i + k_j)y = \text{constant}$, which forms the boundary between the regions of dominant exponentials $E(i, m_2, \dots, m_N)$ and $E(j, m_2, \dots, m_N)$. Equation (5.3) defines an *asymptotic* line-soliton, i.e. $[i, j]$ -soliton, as a result of those two dominant exponentials. In order to identify the set of asymptotic line-solitons associated with a given solution, we need to determine which exponential terms $E(m_1, m_2, \dots, m_N)$ are actually dominant along each line $[i, j] : x = -(k_i + k_j)y$ as $|y| \rightarrow \infty$. For this purpose, first note that along a line $x = -cy$ each exponential term $E(m_1, m_2, \dots, m_N)$ has the form,

$$E(m_1, m_2, \dots, m_N) \propto \exp\left(\sum_{n=1}^N \eta_{m_n}(c)y\right), \quad \eta_m(c) = k_m(k_m - c).$$

Thus for $y \gg 0$ (or $\ll 0$), the dominant exponential corresponds to the largest (or least) value of the sum of $\eta_{m_n}(c)$ for each c . When two dominant exponentials $E(i, m_2, \dots, m_N)$ and $E(j, m_2, \dots, m_N)$ are in balance along the direction of the $[i, j]$ -soliton, we have $\eta_i(c) = \eta_j(c)$ which implies that $c = k_i + k_j$. Since $\eta_m(c) - \eta_i(c) = (k_m - k_i)(k_m + k_i - c)$ and the k -parameters are ordered as $k_1 < k_2 < \dots < k_M$, we have the following order relations among the other $\eta_m(c)$'s along $c = k_i + k_j$,

$$(5.4) \quad \begin{cases} \eta_i = \eta_j < \eta_m & \text{if } m < i \text{ or } j < m, \\ \eta_i = \eta_j > \eta_m & \text{if } i < m < j. \end{cases}$$

The relations among the phases $\eta_j(c)$ can be seen easily from the plots of $\eta_j(c)$ versus c as well as $\eta(k, c) = k(k - c)$ versus k for a fixed value of c illustrated by Figure 5.5. Proposition 5.2 and the relations (5.4) are particularly useful in order to find the asymptotic line-solitons from a given KP τ -function as demonstrated by the example below.

Example 5.3. Let us consider the 2×4 matrix,

$$A = \begin{pmatrix} 1 & 0 & 0 & -a \\ 0 & 1 & b & c \end{pmatrix},$$

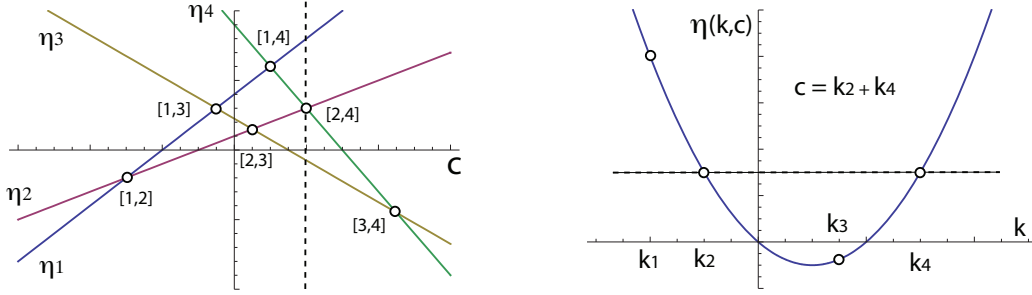


FIGURE 5.5. The left figure shows $\eta_j(c) = k_j(k_j - c)$ for $j = 1, \dots, 4$. Each $[i, j]$ at the intersection point of $\eta_i(c) = \eta_j(c)$ corresponds to $c = k_i + k_j$. We assume that the parameters k_j are generic so that there is at most one intersection point for each c . The right figure is a plot of $\eta(k, c)$ as a function of k with $c = k_2 + k_4$, that is, the η along the dotted line in the left figure passing through the intersection point $\eta_2(c) = \eta_4(c)$. This figure shows the order $\eta_3 < \eta_2 = \eta_4 < \eta_1$.

where a, b, c are positive real numbers. In this case, there are six maximal minors, five of which are positive, namely,

$$\xi(1, 2) = 1, \quad \xi(1, 3) = b, \quad \xi(1, 4) = c, \quad \xi(2, 4) = a, \quad \xi(3, 4) = ab,$$

and $\xi(2, 3) = 0$. Then from (5.1) the τ -function has the form,

$$\begin{aligned} \tau = & (k_2 - k_1)E(1, 2) + b(k_3 - k_1)E(1, 3) + c(k_4 - k_1)E(1, 4) \\ & + a(k_2 - k_4)E(2, 4) + ab(k_4 - k_3)E(3, 4). \end{aligned}$$

Proposition 5.2 implies that the line solitons are localized along the lines $x + cy = \text{constant}$ with $c = k_i + k_j = \tan \Psi_{[i, j]}$. Hence, we look for dominant exponential terms in the τ -function along those directions. For $y \gg 0$, the c -values decrease as we sweep clockwise from negative to positive x -axis starting with the largest value $c = k_3 + k_4$. We have $\eta_1, \eta_2 > \eta_3 = \eta_4$ from the order relations (5.4) for $c = k_3 + k_4$. This means that $\eta_1 + \eta_2$ is the dominant phase combination along this direction. Since $\xi(1, 2) \neq 0$, $\tau(x, y, t) \approx (k_2 - k_1)E(1, 2)$ implying that $u \approx 0$ along the line $[3, 4]$, so there is no $[3, 4]$ line-soliton. By similar reasoning one can verify that the $[1, 4]$ - and $[1, 2]$ -solitons are also impossible. Let us consider the direction $c = k_2 + k_4$ to check for the $[2, 4]$ -soliton. From (5.4) (see also Figure 5.5), $\eta_3 < \eta_2 = \eta_4 < \eta_1$, and since both $\xi(1, 2)$ and $\xi(1, 4) = a$ are nonzero, the τ -function in (5.1) corresponds to a dominant balance of exponentials: $\tau \approx (k_2 - k_1)E(1, 2) + c(k_4 - k_1)E(1, 4)$ along the line $[2, 4]$. Therefore $[2, 4]$ corresponds to an asymptotic line-soliton as $y \rightarrow \infty$. The $[1, 3]$ -soliton also exists by a similar argument. Thus, we have two asymptotic line-solitons $[1, 3]$ - and $[2, 4]$ -types for $y \gg 0$.

We next look for the asymptotic solitons for $y \ll 0$ by sweeping from the negative x -axis to positive x -axis. Recall that in this case the dominant exponential $E(i, j)$ corresponds to the least value of the sum $\eta_i(c) + \eta_j(c)$. It is easy to see that $[1, 2]$ and $[3, 4]$ -solitons are impossible since $E(3, 4)$ and $E(1, 2)$ are respectively, the only dominant exponentials along those directions. Then consider the $[1, 3]$ -soliton. Along $c = k_1 + k_3$, (5.4) implies that $\eta_2 < \eta_1 = \eta_3 < \eta_4$, and so the exponentials $E(1, 2)$ and $E(2, 3)$ would give the dominant balance. But $E(2, 3)$ is not present in the above τ -function because $\xi(2, 3) = 0$. So we conclude that $[1, 3]$ -soliton does not exist as $y \ll 0$, and for similar reasons, $[2, 4]$ -soliton is also impossible. Next, checking for the $[1, 4]$ -soliton, we have $\eta_2, \eta_3 < \eta_1 = \eta_4$ from (5.4). But as seen earlier, the dominant exponential $E(2, 3)$ is *not* present in the τ -function. However, there does exist a balance between the next dominant exponential pairs $\{E(1, 3), E(3, 4)\}$ or $\{E(1, 2), E(2, 4)\}$ depending on whether $\eta_2 > \eta_3$ or $\eta_2 < \eta_3$. In either case, there exists an asymptotic line-soliton along $[1, 4]$. A similar argument applies along the line $[2, 3]$ which corresponds the other asymptotic line-soliton as $y \ll 0$.

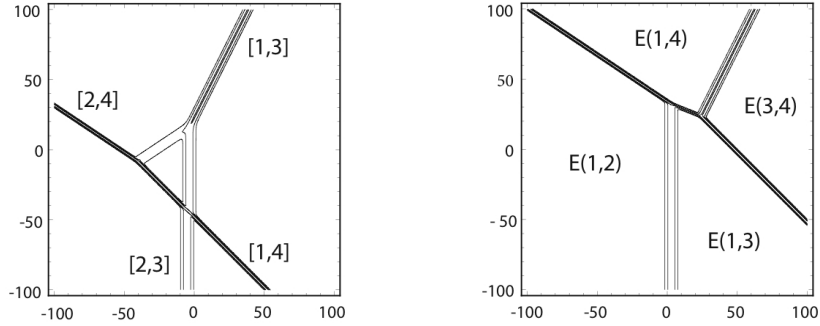


FIGURE 5.6. An example of $(2,2)$ -soliton solution. The left left figure is at $t = -16$ and the right one at $t = 16$. The parameters (k_1, \dots, k_4) are given by $(-1, -0.5, 0.5, 2)$. The intermediate solitons are $[3, 4]$ -type for $t = -16$ and $[1, 2]$ -type for $t = 16$. Note that the middle triangular section at $t = -16$ corresponds to the region with the dominant exponential $E(2, 4)$, and that all five non-zero exponential terms in the τ -function appear in the figure at $t = 16$.

In summary, the τ -function corresponding to the A -matrix given above, generates a KP solution with asymptotic line-solitons $[1, 3]$ and $[2, 4]$ as $y \gg 0$, and asymptotic line-solitons $[1, 4]$ and $[2, 3]$ as $y \ll 0$. This line-soliton solution with the parameters $a = b = c = 1$ in the A -matrix is shown in Figure 5.6.

We note that the line-solitons associated with the resonant $(1, 2)$ - and $(2, 1)$ -soliton solutions can be determined in the same way as the above example by applying for the dominant balance conditions given by Proposition 5.2 and (5.4). We now proceed to discuss a more general characterization of all line-soliton solutions of the KP equation whose τ -functions are given in the Wronskian form (3.10).

5.2. Characterization of the line-solitons. It should be clear from the above examples that a dominant exponential term determined by the relations (5.4) is actually *present* in the given τ -function if its coefficient term given by a maximal minor of the A -matrix is non-zero. Thus, in order to obtain a complete characterization of the asymptotic line solitons, it is necessary to consider the structure of the $N \times M$ coefficient A -matrix in some detail. We consider the matrix A to be in RREF, and we will also assume that A is *irreducible* as defined below:

Definition 5.4. An $N \times M$ matrix A is irreducible if each column of A contains at least one nonzero element, or each row contains at least one nonzero element other than the pivot once A is in RREF.

If an $N \times M$ matrix A is *not* irreducible, then the corresponding τ -function gives the same KP solution u which is obtained from another τ -function associated with a smaller size matrix \tilde{A} derived from A . One can notice from the determinant expansion in (5.1) that

- (a) if the m -th column of A has only zero elements, then $\xi(m_1, \dots, m_N) = 0$ if $m_k = m$ for some k , that is, the exponential E_m will never appear in the τ -function; in terms of the chord diagram, this corresponds to a loop in the lower part of the diagram (m is a non-pivot index),
- (b) if the n -th row of A has the pivot as the only non-zero element, then all $\xi(m_1, \dots, m_N) \neq 0$ contains the index n , that is, the exponential E_n can be factored out from the τ -function; in terms of the chord diagram, this corresponds to a loop in the upper part of the diagram.

So the irreducibility implies that we consider only derangements (i.e. no fixed points) of the permutation.

We now present a classification scheme of the line-soliton solutions by identifying the asymptotic line-solitons as $y \rightarrow \pm\infty$. We denote a line-soliton solution by (N_-, N_+) -soliton whose asymptotic

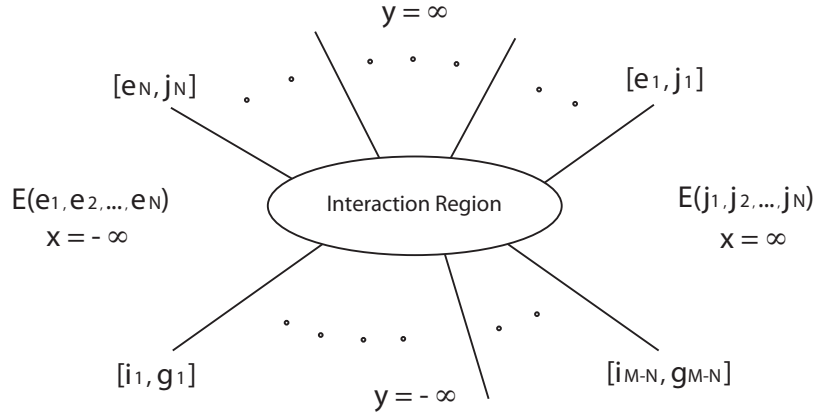


FIGURE 5.7. (N_-, N_+) -soliton solution. The asymptotic line-solitons are denoted by their index pairs $[e_n, j_n]$ and $[i_m, g_m]$. The sets $\{e_1, e_2, \dots, e_N\}$ and $\{g_1, g_2, \dots, g_{M-N}\}$ indicate pivot and non-pivot indices, respectively. Here $N_- = M - N$ and $N_+ = N$ for the τ -function on $\text{Gr}(N, M)$, and $E(\cdot, \dots, \cdot)$ represents the dominant exponential in that region.

form consists of N_- line-solitons as $y \rightarrow -\infty$ and N_+ line-solitons for $y \rightarrow \infty$ in the xy -plane as shown in Figure 5.7. The next Proposition provides a general result characterizing the asymptotic line-solitons of the (N_-, N_+) -soliton solutions (the proof can be found in [8]):

Proposition 5.3. *Let $\{e_1, e_2, \dots, e_N\}$ and $\{g_1, g_2, \dots, g_{M-N}\}$ denote respectively, the pivot and non-pivot indices associated with an irreducible, $N \times M$, TNN A -matrix. Then the soliton solution obtained from the τ -function in (5.1) with this A -matrix has the following structure:*

- (a) *For $y \gg 0$, there are N asymptotic line-solitons of $[e_n, j_n]$ -type for some j_n .*
- (b) *For $y \ll 0$, there are $(M - N)$ asymptotic line-solitons of $[i_m, g_m]$ -type for some i_m .*

An important consequence of Proposition 5.3 is that it defines the *pairing* map $\pi : [M] \rightarrow [M]$ on the integer set $[M] := \{1, 2, \dots, M\}$ according to

$$(5.5) \quad \begin{cases} \pi(e_n) = j_n, & n = 1, 2, \dots, N, \\ \pi(g_m) = i_m, & m = 1, 2, \dots, M - N. \end{cases}$$

Recall that $\{e_n\}_{n=1}^N$ and $\{g_m\}_{m=1}^{M-N}$ are respectively, the pivot and non-pivot indices of the A -matrix and form a disjoint partition of $[M]$. Then the unique index pairings in Proposition 5.3 imply that the map π is a *permutation* of M indices. More precisely, $\pi \in \mathcal{S}_M$ where \mathcal{S}_M is the group of permutations of the index set $[M]$. Furthermore, since $\pi(e_n) = j_n > e_n$, $n = 1, \dots, N$ and $\pi(g_m) = i_m < g_m$, $m = 1, \dots, M - N$, π defined by (5.5) is a permutation with no fixed point, i.e. *derangements*. Yet another feature of π is that it has exactly N *excedances* defined as follows: an element $l \in [M]$ is an *excedance* of π if $\pi(l) > l$. The excedance set of π in (5.5) is the set of pivot indices $\{e_1, e_2, \dots, e_N\}$. The above results can be summarized to deduce the following characterization for the line-soliton solution of the KP equation [8].

Theorem 5.5. *Let A be an $N \times M$, TNN, irreducible matrix which corresponds to a point in the non-negative Grassmannian $\text{Gr}^+(N, M) \subset \text{Gr}(N, M)$. Then the τ -function (5.1) associated with this A -matrix generates an $(M - N, N)$ -soliton solutions. The M asymptotic line-solitons associated with each of these solutions can be identified via a pairing map π defined by (5.5). The map $\pi \in \mathcal{S}_M$ is a derangement of the index set $[M]$ with N excedances given by the pivot indices $\{e_1, e_2, \dots, e_N\}$ of the A -matrix in RREF.*

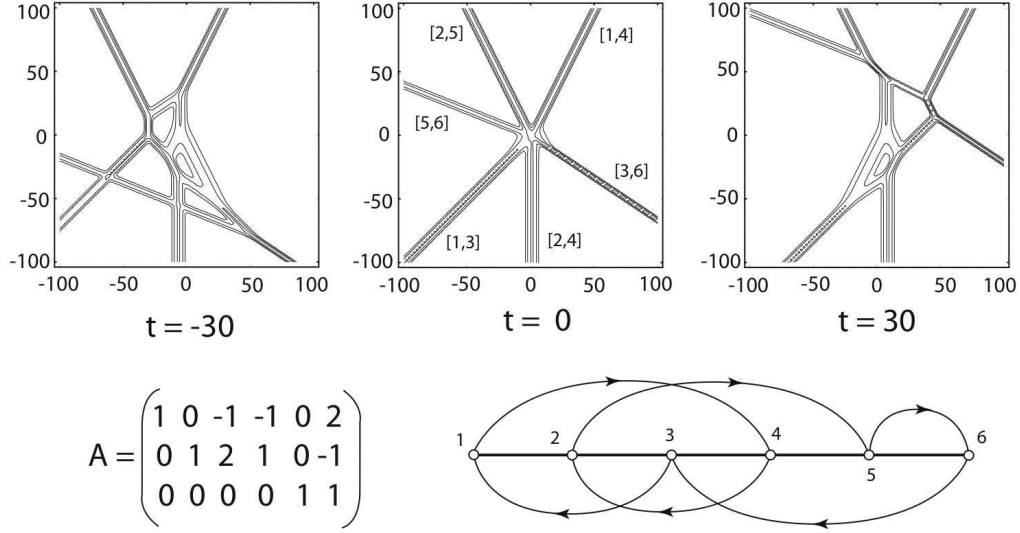


FIGURE 5.8. An example of $(3,3)$ -soliton solution. The permutation of this solution is $\pi = (451263)$. The k -parameters are chosen as $(k_1, k_2, \dots, k_6) = (-1, -\frac{1}{2}, 0, \frac{1}{2}, 1, \frac{3}{2})$. The dominant exponential for $x \ll 0$ is $E(1, 2, 5)$, and each dominant exponential is obtained through the derangement representing the solution, e.g. after crossing $[5, 6]$ -soliton in the clockwise direction, the dominant exponential becomes $E(1, 2, 6)$. That is, $[5, 6]$ -soliton is given by the balance of those two exponentials.

As explained in Section 4, the derangements $\pi \in \mathcal{S}_M$ are represented by the chord diagrams with the arrows above the line pointing from e_n to j_n for $n = 1, 2, \dots, N$, while arrows below the line point from g_m to i_m for $m = 1, 2, \dots, M - N$. Figure 5.8 illustrates the time evolution of an example of $(3, 3)$ -soliton solution. The chord diagram shows all asymptotic line-solitons for $y \rightarrow \pm\infty$.

Theorem 5.5 provides a unique parametrization of each TNN Grassmannian cell in terms of the derangement of S_M . This agrees with the result obtained by Postnikov et al in [38, 45]. One should, however, note that Theorem 5.5 does not give us the indices j_n and i_m in the $[e_n, j_n]$ and $[i_m, g_m]$ line-solitons. The specific conditions that an index pair $[i, j]$ identifies an asymptotic line-soliton are obtained by identifying the dominant exponential in each domain in the xy -plane. The example below illustrates how to apply Theorem 5.5, and identify all the asymptotic line-solitons for a given irreducible TNN A -matrix.

Example 5.6. Let us consider the 3×5 matrix,

$$A = \begin{pmatrix} 1 & 0 & -a & 0 & b \\ 0 & 1 & c & 0 & -d \\ 0 & 0 & 0 & 1 & e \end{pmatrix} \quad \text{with } ad - bc = 0,$$

where a, b, c, d and e are positive constants, that is, the A -matrix marks a point on $\text{Gr}^+(3, 5)$. Then the purpose is to find asymptotic line-solitons generated by the τ -function (3.10) associated with this A -matrix. From Proposition 5.3, one can see that the τ -function with this matrix will produce a $(3, 2)$ -soliton solution since $N = 3$ and $M = 5$. Moreover, the asymptotic line-solitons for this solution are labeled by $[1, j_1], [2, j_2]$ and $[4, j_3]$ for $y \gg 0$ for some $j_1 > 1, j_2 > 2$ and $j_3 > 4$. Similarly, the line-solitons for $y \ll 0$ are labeled by $[i_1, 3]$ and $[i_2, 5]$ for some $i_1 < 3$ and $i_2 < 5$. The basic idea to determine those indices j_1, j_2, j_3 and i_1, i_2 is to apply Proposition 5.3 and the dominant relations (5.4).

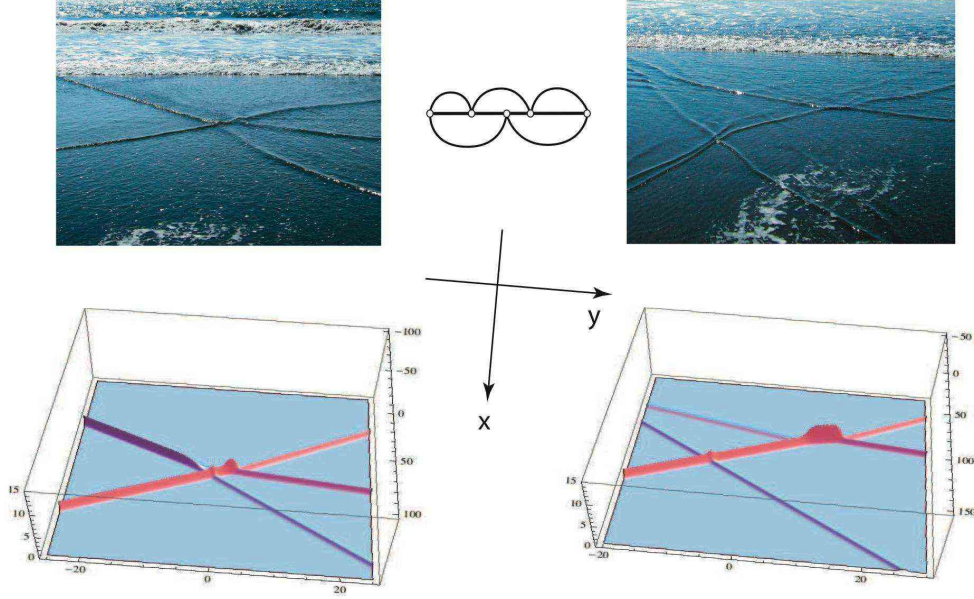


FIGURE 5.9. Example of shallow water waves. The upper photos are taken at a beach in Mexico. The lower figures show the evolution of the corresponding exact $(3, 2)$ -soliton solution of (24153) -type shown in the chord diagram (see Example 5.6): the left one at $t = 1.5$ and the right one at $t = 10$. (Photographs by courtesy of Mark J. Ablowitz.)

Let us first consider the case for $y \gg 0$. Starting with the last pivot $e_3 = 4$, it is immediate to find $j_3 = 5$, because of $j_3 > 4$ (just Proposition 5.3). We now take the next pivot $e_2 = 2$ and find the index j_2 . Since the index 5 is already taken as the pair index of $e_3 = 4$, we need to check only the cases $[2, 4]$ and $[2, 3]$. For the existence of $[2, 4]$ -soliton, the dominant relation (5.4) requires that both $\xi(1, 2, 5)$ and $\xi(1, 4, 5)$ are not zero. Calculating those minors for our A -matrix, we have

$$\xi(1, 2, 5) = e \neq 0, \quad \xi(1, 4, 5) = d \neq 0,$$

and hence $[2, 4]$ -soliton exists. Now we consider the case with $e_1 = 1$, that is, we have only $[1, 2]$ and $[1, 3]$ possibility. In the case of $[1, 3]$, we use again the dominant relation (5.4), and check the minors $\xi(1, 4, 5)$ and $\xi(3, 4, 5)$ which corresponds to the dominant exponentials. We then find $\xi(1, 4, 5) = d \neq 0$ but $\xi(3, 4, 5) = bc - ad = 0$. This implies that $[1, 3]$ -soliton is impossible for $y \gg 0$. So the last one is $[1, 2]$ -type, which can be confirmed by the condition $\xi(1, 4, 5) = d \neq 0$ and $\xi(2, 4, 5) = b \neq 0$.

Now we consider the case for $y \ll 0$. Theorem 5.5 tells us that for the non-pivot index $g_1 = 3$, only the pair $[1, 3]$ is possible (the index 2 is already taken because $[1, 2]$ -soliton exists, i.e. $\pi(1) = 2$). Then the final soliton must be $[3, 5]$ -type from the non-pivot index $g_2 = 5$. The last one can be confirmed by the least condition in (5.4) with $\xi(2, 3, 4) = a \neq 0$ and $\xi(2, 4, 5) = b \neq 0$.

Thus we have a $(2, 3)$ -soliton solution of $\pi = (24153)$ -type for the τ -function (3.10) with the A -matrix considered. The photos in Figure 5.9 show some interacting shallow water waves, which we think a realization of this example. We demonstrate an exact solution whose parameters are given by $(k_1, k_2, \dots, k_5) = (-2, -1, 0, 0.5, 2)$ and the A -matrix with $(a, b, c, d, e) = (1, 2, 1, 2, 1)$.

6. $(2, 2)$ -SOLITON SOLUTIONS

Here we give a summary of all soliton solutions of the KP equation generated by the 2×4 irreducible, TNN A -matrices. Proposition 5.3 implies that each of the soliton solutions consists of

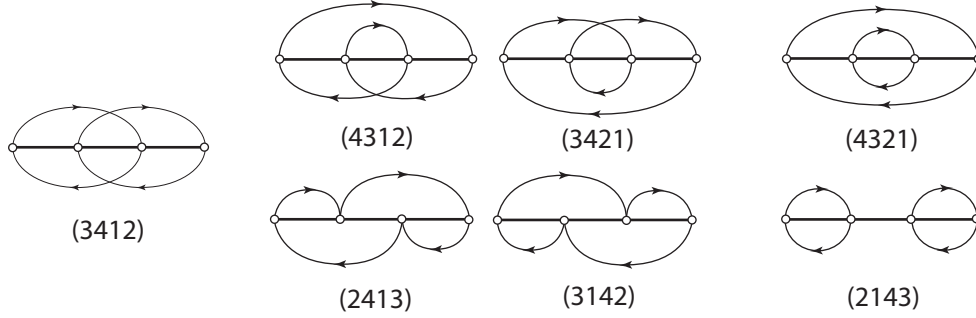


FIGURE 6.1. The chord diagrams for seven different types of $(2, 2)$ -soliton solutions. Each diagram corresponds to a totally non-negative Grassmannian cell in $\text{Gr}(2, 4)$.

two asymptotic line-solitons as $y \rightarrow \pm\infty$. That is, they are $(2, 2)$ -soliton solutions. We outline below the classification scheme for the $(2, 2)$ -soliton solutions, and discuss some of the exact solutions in details for the applications discussed in the following sections. First note that for 2×4 matrices, there are only two types given by

$$\begin{pmatrix} 1 & 0 & -c & -d \\ 0 & 1 & a & b \end{pmatrix} \quad \text{and} \quad \begin{pmatrix} 1 & a & 0 & -c \\ 0 & 0 & 1 & b \end{pmatrix},$$

The fact that A is TNN implies that the constants a, b, c and d must be non-negative. For the first type, one can easily see that $ad = 0$ is impossible because then either $\xi(3, 4) < 0$ or A is not irreducible. Then there are 5 possible cases with $ad \neq 0$, namely,

$$(1) \quad ad - bc > 0, \quad (2) \quad ad - bc = 0, \quad (3) \quad b = 0, c \neq 0, \\ (4) \quad c = 0, b \neq 0, \quad (5) \quad b = c = 0.$$

For the second type, $ab \neq 0$ due to irreducibility. Hence, we have only two cases:

$$(6) \quad c \neq 0, \quad (7) \quad c = 0.$$

Thus we have total seven different types of A -matrices, and using Theorem 5.5, we can show that each A -matrix gives a different $(2, 2)$ -soliton solution which can be enumerated according to the seven derangements of the index set $[4] = \{1, 2, 3, 4\}$ with two excedances. Namely, for those cases from (1) to (7) we have

$$(1) \quad \pi = (3412), \quad (2) \quad \pi = (2413), \quad (3) \quad \pi = (4312), \quad (4) \quad \pi = (3421), \\ (5) \quad \pi = (4321), \quad (6) \quad \pi = (3142), \quad (7) \quad \pi = (2143).$$

In Figure 6.1, we show the chord diagrams for all those seven cases. One should note that any derangement of \mathcal{S}_4 with exactly two excedances should be one of the graphs. This uniqueness in the general case has been used to count the number of totally non-negative Grassmann cells [38, 45].

Let us now summarize the results for all those seven cases of the $(2, 2)$ -soliton solutions:

- (1) $\pi = (3412)$: This case corresponds to the *T-type* 2-soliton solution which was first obtained as the solution of the *Toda* lattice hierarchy [4]. This is why we call it “T-type” (see also [22]). The asymptotic line-solitons are $[1, 3]$ - and $[2, 4]$ -types for $|y| \rightarrow \infty$. The A -matrix is given by

$$A = \begin{pmatrix} 1 & 0 & -c & -d \\ 0 & 1 & a & b \end{pmatrix},$$

where $a, b, c, d > 0$ are free parameters with $ad - bc > 0$. This is the generic solution on the maximum dimensional cell of $\text{Gr}^+(2, 4)$, and the corresponding line-soliton has the most complicated pattern due to the fully resonant interactions among all line-solitons.

- (2) $\pi = (2413)$: The asymptotic line-solitons are given by $[1, 2]$ - and $[2, 4]$ -solitons for $y \gg 0$, and $[1, 3]$ - and $[3, 4]$ -solitons for $y \ll 0$. The A -matrix is given by

$$A = \begin{pmatrix} 1 & 0 & -c & -d \\ 0 & 1 & a & b \end{pmatrix},$$

where $a, b, c, d > 0$ with $\xi(3, 4) = ad - bc = 0$. Note the change of the solution structure by imposing just one constraint $\xi(3, 4) = 0$ to the previous case (1).

- (3) $\pi = (4312)$: The asymptotic line-solitons for this case are $[1, 4]$ - and $[2, 3]$ -solitons for $y \gg 0$, and $[1, 3]$ - and $[2, 4]$ -solitons for $y \ll 0$. The A -matrix is given by

$$A = \begin{pmatrix} 1 & 0 & -b & -c \\ 0 & 1 & a & 0 \end{pmatrix},$$

where $a, b, c > 0$ are free parameters. Notice that two line-solitons for $y \ll 0$ are the same as in the T-type solution (see the crossing in the lower chords in Figure 6.1).

- (4) $\pi = (3421)$: The asymptotic line-solitons are given by $[1, 3]$ and $[2, 4]$ for $y \gg 0$, and for $y \ll 0$, these are the $[1, 4]$ - and $[2, 3]$ -solitons. The A -matrix is given by

$$A = \begin{pmatrix} 1 & 0 & 0 & -c \\ 0 & 1 & a & b \end{pmatrix},$$

where $a, b, c > 0$ are positive free parameters. This solution can be considered as a dual of the previous case (3), that is, two sets of line-solitons for $y \gg 0$ and $y \ll 0$ are exchanged (also notice the duality in the chord diagrams in Figure 6.1). The example discussed after Proposition 5.3 corresponds to this solution (see Figure 5.6).

- (5) $\pi = (4321)$: The solution in this case is called the *P-type* 2-soliton solution which has asymptotic line-solitons of $[1, 4]$ - and $[2, 3]$ -types as $|y| \rightarrow \infty$. This type of solutions fits better with the *physical* assumption of quasi-two dimensionality with weak y -dependence underlying the derivation of the KP equation. This is why we call it “P-type” (see [22]). The A -matrix is given by

$$A = \begin{pmatrix} 1 & 0 & 0 & -b \\ 0 & 1 & a & 0 \end{pmatrix}.$$

The chord diagram indicates that those two line-solitons must have the different amplitudes, i.e. $A[1, 4] > A[2, 3]$, but they can propagate in the same direction, which correspond to the two soliton solution of the KdV equation.

- (6) $\pi = (3142)$: The asymptotic line-solitons are given by $[1, 3]$ - and $[3, 4]$ -solitons for $y \gg 0$, and $[1, 2]$ - and $[2, 4]$ -solitons for $y \ll 0$. The A -matrix is given by

$$A = \begin{pmatrix} 1 & a & 0 & -c \\ 0 & 0 & 1 & b \end{pmatrix},$$

where $a, b, c > 0$. This solution is dual to the case (2) in the sense that the two sets of asymptotic line-solitons for $y \gg 0$ and $y \ll 0$ are switched, as well as the missing minors are switched by $\xi(3, 4) \leftrightarrow \xi(1, 2)$. Also note the duality between the corresponding chord diagrams.

- (7) $\pi = (2143)$: This case is called the *O-type* 2-soliton solution. The asymptotic line-solitons are of $[1, 2]$ - and $[3, 4]$ -types as $|y| \rightarrow \infty$. The letter “O” for this type is due to the fact that this solution was *originally* found to describe the two-soliton solution of the KP equation (see for example [14]). The A -matrix for the O-type 2-soliton solution is given by

$$A = \begin{pmatrix} 1 & a & 0 & 0 \\ 0 & 0 & 1 & b \end{pmatrix}.$$

Notice that this A -matrix is obtained as a limit $c \rightarrow 0$ in the previous one of the case (6), i.e. (3142)-soliton solution.

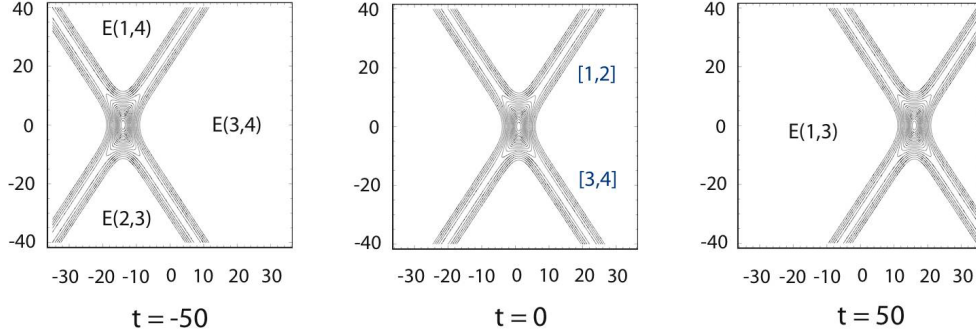


FIGURE 6.2. The time evolution of an O-type soliton solution. Each $E(i, j)$ indicates the dominant exponential in that region. The parameters are chosen as $A_{[1,2]} = A_{[3,4]} = 0.1$ and $\Psi_{[3,4]} = -\Psi_{[1,2]} = 30^\circ$.

Now let us describe the details of some of the (2, 2)-soliton solutions, which will be important for an application of those solutions to shallow water problem discussed in the next Section. In particular, we explain how the A -matrix uniquely determines the structure of the corresponding soliton solution such as the location of the solitons and their phase shifts.

6.1. O-type soliton solutions. This is the original two-soliton solution, and the solutions correspond to the chord diagram of $\pi = (2143)$. A solution of this type consists of two full line-solitons of $[1, 2]$ and $[3, 4]$ (see Figure 6.2). Note here that they have phase shifts due to their collision. Let us describe explicitly the structure of the solution of this type: The τ -function defined in (5.1) for this case is given by

$$\tau = E(1, 3) + bE(1, 4) + aE(2, 3) + abE(2, 4),$$

where $a, b > 0$ are the free parameters given in the A -matrix listed above. As we will show that those two parameters can be used to fix the locations of those solitons, that is, they are determined by the asymptotic data of the solution for large $|y|$.

For the later application of the solution, we assume that $[1, 2]$ -soliton has a “negative” y -component in the wave-vector (i.e. $\tan \Psi_{[1,2]} < 0$), and $[3, 4]$ -soliton has a “positive” y -component, (i.e. $\tan \Psi_{[3,4]} > 0$, see Figure 3.1). Then for the region with large positive x , we have $[1, 2]$ -soliton in $y > 0$ and $[3, 4]$ -soliton in $y < 0$.

For $[1, 2]$ -soliton in $x > 0$ (and $y \gg 0$), we have the dominant balance between $E(1, 4)$ and $E(2, 4)$. Then the τ -function can be written in the following form,

$$\begin{aligned} \tau &\approx bE(1, 4) + abE(2, 4) \\ &= 2be^{\theta_4 + \frac{1}{2}(\theta_1 + \theta_2)} \cosh \frac{1}{2} (\theta_1 - \theta_2 + \theta_{12}^+) , \end{aligned}$$

which leads to the $[1, 2]$ -soliton solution in the region near $\theta_1 \approx \theta_2$ for $x \gg 0$,

$$u = 2\partial_x^2 \ln \tau \approx \frac{1}{2}(k_2 - k_1)^2 \operatorname{sech}^2 \frac{1}{2} (\theta_1 - \theta_2 + \theta_{12}^+) .$$

Here the shift θ_{12}^+ (+ indicates $x > 0$) is related to the parameter a in the A -matrix (see below).

For $[3, 4]$ -soliton in $x > 0$ (and $y \ll 0$), from the balance $\tau \approx aE(2, 3) + abE(2, 4)$, we have

$$u \approx \frac{1}{2}(k_4 - k_3)^2 \operatorname{sech}^2 \frac{1}{2} (\theta_3 - \theta_4 + \theta_{34}^+) .$$

The shifts θ_{12}^+ and θ_{34}^+ are related to the parameters in the A -matrix,

$$(6.1) \quad a = \frac{k_4 - k_1}{k_4 - k_2} e^{-\theta_{12}^+}, \quad b = \frac{k_3 - k_2}{k_4 - k_2} e^{-\theta_{34}^+} .$$

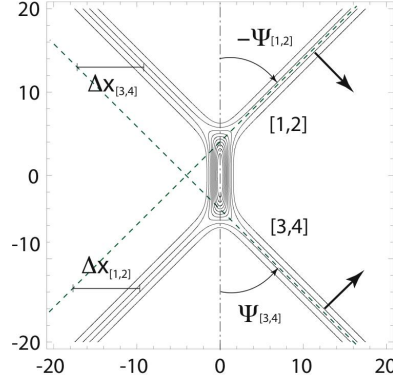


FIGURE 6.3. O-type interaction for two equal amplitude solitons. The parameters k_i 's are taken to be $(k_1, k_2, k_3, k_4) = (-1 - 10^{-4}, -10^{-4}, 10^{-4}, 1 + 10^{-4})$, which give $A_{[1,2]} = A_{[3,4]} = \frac{1}{2}$ and $\tan \Psi_{[3,4]} = -\tan \Psi_{[1,2]} = 1 + 2 \times 10^{-4}$ (i.e. $\Psi_{[3,4]} \approx 45.0057^\circ$). The constants a, b in the A -matrix are chosen so that the center of interaction point is located at the origin, and $u_{\max} = u(0, 0, 0) \approx 1.96$ and the phase shift $\Delta x_{[1,2]} = \Delta_{[3,4]} \approx 7.8$.

Thus the parameters in the A -matrix can be determined by the asymptotic data of the locations of those $[1, 2]$ - and $[3, 4]$ -solitons for $x \gg 0$ and $|y| \gg 0$.

The most important feature of the O-type solution is the phase shift due to the interaction of those two oblique line-solitons. The phase shift for $[i, j]$ -soliton is defined by $\theta_{ij} = \theta_{ij}^- - \theta_{ij}^+$ where \pm indicate the values for $x \rightarrow \pm\infty$. The values θ_{12} and θ_{34} turn out to be the same (see for example [16]),

$$\theta_{12} = \theta_{34} = -\ln \Delta_{\text{O}}.$$

where we note

$$\Delta_{\text{O}} := \frac{(k_3 - k_2)(k_4 - k_1)}{(k_4 - k_2)(k_3 - k_1)} = 1 - \frac{(k_2 - k_1)(k_4 - k_3)}{(k_4 - k_2)(k_3 - k_1)} < 1.$$

This implies that $\theta_{12} = \theta_{34} > 0$, and each $[i, j]$ -soliton shifts in x with

$$(6.2) \quad \Delta x_{[i,j]} = \frac{1}{k_j - k_i} \theta_{ij}.$$

The positive phase shifts $\Delta x_{[1,2]} > 0$ and $\Delta x_{[3,4]} > 0$ indicate an *attractive* force in the interaction. Figure 6.3 illustrates an O-type interaction of two solitons which have the same amplitude, $A_{[1,2]} = A_{[3,4]} = \frac{1}{2}$, and are symmetric with respect to the y -axis, $\Psi_{[3,4]} = -\Psi_{[1,2]} \approx 45^\circ$. Since the solution is close to the resonance, we have the large phase shifts $\Delta x_{[1,2]} = \Delta x_{[3,4]} \approx 7.8$ and the maximum value of the soliton $u_{\max} \approx 1.96$ (almost four times larger than $A_{[1,2]}$).

O-type soliton solution has a steady X-shape with phase shifts in both line-solitons. One can also find the formula of the maximum amplitude which occurs at the center of intersection point (center of the X-shape), which is given by

$$(6.3) \quad u_{\max} = A_{[1,2]} + A_{[3,4]} + 2 \frac{1 - \sqrt{\Delta_{\text{O}}}}{1 + \sqrt{\Delta_{\text{O}}}} \sqrt{A_{[1,2]} A_{[3,4]}}.$$

(see for example [8, 12, 42].) Since $0 < \Delta_{\text{O}} < 1$, we have the bound

$$A_{[1,2]} + A_{[3,4]} < u_{\max} < \left(\sqrt{A_{[1,2]}} + \sqrt{A_{[3,4]}} \right)^2.$$

It is also interesting to note that the formula Δ_{O} has critical cases at the values $k_1 = k_2$ or $k_2 = k_3$ or $k_3 = k_4$. For the case with $k_1 = k_2$ or $k_3 = k_4$ (i.e. $\Delta_{\text{O}} = 1$), one can see that one of the line-soliton becomes small, and the limit consists of just one-soliton solution. On the other hand, for

the case $k_2 = k_3$ (i.e. $\Delta_O = 0$), the τ -function has only three terms, which corresponds to a solution showing a Y-shape interaction (i.e. the phase shift becomes infinity and the middle portion of the interaction stretches to infinity). This limit has been discussed in [28, 32] as a resonant interaction of three waves to make Y-shape soliton. This limit gives a critical angle between those solitons which can be found as follows: First let us express each k_j parameter in terms of the amplitude and the slope,

$$\begin{aligned} k_{1,2} &= \frac{1}{2} \left(\tan \Psi_{[1,2]} \mp \sqrt{2A_{[1,2]}} \right), \\ k_{3,4} &= \frac{1}{2} \left(\tan \Psi_{[3,4]} \mp \sqrt{2A_{[3,4]}} \right), \end{aligned}$$

where the angle $\Psi_{[i,j]}$ is measured in the counterclockwise direction from the y -axis (see Figure 6.3). In particular, we have

$$\tan \Psi_{[1,2]} = -\sqrt{2A_{[1,2]}} + 2k_2, \quad \tan \Psi_{[3,4]} = \sqrt{2A_{[3,4]}} + 2k_3.$$

For simplicity, let us consider the special case when both solitons are of equal amplitude and symmetric with respect to the y -axis i.e., $A_{[1,2]} = A_{[3,4]} = A_0$ and $\Psi_{[3,4]} = -\Psi_{[1,2]} = \Psi_0 > 0$. This corresponds to setting $k_1 = -k_4$ and $k_2 = -k_3$. Then, for fixed amplitude A_0 , the angle Ψ_0 has a lower bound given by

$$\tan \Psi_0 = \sqrt{2A_0} + 2k_3 \geq \sqrt{2A_0} := \tan \Psi_c.$$

The lower bound is achieved in the limit $k_2 = k_3 = 0$, and the critical angle Ψ_c is given by

$$(6.4) \quad \Psi_c = \tan^{-1} \sqrt{2A_0}.$$

In [28], Miles introduced the following parameter to describe the interaction properties for O-type solution,

$$(6.5) \quad \kappa := \frac{\tan \Psi_0}{\sqrt{2A_0}} = \frac{\tan \Psi_0}{\tan \Psi_c}.$$

With this parameter, the maximum amplitude of (6.3) for this symmetric case is given by

$$(6.6) \quad u_{\max} = \frac{4A_0}{1 + \sqrt{\Delta_O}}, \quad \text{with } \Delta_O = 1 - \frac{1}{\kappa^2}.$$

Thus, at the critical angle $\Psi_0 = \Psi_c$ (i.e., $\kappa = 1$), we have $u_{\max} = 4A_0$ and the phase shift $\theta_{[12]} \rightarrow \infty$, leading to the resonant Y-shape interaction (see also [28, 12, 42]).

One should note that if we use the form of the O-type solution even beyond the critical angle, i.e. $k_3 < k_2$, then the solution becomes singular (note that the sign of $E(2, 3)$ changes). In earlier works, this was considered to be an obstacle for using the KP equation to describe an interaction of two line-solitons with a smaller angle. On the contrary, the KP equation should give a better approximation to describe oblique interactions of solitons with smaller angles. Thus one should expect to have explicit solutions of the KP equation describing such phenomena. It turns out that the new types of (2, 2)-soliton solutions discussed above can indeed serve as good models for describing line-soliton interactions of solitons with small angles. We will show in Section 8 how these solutions are related to the *Mach reflections* in shallow water waves.

6.2. (3142)-type soliton solutions. We consider a solution of this type which consists of two line-solitons for large positive x and two other line-solitons for large negative x . We then assume that the slopes of two solitons in each region have opposite signs, i.e. one in $y > 0$ and other in $y < 0$ (see Figure 6.4). The line-solitons for the (3142)-type solution are determined from the balance between two appropriate exponential terms in its τ -function which has the form,

$$\tau = E(1, 3) + bE(1, 4) + aE(2, 3) + abE(2, 4) + cE(3, 4).$$

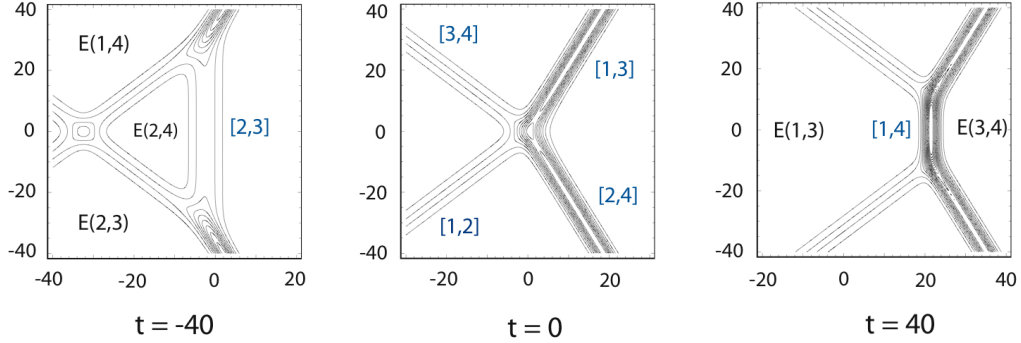


FIGURE 6.4. The time evolution of a (3142)-type soliton solution. The line-solitons have $A_{[1,3]} = A_{[2,4]} = 0.5$ and $\Psi_{[2,4]} = -\Psi_{[1,3]} = 25^\circ$. The critical angle is given by $\Psi_c = \tan^{-1} \sqrt{2A_0} = 45^\circ$, which also gives $\Psi_c = \Psi_{[3,4]} = -\Psi_{[1,2]}$. The parameters in the A -matrix are given by (6.9) with $\theta_{13}^+ = \theta_{24}^+ = 0$ and $s = 1$. The amplitude of the intermediate $[1, 4]$ -soliton approaches asymptotically to 1.075.

The solution contains three free parameters a, b and c , which can be used to determine the locations of three (out of four) asymptotic line-solitons (e.g. two in $x \gg 0$ and one in $x \ll 0$). Thus, the parameters are completely determined from the asymptotic data on large $|y|$.

Let us first consider the line-solitons in $x \gg 0$: There are two line-solitons which are $[1, 3]$ -soliton in $y \gg 0$ and $[2, 4]$ -soliton in $y \ll 0$. The $[1, 3]$ -soliton is obtained by the balance between the exponential terms $bE(1, 4)$ and $cE(3, 4)$, and the $[2, 4]$ -soliton is by the balance between $aE(2, 3)$ and $cE(3, 4)$. Consequently, the phase shifts of $[1, 3]$ - and $[2, 4]$ -solitons for $x \gg 0$ are given by

$$(6.7) \quad \theta_{13}^+ = \ln \frac{k_4 - k_1}{k_4 - k_3} + \ln \frac{b}{c}, \quad \theta_{24}^+ = \ln \frac{k_3 - k_2}{k_4 - k_3} + \ln \frac{a}{c}.$$

Now we consider the line-solitons in $x \ll 0$: They are $[3, 4]$ -soliton in $y \gg 0$ and $[1, 2]$ -soliton in $y \ll 0$. The phase shifts are given respectively by

$$\theta_{34}^- = \ln \frac{k_3 - k_1}{k_4 - k_1} - \ln b, \quad \theta_{12}^- = \ln \frac{k_3 - k_1}{k_3 - k_2} - \ln a$$

We then define the parameter s (representing the total phase shifts $\theta_{13}^+ + \theta_{34}^- = \theta_{24}^+ + \theta_{12}^-$),

$$(6.8) \quad s := \exp(-\theta_{13}^+ - \theta_{34}^-),$$

which leads to

$$(6.9) \quad a = \frac{k_3 - k_1}{k_3 - k_2} s e^{\theta_{24}^+}, \quad b = \frac{k_3 - k_1}{k_4 - k_1} s e^{\theta_{13}^+}, \quad c = \frac{k_3 - k_1}{k_4 - k_3} s.$$

The s -parameter represents the relative locations of the intersection point of the $[1, 3]$ - and $[3, 4]$ -solitons with the x -axis, in particular, $\theta_{13}^+ + \theta_{34}^- = 0$ when $s = 1$ (see Figure 6.5). Thus the parameters a, b and c are related to the locations of $[1, 3]$ -soliton (with θ_{13}^+), of $[2, 4]$ -soliton (with θ_{24}^+), and the intersection point of $[1, 3]$ - and $[3, 4]$ -solitons (with s).

Now we consider the case where the $[1, 3]$ - and $[2, 4]$ -solitons have the same amplitude ($A_{[1,3]} = A_{[2,4]} = A_0$) and they are symmetric with respect to the x -axis ($\Psi_{[2,4]} = -\Psi_{[1,3]} = \Psi_0$). Then in terms of the k -parameters, we have

$$k_3 - k_1 = k_4 - k_2 = \sqrt{2A_0}.$$

Also the symmetry of the wave-vectors, i.e. $\Psi_{[2,4]} = \Psi_0 = -\Psi_{[1,3]}$, gives

$$k_2 + k_4 = -(k_1 + k_3) = \tan \Psi_0.$$

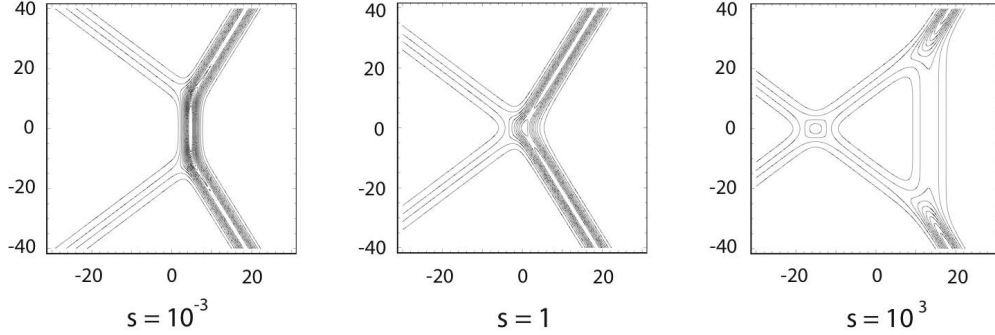


FIGURE 6.5. (3142)-type soliton solution with the s -parameter. The line-solitons are given by $A_{[1,3]} = A_{[2,4]} = 0.5$ and $\Psi_{[2,4]} = -\Psi_{[1,3]} = 25^\circ$ (these then gives the other two solitons uniquely). The parameters in the A -matrix are chosen as (6.9) with $\theta_{[1,3]}^+ = \theta_{[2,4]}^+ = 0$. Then at $s = 1$, all the solitons meet at the origin, i.e. the s -parameter shifts $[1, 2]$ - and $[3, 4]$ -solitons.

This implies that we have

$$(6.10) \quad k_4 = -k_1 > 0, \quad k_3 = -k_2 > 0.$$

The angle Ψ_0 takes the value in $(0, \Psi_c)$, where the critical angle is given by the condition $k_2 = k_3 = 0$, i.e.

$$\Psi_c = \tan^{-1} \sqrt{2A_0}.$$

Notice that this formula is the same as that of the O-type soliton solution (see (6.4)), and the (3142)-type exists when the κ -parameter is less than one, i.e. for (3142)-type, we have

$$\kappa = \frac{\tan \Psi_0}{\sqrt{2A_0}} < 1.$$

From (6.10), one can easily deduce the following facts for $[1, 2]$ - and $[3, 4]$ -solitons in $x < 0$:

- (a) Those solitons have the same amplitude, i.e.

$$A_{[1,2]} = A_{[3,4]} = \frac{1}{2}(k_4 - k_3)^2 = \frac{1}{2}(k_4 + k_2)^2 = \frac{1}{2} \tan^2 \Psi_0 = \kappa^2 A_0.$$

Thus, if the $[1, 3]$ - and $[2, 4]$ -solitons in $x > 0$ are close to the y -axis (i.e. a small Ψ_0), then the amplitudes of the solitons in $x < 0$ are small; whereas at the critical angle $\Psi_0 = \Psi_c$, the solitons $[1, 2]$ and $[3, 4]$ in $x < 0$ take the maximum amplitude $A_{[1,2]} = A_{[3,4]} = A_0$.

- (b) The directions of the wave-vectors for the $[1, 2]$ and $[3, 4]$ -solitons are also symmetric, i.e.

$$\tan \Psi_{[3,4]} = -\tan \Psi_{[1,2]} = k_3 + k_4.$$

Moreover, the symmetry (6.10) implies that $\tan \Psi_{[3,4]} = k_4 - k_2 = \sqrt{2A_{[2,4]}} = \sqrt{2A_0}$, so

$$\Psi_{[3,4]} = \Psi_c = \tan^{-1} \sqrt{2A_0}.$$

Thus the directions of the wave-vectors for the $[1, 2]$ and $[3, 4]$ -solitons in $x < 0$ depend only on the amplitude of the solitons in $x > 0$ but not on their directions (i.e., angle of their V-shape).

Let us choose the parameters in the A -matrix for the (3142)-soliton solution appropriately, so that at $t = 0$ all the solitons intersect at the origin (see Figure 6.4). Then for $t < 0$, the resonant interaction between $[1, 3]$ - and $[3, 4]$ -solitons (as well as $[2, 4]$ - and $[1, 2]$ -solitons) generates an intermediate line-soliton (called ‘‘stem’’ soliton) which is $[1, 4]$ soliton. The amplitude of this soliton is

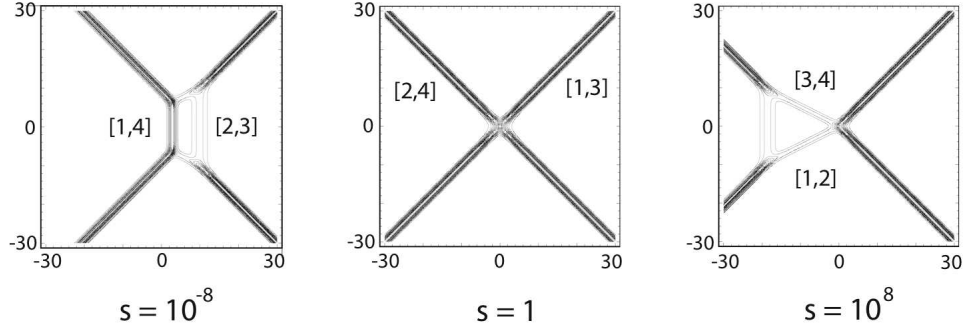


FIGURE 6.6. T-type interaction with the s -parameter. The k -parameters are chosen as $(k_1, k_2, k_3, k_4) = (-\frac{3}{2}, -\frac{1}{2}, \frac{1}{2}, \frac{3}{2})$. The A -matrix is chosen as (6.12) and (6.13) with $\theta_{13}^+ = \theta_{24}^+ = 0$ and $r = 1$. The s -parameter gives the phase shift for the $[1, 2]$ - and $[3, 4]$ -solitons in $x < 0$.

given by

$$(6.11) \quad A_{[1,4]} = \frac{1}{2}(k_4 - k_1)^2 = \frac{1}{2} \left(\sqrt{2A_0} + \tan \Psi_0 \right)^2 = A_0(1 + \kappa)^2.$$

Note here that at the critical angle $\Psi_0 = \Psi_c$, the amplitude takes the maximum $A_{[1,4]} = 4A_0$ (see [43, 37]).

For $t > 0$, the resonant interaction between $[1, 3]$ - and $[1, 2]$ -solitons (as well as $[2, 4]$ - and $[3, 4]$ -solitons) generates an intermediate line-soliton of $[2, 3]$ -soliton. The amplitude of $[2, 3]$ -soliton is given by

$$A_{[2,3]} = \frac{1}{2}(k_3 - k_2)^2 = \frac{1}{2} \left(\sqrt{2A_0} - \tan \Psi_0 \right)^2 = A_0(1 - \kappa)^2.$$

Because of the symmetry (6.10), both $[1, 4]$ - and $[2, 3]$ -solitons are parallel to the y -axis, i.e. $\tan \Psi_{[1,4]} = \tan \Psi_{[2,3]} = 0$.

6.3. T-type soliton solutions. There are four parameters in the A -matrix for T-type soliton solution. Here we explain that those parameters give the information of the locations of those line-solitons, the phase shift and on-set of the opening of a box. Thus three of those four parameters are determined by the asymptotic data on large $|y|$, and we need an internal data for the other one.

Following the arguments in the previous section, one can find the phase shifts of the line-solitons of $[1, 3]$ and $[2, 4]$: For $[1, 3]$ -soliton in $x > 0$ (and $y \gg 0$), the phase shift is calculated as

$$\theta_{13}^+ = \ln \frac{k_4 - k_1}{k_4 - k_3} - \ln \frac{D}{b},$$

where $D = ad - bc = \xi(3, 4)$. For the same soliton in $x < 0$ (and $y \ll 0$), we have

$$\theta_{13}^- = \ln \frac{k_2 - k_1}{k_3 - k_2} - \ln c.$$

So the total phase shift $\theta_{13} := \theta_{13}^- - \theta_{13}^+$ depends on the A -matrix unlike the cases of O- and P-types, and it can take any value.

For $[2, 4]$ -soliton in $x > 0$ (and $y \ll 0$), we have

$$\theta_{24}^+ = \ln \frac{k_3 - k_2}{k_4 - k_3} - \ln \frac{D}{c}$$

and for the same one in $x < 0$ (and $y \gg 0$), we have

$$\theta_{24}^- = \ln \frac{k_2 - k_1}{k_4 - k_1} - \ln b.$$

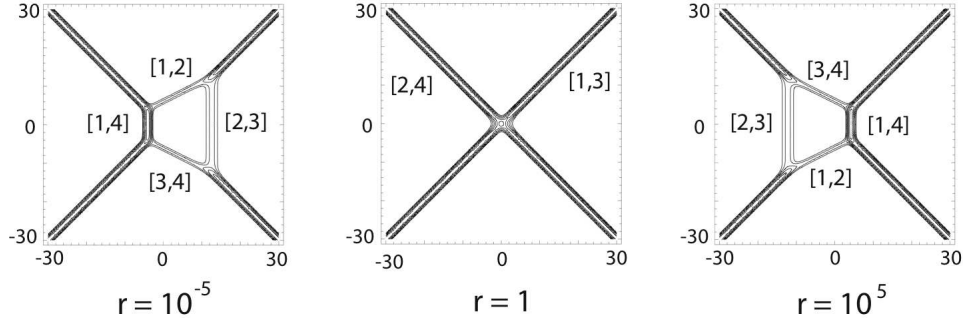


FIGURE 6.7. T-type interaction with the r -parameter. The k -parameters are the same as those in Figure 6.6. The A -matrix are chosen as (6.12) with $\theta_{13}^+ = \theta_{24}^+ = 0$ and $s = 1$. The r -parameter gives the on-set of the box, and it does not affect the locations of all four line-solitons, that is, r is an *internal* parameter.

Note that the total phase shift $\theta_{24} = \theta_{24}^+ - \theta_{24}^-$ is the same as that for $[1, 3]$ -soliton, i.e. the phase conservation along the y -axis $\theta_{13}^+ + \theta_{24}^- = \theta_{13}^- + \theta_{24}^+$ holds. Then as in (6.8) for the case of (3142)-type, we define the s -parameter,

$$s := \exp(-\theta_{13}^+ - \theta_{24}^-),$$

which represents the intersection point of $[1, 3]$ - and $[2, 4]$ -soliton. With the s -parameter, we have

$$(6.12) \quad b = \frac{k_2 - k_1}{k_4 - k_1} s e^{\theta_{13}^+}, \quad c = \frac{k_2 - k_1}{k_3 - k_2} s e^{\theta_{24}^+}, \quad D = \frac{k_2 - k_1}{k_4 - k_3} s.$$

Namely, the three parameters b, c and $D = ad - bc$ determine the locations and the phase shift (i.e. the intersection point of $[1, 3]$ - and $[2, 4]$ -solitons). One other parameter is then related to an on-set of a box at the intersection point (see Figure 6.7).

In order to characterize this parameter, let us consider the intermediate solitons of $[1, 4]$ and $[2, 3]$. First note that for $t \gg 0$, $[1, 4]$ -soliton appears as the dominant balance between $E(1, 2)$ and $E(2, 4)$. Then one can find the phase shift θ_{14}^+ (here $+$ indicates $t > 0$),

$$\theta_{14}^+ = \ln \frac{k_2 - k_1}{k_4 - k_2} - \ln d.$$

Similarly one can get the phase shift θ_{14}^- for $t \ll 0$ as

$$\theta_{14}^- = \ln \frac{k_3 - k_1}{k_4 - k_3} - \ln \frac{D}{a}.$$

Now consider the sum of θ_{14}^\pm , i.e.

$$\theta_{14}^+ + \theta_{14}^- = \ln \frac{(k_2 - k_1)(k_3 - k_1)}{(k_4 - k_2)(k_4 - k_3)} - \ln \frac{dD}{a}.$$

Also, for the $[2, 3]$ -soliton, one can get

$$\theta_{23}^+ + \theta_{23}^- = \ln \frac{(k_2 - k_1)(k_4 - k_2)}{(k_3 - k_1)(k_4 - k_3)} - \ln \frac{aD}{d}.$$

Now we introduce a parameter r in the form,

$$(6.13) \quad \frac{a}{d} = r \frac{k_4 - k_2}{k_3 - k_1},$$

so that we have

$$\theta_{14}^+ + \theta_{14}^- = \ln \frac{r}{s}, \quad \theta_{23}^+ + \theta_{23}^- = -\ln(rs).$$

Suppose that at $t = 0$, [1, 3]- and [2, 4]-solitons in $x > 0$ are placed so that they meet at the origin, that is, we choose $\theta_{13}^+ = \theta_{24}^+ = 0$. Also if there is no phase shifts for those solitons, i.e. $s = 1$. then the sums become

$$\theta_{14}^+ + \theta_{14}^- = \ln r = -(\theta_{23}^+ + \theta_{23}^-).$$

This implies that at $t = 0$ (and $s = 1$) if $r = 1$, then the T-type soliton solution has an exact shape of “X” without any opening of a box at the intersection point on the origin. Moreover, at $t = 0$ if $r > 1$, then [1, 4]-soliton appears in $x > 0$ and [2, 3]-soliton in $x < 0$; whereas if $0 < r < 1$, then [1, 4]-soliton appears in $x < 0$ and [2, 3]-soliton in $x > 0$. Figure 6.7 illustrates those cases with $s = 1$. The parameter r determines the exponential term that is dominant in the region inside the box. When $r < 1$, $E(2, 4)$ is the dominant exponential term, and when $r > 1$ the dominant exponential is $E(1, 3)$. One should note that the parameter r cannot be determined by the asymptotic data, that is, r is considered as an “internal” parameter.

7. NUMERICAL SIMULATION AND THE STABILITY OF THE SOLITON SOLUTIONS

In this section, we present some numerical simulations of the KP equation with “V-shape” initial wave form related to a physical situation (see for examples [37, 43, 15]). The main purpose of the numerical simulation is to study the interaction properties of line-solitons, and we will show that the solutions of the initial value problems with V-shape incident waves approach asymptotically to some of the exact soliton solutions of the KP equation discussed in the previous section. This implies a stability of those exact solutions under the influence of certain deformations (notice that the deformation in our cases are not so small).

The initial value problem considered here is essentially an infinite energy problem in the sense that each line-soliton in the initial wave is supported asymptotically in either $y \gg 0$ or $y \ll 0$, and the interactions occur only in a finite domain in the xy -plane. In the numerical scheme, we consider the rectangular domain $D = \{(x, y) : |x| \leq L_x, |y| \leq L_y\}$, and each line-soliton is matched with a KdV soliton at the boundaries $y = \pm L_y$. The details of the numerical scheme and the results can be found in [20].

We consider the initial data given in the shape of “V” with the amplitude A_0 and the oblique angle $\Psi_0 > 0$,

$$(7.1) \quad u(x, y, 0) = A_0 \operatorname{sech}^2 \sqrt{\frac{A_0}{2}} (x - |y| \tan \Psi_0).$$

Note here that two semi-infinite line-solitons are propagating toward each other into the positive x -direction, so that they interact strongly at the corner of the V-shape. At the boundaries $y = \pm L_y$ of the numerical domain, those line-solitons are patched to the KdV one-soliton solutions given by

$$u(x, \pm L_y, t) = A_0 \operatorname{sech}^2 \sqrt{\frac{A_0}{2}} (x \mp L_y \tan \Psi_0 - \nu t),$$

with $\nu = \frac{3}{4} \tan^2 \Psi_0 + \frac{1}{2} A_0$. Note here that these solitons correspond to the exact one-soliton solution of the KdV equation with the velocity shift due to the oblique propagation of the line-soliton, i.e. $\partial^2 u / \partial y^2 = \tan^2 \Psi_0 \partial^2 u / \partial x^2$. The numerical simulations are based on a spectral method with window-technique similar to the method used in [43] (see [20] for the details). The V-shape initial wave was first considered by Oikawa and Tsuji (see for example [37, 43]) in order to study the generation of freak (or rogue) waves. They noticed generations of different types of asymptotic solutions depending on the initial oblique angle Ψ_0 , and found the resonant interactions which create localized high amplitude waves. In this section, we present the results for the cases corresponding to $A_0 = 2$ and two different angles, Ψ_1 and Ψ_2 with $\Psi_1 < \Psi_c < \Psi_2$. where the critical angle is given by $\Psi_c = \tan^{-1} \sqrt{2A_0} \approx 63.4^\circ$. Then we explain these results in terms of certain (2, 2)-soliton solutions discussed in the previous section, and in particular, we describe the connection with the Mach reflection (this will be further discussed in Section 8).

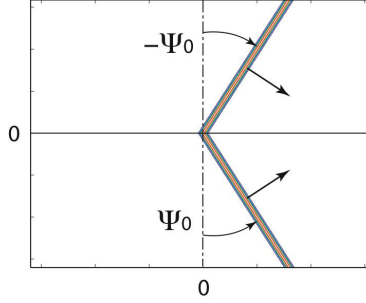


FIGURE 7.1. Initial data with V-shape wave. Each line of the V-shape is locally a line-soliton solution. We set those line-solitons to meet at the origin.

The main idea here is to consider the V-shape initial wave as the part of some $(2, 2)$ -soliton solutions listed in the previous section. In order to identify those soliton solutions from the V-shape initial wave form, let us first denote them as $[i_1, j_1]$ -soliton for $y \gg 0$ and $[i_2, j_2]$ -soliton for $y \ll 0$. Then using the relations, $k_j - k_i = \sqrt{2A_0} = 2$ and $k_j + k_i = \tan \Psi_0$, for $[i, j]$ -soliton and the Miles parameter $\kappa = \tan \Psi_0 / \sqrt{2A_0}$ of (6.5), we have

$$(7.2) \quad \begin{cases} k_{i_1} = -(1 + \kappa), & k_{j_1} = 1 - \kappa, \\ k_{i_2} = -(1 - \kappa), & k_{j_2} = 1 + \kappa. \end{cases}$$

Notice that $k_{j_2} = -k_{i_1}$ and $k_{i_2} = -k_{j_1}$ because of the symmetry in the initial wave. Moreover, at the critical angle $\Psi_0 = \Psi_c$ (i.e. $\kappa = 1$), we have $k_{i_2} = k_{j_1} = 0$. We also note k_{i_1} as the smallest parameter and k_{j_2} as the largest one, so that depending on the angle Ψ_0 , we obtain the following ordering in the k -parameters:

For $0 < \Psi_0 < \Psi_c$ (i.e. $\kappa < 1$), we have

$$k_{i_1} < k_{i_2} < 0 < k_{j_1} < k_{j_2},$$

implying that the corresponding chords of the $[i_1, j_1]$ - and the $[i_2, j_2]$ -solitons overlap. That is, $[1, 3]$ chord appears on the upper side of the diagram, and $[2, 4]$ chord on the lower side. This means that the two solitons can be identified as part of either the (3412) -type (T-type) or the (3142) -type solution (see the chord diagrams in Figure 6.1).

For $\Psi_c < \Psi_0 < \frac{\pi}{2}$ (i.e. $\kappa > 1$), we have

$$k_{i_1} < k_{j_1} < 0 < k_{i_2} < k_{j_2}.$$

In this case, the corresponding chords are separated, and the two solitons form part of either (2413) - or (2143) -type (O-type) solution. Here $[1, 2]$ - and $[3, 4]$ -chords appear on the upper and lower sides of the chord diagram, respectively.

Then the numerical simulations show that we have the following types of the asymptotic solutions depending on the values Ψ_0 :

- (a) If the angle satisfies $\Psi_0 < \Psi_c$ (i.e. $\kappa < 1$), then the solution converges asymptotically to (3142) -type soliton solution (not T-type)
- (b) If the angle satisfies $\Psi_c < \Psi_0$ (i.e. $\kappa > 1$), then the solution converges asymptotically to an O-type soliton solution (not (2413) -type).

The convergence here is in a locally defined L^2 -sense with the usual norm,

$$\|f\|_{L^2(D)} := \left(\iint_D |f(x, y)|^2 dx dy \right)^{\frac{1}{2}}.$$

where $D \subset \mathbb{R}^2$ is a compact set which covers the main structure of the interactions in the solution. To confirm the convergence statements, we define the (relative) error function,

$$(7.3) \quad E(t) := \|u^t - u_{\text{exact}}^t\|_{L^2(D_r^t)}^2 / \|u_{\text{exact}}^t\|_{L^2(D_r^t)}^2,$$

with the solution $u^t(x, y) := u(x, y, t)$ and an exact solution $u_{\text{exact}}^t(x, y)$, where D_r^t is the circular disc given by

$$D_r^t := \{(x, y) \in \mathbb{R}^2 : (x - x_0(t))^2 + (y - y_0(t))^2 \leq r^2\}.$$

The center $(x_0(t), y_0(t))$ of the circular domain D_r^t is chosen as the intersection point of two lines determined from the corresponding exact solution. We find the exact solution $u_{\text{exact}}^t(x, y)$ by minimizing $E(t)$ at certain large time $t = T_0$: In the minimization process, we assume that the k -parameters remain the same as those given by (7.2), and vary the corresponding A -matrix to adjust the solution pattern (recall that the A -matrix determines the locations of the line-solitons in the solution, see Section 5). After minimizing $E(t)$, that is, finding the corresponding exact solution, we check that $E(t)$ further decreases for a larger time $t > T_0$ up to a time $t = T_1 > T_0$, just before the effects of the boundary enter the disc D_r^t (those effects include the periodic condition in x and a mismatch on the boundary patching). We take the radius r in D_r^t large enough so that the main interaction area is covered for all $t < T_0$, but D_r^t should be kept away from the boundary to avoid any influence coming from the boundaries. The time $T_1 > T_0$ gives an optimal time to develop a pattern close to the corresponding exact solution, but it is also limited to avoid any disturbance from the boundaries for $t < T_1$. Thus, our convergence implies the separation of the radiations from the soliton solution, just like the case of the KdV equation (see the end of Section 3).

We also note that the convergence here implies a *completion* of the partial chord diagram consisting of only two chords which corresponds to the semi-infinite solitons in the initial V-shape wave. Namely, the asymptotic solution of the initial value problem with V-shape initial wave is given by an exact solution parametrized by a unique chord diagram, and the initial (partial) chord diagram is completed by adding two other solitons (chords) generated by the interaction. The completion may not be unique, and in [23], we proposed a concept of *minimal* completion in the sense that the completed diagram has the minimum total length of the chords and the corresponding TNN Grassmannian cell has the minimum dimension. However, this problem is still open, and we need to make a precise statement of the minimal completion of partial chord diagram given by the initial wave profile.

7.1. Regular reflection: $\kappa > 1$. We consider the V-shape initial wave with $A_0 = 2$ and $\tan \Psi_0 = \frac{12}{5}$, ($\Psi_0 \approx 67.3^\circ$) which gives $\kappa = 1.2$. Here the critical angle is $\Psi_c = \tan^{-1}(2) \approx 63.4^\circ$, and we expect asymptotically an O-type soliton solution. The corresponding k -parameters are obtained from (7.2), i.e.

$$(k_1, k_2, k_3, k_4) = \left(-\frac{11}{5}, -\frac{1}{5}, \frac{1}{5}, \frac{11}{5}\right).$$

Figure 7.2 illustrates the result of the numerical simulation. The top figures show the direct simulation of the KP equation. The wake behind the interaction point has a large negative amplitude, and it disperses and decays in the negative x -direction. This shows a separation of the radiations from the exact solution similar to the case of KdV soliton. The steady pattern left after shedding the radiations can be identified as an O-type solution. The middle figures show the corresponding O-type exact solution whose A -matrix is determined by minimizing the error function $E(t)$ at $t = 6$,

$$A = \begin{pmatrix} 1 & 1.91 & 0 & 0 \\ 0 & 0 & 1 & 0.17 \end{pmatrix}$$

Using (6.1), we obtain the shift of the initial line-solitons,

$$x_{[1,2]} = x_{[3,4]} = -0.020.$$

(Note here that because of the symmetric profile, the shifts for initial solitons are the same.) The negative shifts imply the slow-down of the incidence waves due to the generation of the solitons

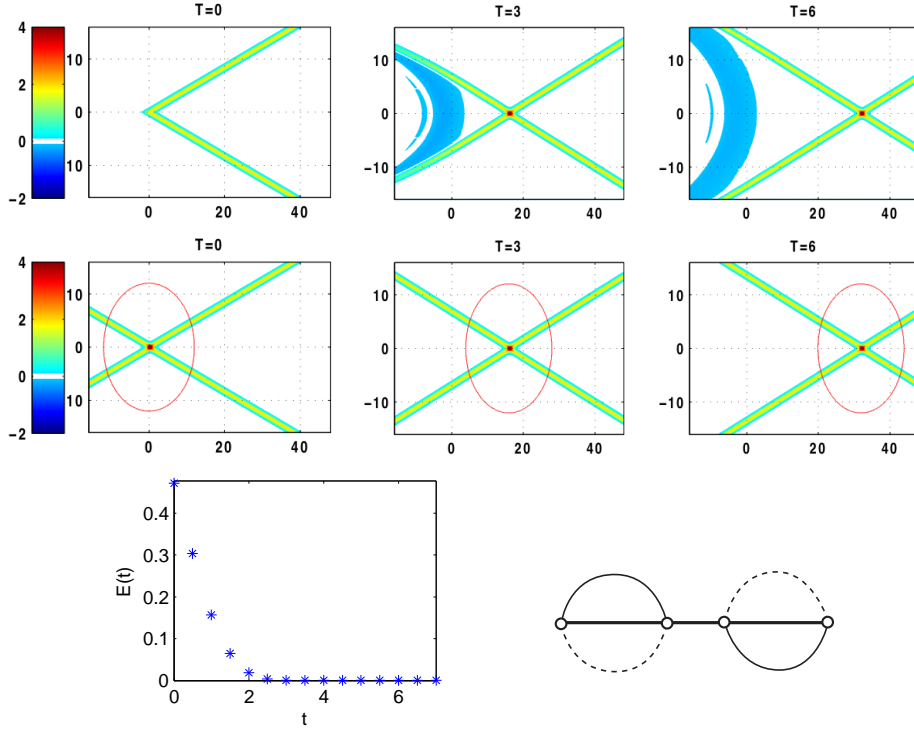


FIGURE 7.2. Numerical simulation of V-shape initial wave for $\kappa > 1$ (regular reflection). The initial wave consists of $[1, 2]$ -soliton in $y > 0$ and $[3, 4]$ -soliton in $y < 0$, with $A_{[1,2]} = A_{[3,4]} = 2$ and $\Psi_0 \approx 67.3^\circ$ ($\Psi_c = 63.4^\circ$). The upper figures show the result of the direct simulation. Notice a large wake behind the interaction point which extends the initial solitons. The middle figures show the corresponding exact solution of O-type. The circle in these figures show the domain D_r^t with $r = 12$. About $t = 3$, the wakes seem to be out of the domain. The bottom graph shows the error function $E(t)$ which is minimized at $t = 6$. The solid chords in the diagram indicates the incident solitons, and the dotted ones show the reflected solitons (i.e. a completion of the chord diagram [23]).

extending the initial solitons in the negative x -direction. The phase shifts $\Delta x_{[i,j]}$ for the O-type exact solution are calculated from (6.2), and they are

$$\Delta x_{[1,2]} = \Delta x_{[3,4]} = 0.593.$$

The positivity of the phase shifts is due to the attractive force between the line-solitons, and this explains the slow-down of the initial solitons, i.e. the small negative shifts of $x_{[i,j]}$. The bottom graph in Figure 7.2 shows $E(t)$ of (7.3), where we take $r = 12$ for the domain D_r^t . One can see a rapid convergence of the solution to the O-type exact solution with those parameters. One should however remark that when Ψ_0 is close to the critical one, i.e. $k_2 \approx k_3$, there exists a large phase shift in the soliton solution, and the convergence is very slow. Note that in the limit $k_2 = k_3$ the amplitude of the intermediate soliton generated at the intersection point reaches *four* times larger than the initial solitons. This large amplitude wave generation has been considered as the Mach reflection problem of shallow water wave [28, 37, 8, 23] (see also Section 8). The chord diagram in Figure 7.2 shows a *completion* of the (partial) chord diagram: The solid chords indicate the initial solitons forming V-shape, and the dotted chords corresponds to the solitons generated by the interaction (see [23] for further discussion).

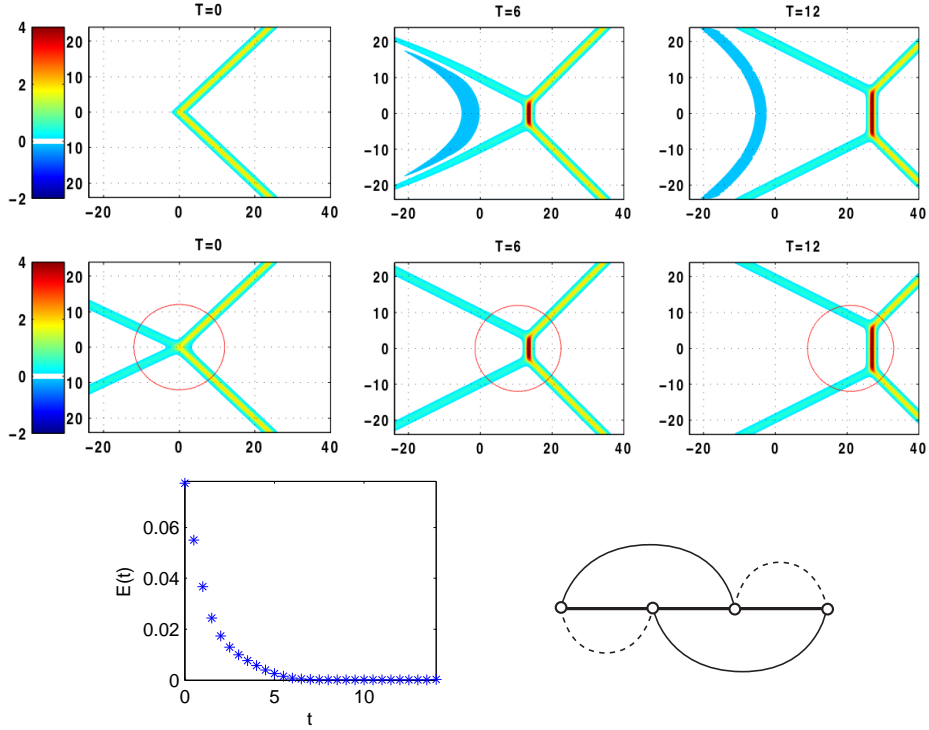


FIGURE 7.3. Numerical simulation of V-shape initial wave for $\kappa < 1$ (Mach reflection): The initial wave consists of $[1, 3]$ -soliton in $y > 0$ and $[2, 4]$ -soliton in $y < 0$ with $A_0 = 2$ and $\Psi_0 = 45^\circ$. The top figures show the result of the direct simulation, and the middle figures show the corresponding exact solution of (3142)-type. Notice that a large amplitude intermediate soliton is generated at the intersection point, and it corresponds to the $[1, 4]$ -soliton with the amplitude $A_{[1,4]} = 4.5$. The circles in the middle figures are D_r^t with $r = 12$, which cover well the main part of the interaction regions up to $t = 12$. The bottom graph of the error function $E(t)$ which is minimized at $t = 10$. The solid chords in the diagram indicate the incident solitons, and the dotted ones show the reflected solitons.

7.2. The Mach reflection: $\kappa < 1$. We consider the initial V-shape wave with $A_0 = 2$ and $\Psi_0 = 45^\circ$ (i.e. $\kappa = 0.5$). The angle Ψ_0 is now less than the critical angle $\Psi_c \approx 63.4^\circ$. The asymptotic solution is expected to be of (3142)-type whose k -parameters are obtained from (7.2), i.e.

$$(k_1, k_2, k_3, k_4) = \left(-\frac{3}{2}, -\frac{1}{2}, \frac{1}{2}, \frac{3}{2}\right).$$

Figure 7.3 illustrates the result of the numerical simulation. The top figures show the direct simulation of the KP equation. We again observe a bow-shape wake behind the interaction point. The wake expands and decays, and then we see the appearance of new solitons which form resonant interactions with the initial solitons. One should note that the solution generates a large amplitude intermediate soliton at the interaction point, and this soliton is identified as $[1, 4]$ -soliton with the amplitude $A_{[1,4]} = 4.5$. This $[1, 4]$ -soliton is called the Mach stem in the Mach reflection [8, 23] (see also Section 8).

The middle figures in Figure 7.3 show the corresponding exact solution of (3142)-type whose A -matrix is found by minimizing $E(t)$ at $t = 10$,

$$A = \begin{pmatrix} 1 & 1.92 & 0 & -1.96 \\ 0 & 0 & 1 & 0.64 \end{pmatrix}$$

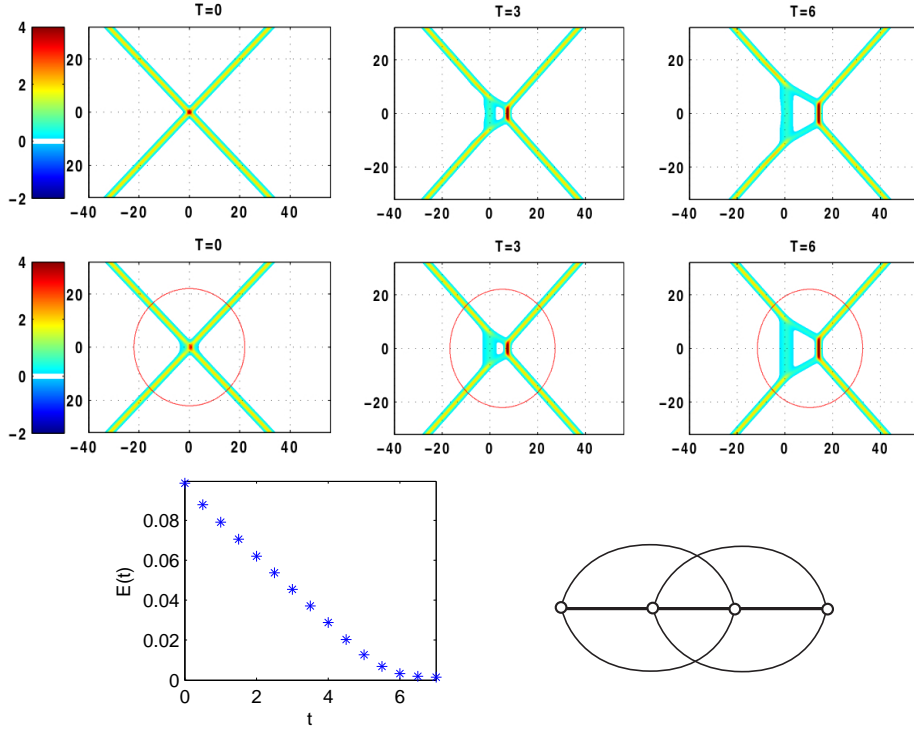


FIGURE 7.4. Numerical simulation for X-shape initial wave with $A_0 = 2$ and $\Psi_0 = 45^\circ$ (i.e. $\kappa = 0.5 < 1$): The initial wave is the sum of $[1, 3]$ - and $[2, 4]$ -solitons. The top figures show the numerical simulation, and the middle figures show the corresponding exact solution of (3412)-type, i.e. T-type. Notice that the circle showing D_r^t with $r = 22$ covers well the box generated by the resonant interaction up to $t = 7$. The bottom graph shows the error function $E(t)$ of (7.3) which is minimized at $t = 6$. The four solid chords in the diagram show the asymptotic solitons in the incident wave, and they form a T-type soliton solution.

Using (6.9), we obtain the phase shifts $x_{[i,j]}$ for the initial solitons of $[1, 3]$ - and $[2, 4]$ -type in $x > 0$, and the s -parameter,

$$x_{[1,3]} = x_{[2,4]} = -0.01, \quad s = 0.980.$$

Those values indicate that the solution is very close to the exact solution for all the time. The negative value of the shifts $x_{[i,j]}$ is due to the generation of a large amplitude soliton $[1, 4]$ -type (i.e. the initial solitons slow down), and $s < 1$ implies that the $[1, 4]$ -soliton is generated after $t = 0$. Also note that the $[1, 4]$ -soliton now resonantly interact with $[1, 3]$ - and $[2, 4]$ -solitons to create new solitons $[1, 2]$ - and $[3, 4]$ -solitons (called the reflected waves in the Mach reflection problem [28, 8, 23]). This process then seems to compensate the shifts of incident waves, even though we observe a large wake behind the interaction point.

The bottom graph in Figure 7.3 shows a rapid convergence of the initial wave to (3142)-type soliton solution with those parameters of the A -matrix and k values given above, and for the error function $E(t)$, we minimize it at $t = 10$ for D_r^t with $r = 12$.

7.3. T-type interaction with X-shape initial wave. In this example, we consider an X-shape initial wave given by the sum of two line-solitons. For simplicity, we consider a symmetric initial wave with $A_0 = 2$ and $\Psi_0 = 45^\circ$ (i.e. extend the initial wave in Figure 7.3 into the negative x -region). Since $\kappa = 0.5 < 1$, the corresponding chord diagram shows the T-type with the k -parameters

$(k_1, k_2, k_3, k_4) = (-\frac{3}{2}, -\frac{1}{2}, \frac{1}{2}, \frac{3}{2})$. Although T-type soliton appears for smaller angle Ψ_0 , one should not take so small value. For an example of the symmetric case, if we take $\Psi_0 = 0$ giving twice higher amplitude than one-soliton case, we obtain KdV 2-soliton solution with different amplitudes (as can be shown by the method of IST). So for the case with very small angle Ψ_0 , we expect to see those KdV solitons near the intersection point. However, the solitons expected from the chord diagram have almost the same amplitude as the incidence solitons for the case with a small angle. The detailed study also shows that near the intersection point for T-type solution at the time when all four solitons meet at this point (i.e X-shape), the solution at the intersection point has a small amplitude due to the repulsive force similar to the KdV solitons. Then the initial X-shape wave with small angle generates a large soliton at the intersection point. This then implies that our initial wave given by the sum of two line-solitons creates a large dispersive perturbation at the intersection point, and one may need to wait a long time to see the convergence.

The top figures in Figure 7.4 illustrate the numerical simulation, which clearly shows an opening of a resonant box as expected by the feature of T-type. The corresponding exact solution is illustrated in the middle figures, where the A -matrix of the solution is obtained by minimizing the error function $E(t)$ of (7.3) at $t = 6$,

$$A = \begin{pmatrix} 1 & 0 & -0.368 & -0.330 \\ 0 & 1 & 1.198 & 0.123 \end{pmatrix}$$

In the minimization process, we take $x_{[1,3]} = x_{[2,4]}$ due to the symmetric profile of the solution, and adjust the on-set of the box (see subsection 6.3). Note that the symmetry reduces the number of free parameters to three. We obtain

$$x_{[1,3]} = x_{[2,4]} = 0.025, \quad r = 3.63, \quad s = 0.350.$$

The positive shifts of those $[1, 3]$ - and $[2, 4]$ -solitons in the wavefront indicate also the positive shift of the newly generated soliton of $[1, 4]$ -type at the front. This is due to the repulsive force which exists in the KdV type interaction as explained above, that is, the interaction part in the initial wave has a larger amplitude than that of the exact solution, so that this part of the solution moves faster than that in the exact solution. This difference may result in a shift of the location of the $[1, 4]$ -soliton. The relatively large value $r > 1$ indicates that the onset of the box is actually much earlier than $t = 0$, and $s < 1$ shows the positive phase shifts as calculated from (6.12).

The bottom graph in Figure 7.4 shows the evolution of the error function $E(t)$ of (7.3) which is minimized at $t = 6$. Note here that the circular domain D_r^t with $r = 22$ covers well the main feature of the interaction patterns for all the time computed for $t \leq 7$. The chord diagram in the figure shows four asymptotic solitons in the initial wave which form a T-type soliton solution (see [20] for further discussion).

8. SHALLOW WATER WAVES: THE MACH REFLECTION

In this last section, we discuss a real application of the exact soliton solutions of the KP equation described in the previous sections to the Mach reflection phenomena in shallow water. In [28], J. Miles considered an oblique interaction of two line-solitons using O-type solutions. He observed that resonance occurs at the critical angle Ψ_c , and when the initial oblique angle Ψ_0 is smaller than Ψ_c , the O-type solution becomes singular (recall that at the critical angle Ψ_c , one of the exponential term in the τ -function vanishes, see subsection 6.1). He also noticed a similarity between this resonant interaction and the Mach reflection found in shock wave interaction (see for example CF:48,Wh:64). This is illustrated by the left figure of Figure 8.1, where an incidence wave shown by the vertical line is propagating to the right, and it hits a rigid wall with the angle $-\Psi_0$ measured counterclockwise from the axis perpendicular to the wall (see also [15]). If the angle Ψ_0 (equivalently the inclination angle of the wall) is large, the reflected wave behind the incidence wave has the same angle Ψ_0 , i.e. a regular reflection occurs. However, if the angle is small, then an intermediate wave called the Mach stem appears as illustrated in Figure 8.1. The Mach stem, the incident wave and the reflected wave interact resonantly, and those three waves form a resonant triplet. The right panel in Figure 8.1

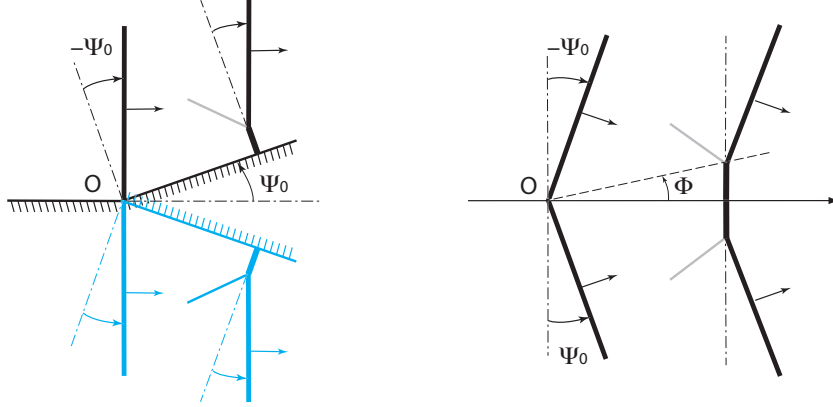


FIGURE 8.1. The Mach reflection. The left panel illustrates a semi-infinite line-soliton (incidence wave) propagating parallel to the wall with the mirror image. The right panel is an equivalent system to the left one when we ignore the viscous effect on the wall. The incident wave then forms a V-shape wave at $t = 0$ as discussed in Section 7. The resulting wave pattern shown here is a (3142)-soliton solution.

illustrates the wave propagation which is equivalent to that in the left panel, if one ignores the effect of viscosity on the wall (i.e. no boundary layer). At the point O , the initial wave has V-shape with the angle Ψ_0 , which forms the initial data for our simulation discussed in the previous section. Then as we presented, the numerical simulation describes the reflection of line-soliton with an inclined wall, and these results explain well the Mach reflection phenomena in terms of the exact soliton solutions of the KP equation.

8.1. Previous numerical results of the Boussinesq-type equations. One of the most interesting things of the Mach reflection is that the KP theory predicts an extraordinary four-fold amplification of the stem wave at the critical angle [28]. We recall the formulae of the maximum amplitudes which are given by (6.6) for the O-type solution ($\kappa > 1$) and (6.11) for (3142)-type solution ($\kappa < 1$). Let α denote the amplification factor in terms of the Miles parameter κ of (6.5), i.e.

$$(8.1) \quad \alpha = \begin{cases} (1 + \kappa)^2, & \text{for } \kappa < 1, \\ \frac{4}{1 + \sqrt{1 - \kappa^{-2}}}, & \text{for } \kappa > 1. \end{cases}$$

Several laboratory and numerical experiments tried to confirm the formula (8.1), in particular, the four-fold amplification at the critical value $\kappa = 1$ (see for example [36, 27, 15, 41, 46]). In [15], Funakoshi made a numerical simulation of the Mach reflection problem using the system of equations,

$$\begin{cases} \eta_t + \Delta\psi + \alpha \nabla \cdot (\eta \nabla \psi) - \frac{\beta}{6} \Delta^2 \psi = 0, \\ \left(\psi - \frac{\beta}{2} \Delta \psi \right)_t + \eta + \frac{\alpha}{2} |\nabla \psi|^2 = 0, \end{cases}$$

which is equivalent to the Boussinesq-type equation (2.4) up to this order. He considered the initial wave to be the KdV soliton with higher order corrections up to $\mathcal{O}(\epsilon)$. In his paper, he mainly presented the results for the incidence waves with the amplitude $a_i = 0.05 = \hat{a}_0/h_0$ and the angles $\frac{\pi}{40} \leq \Psi_0 \leq \frac{\pi}{3}$. He concluded that his results agree very well with the resonantly interacting solitary wave solution predicted by Miles. However his results on the amplification parameter α are slightly shifted to the lower values of the Miles κ -parameter. Tanaka in [41] then re-examined Funakoshi's

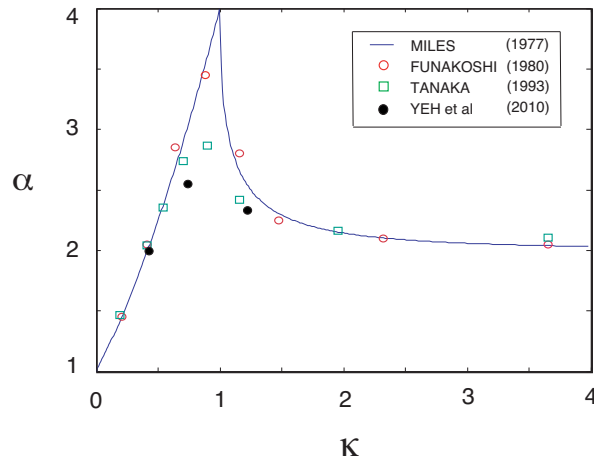


FIGURE 8.2. Numerical results of the amplification factor α versus the κ -parameter. The circles show Funakoshi's result [15], the squares show Tanaka's result [41]. The black dots shows the experimental results by Yeh et al [46].

results for higher amplitude incidence waves with $a_i = 0.3$ using the high-order spectral method. He noted that the effect of large amplitude tends to prevent the Mach reflection to occur, and all the parameters such as the critical angle Ψ_c are shifted toward the values corresponding to the regular reflection (i.e. O-type). For example, he obtained the maximum amplification $\alpha = 2.897$ at $\kappa = 0.695$.

However, we claim in our recent paper [47] that those previous results did not properly interpret their comparisons with the theory, and in fact their results are in good agreement with the the predictions given by the KP theory except for the cases near $\kappa = 1$. One should emphasize that the KP equation is derived under the assumptions of quasi-two dimensionality and weak nonlinearity. Thus the key ingredient is to include higher order corrections to those assumptions when we compare the numerical or experimental results with the theory. In particular, the quasi-two dimensionality can be corrected by comparing the KP soliton with the KdV soliton in the propagation direction as mentioned in Section 3. More precisely, we have the amplitude correction (3.6), i.e.

$$\hat{a}_0 = \frac{a_0}{\cos^2 \Psi_0} = \frac{2h_0 A_0}{3 \cos^2 \Psi_0},$$

where \hat{a}_0 is the amplitude observed in the numerical computation of the Boussinesq-type equation (which has rotational symmetry in \mathbb{R}^2). This then suggests that the κ -parameter should be evaluated by the following formula using the experimental amplitude \hat{a}_0 ,

$$(8.2) \quad \kappa := \frac{\tan \Psi_0}{\sqrt{2A_0}} = \frac{\tan \Psi_0}{\sqrt{3(\hat{a}_0/h_0)} \cos \Psi_0}.$$

Because of the quasi-two dimensional approximation, i.e. $|\Psi_0| \ll 1$, Miles in his paper [28] replaced $\tan \Psi_0$ by Ψ_0 , and then in [15, 41], the authors continued on to use this replacement. Then their computations with rather large values of Ψ_0 gave significant shifts of the κ -parameter. We then re-evaluate their results with our formula (8.2), and the new results are shown in Figure 8.2. Since Funakoshi's simulations are based on small amplitude incidence waves, his results agree quite well with the KP predictions. Tanaka's results are also in good agreement with the KP theory except for the cases near the critical angle (i.e. $\kappa = 1$), where the amplification parameter α gets close to 3. This region clearly violates the assumption of the weak nonlinearity. Although one needs to make higher order corrections to weak nonlinearity, the original plots of Tanaka's are significantly improved with the formula (8.2). The black dots in Figure 8.2 indicate the results of recent laboratory experiments

TABLE 1. Amplification factor α for different values of $\kappa = \tan \Psi_0 / \sqrt{2A_0}$: $\alpha_{\tilde{x}=71.1}$ (Exp.) are the laboratory data at $x = 71.1$ ($\tilde{x} = 4.27$ m), $\alpha_{x=71.1}$ (KP) are calculated from the corresponding KP exact solutions at $t = 41.05$, and $\alpha_{x=\infty}$ (KP) are from (6.6) and (6.11). In the row of $A_0 = 0.413$ with $\Psi_0 = 30^\circ$, the values of α in the brackets are obtained at $x = 50.8$, because of the wave breaking immediately after this point; hence, the greater amplification cannot be realized [47].

κ	A_0	Ψ_0	$\alpha_{x=71.1}$ (Exp.)	$\alpha_{x=71.1}$ (KP)	$\alpha_{x=\infty}$ (KP)
1.392	0.086	30°	2.10	2.36	2.36
1.242	0.108	30°	2.13	2.51	2.51
1.017	0.161	30°	2.24	3.38	3.38
0.887	0.212	30°	2.33	2.43	3.56
0.731	0.312	30°	2.52	2.61	2.99
0.722	0.127	20°	1.89	1.84	2.96
0.635	0.413	30°	(2.48)	(2.54)	2.67
0.591	0.189	20°	1.95	1.93	2.53
0.516	0.249	20°	1.99	2.08	2.30
0.425	0.367	20°	2.01	1.99	2.03

done by Yeh and his colleagues [46]. We will discuss their experimental results in the next section.

Before closing this section, we remark on the length of the Mach stem (i.e. the intermediate soliton of [1, 4]-type). From (3142)-soliton solution, one can find the point (x_*, y_*) of the interaction of the triplet with [1, 3]-, [3, 4]- and [1, 4]-solitons [8],

$$\begin{cases} x_* = \frac{1}{4} (\tan \Psi_c + \tan \Psi_0)^2 t = \frac{A_0}{2} (1 + \kappa)^2 t, \\ y_* = \frac{1}{2} (\tan \Psi_c - \tan \Psi_0) t = \sqrt{\frac{A_0}{2}} (1 - \kappa) t, \end{cases}$$

(see Figure 8.1). In the physical coordinates with $(\tilde{x}_*, \tilde{y}_*, \tilde{t})$, we have

$$\tilde{x}_* = c_0 \left(1 + \frac{\hat{a}_0 \cos^2 \Psi_0}{h_0} (1 + \kappa)^2 \right) \tilde{t}, \quad \tilde{y}_* = c_0 \sqrt{\frac{\hat{a}_0 \cos^2 \Psi_0}{3h_0}} (1 - \kappa) \tilde{t}.$$

The angle Φ in Figure 8.1 is then given by $\tan \Phi = \tilde{y}_*/\tilde{x}_*$, which is approximated in [28, 15] by

$$\tan \Phi \approx \sqrt{\frac{\hat{a}_0}{3}} (1 - \kappa).$$

Using the corrected formula $\tan \Phi = \tilde{y}_*/\tilde{x}_*$, one can see again a good agreement with the KP theory (see Figure 8 in [15]).

8.2. Experiments. Recently, Yeh and his colleagues [46] performed several laboratory experiments on the Mach reflection phenomena using 7.3 m long and 3.6 m wide wave tank with a water depth of 6.0 cm. Here we briefly describe their results and show that our KP theory can predict very well the evolution of the waves observed in the experiments.

The wave tank is equipped with 16 axis directional-wave maker system along the 3.6 m long side wall marked by $x = 0$. An oblique incident solitary wave is created by driving those 16 paddles synchronously along the sidewall, and the wave maker is designed to generate a KdV soliton with any heights before the breaking. The temporal and spatial variations of water-surface profiles are measured by the Laser Induced Fluorescent (LIF) method (a highly accurate measurement technique). The water dyed with fluorescein (green) fluoresces when excited by the laser sheet. The illuminated image of the water-profiles are recorded by a high-speed and high-resolution video camera.

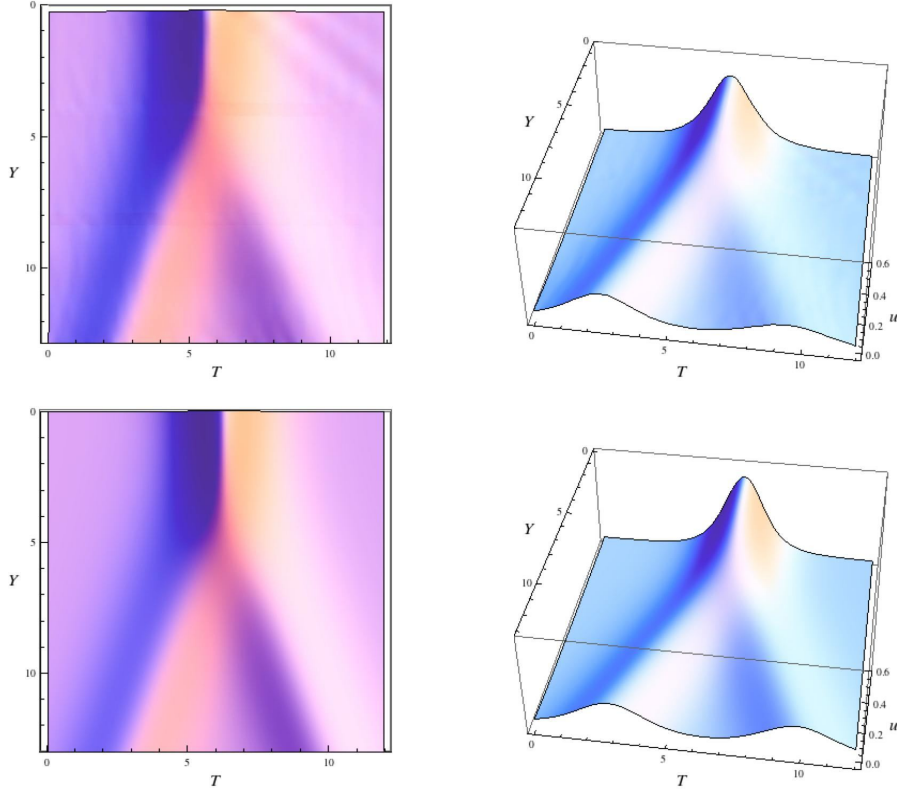


FIGURE 8.3. Two views of the temporal variation of the water-surface profile in the y -direction (perpendicular to the wall) at $x = 71.1$ [47]: The top panels show the experimental result, and the bottom ones show the corresponding (3142)-type exact soliton solution of the KP equation. The incident wave amplitude $A_0 = 0.212$, and the angle $\Psi_0 = 30^\circ$. The amplification factors obtained from the experiment and the exact solutions are close, and they are $\alpha_{x=71.1}(\text{Exp.}) = 2.33$ and $\alpha_{x=71.1}(\text{KP}) = 2.43$ (see Table 1).

8.2.1. *The Mach reflection.* In Table 1, their experimental results of the amplification factors α are compared with those obtained from the exact solutions of the KP equation (i.e. O-type for $\kappa > 1$ and (3142)-type for $\kappa < 1$). The waves were measured at $\tilde{x} = 4.27$ m ($x = \tilde{x}/h_0 = 71.1$) which is the farthest measuring location in the experiments, except for the case with $A_0 = 0.413$. In the later case, the α values in the brackets are measured at $x = 50.8$ because of the wave-breaking (notice that at this point $\alpha = 2.48$ implies $a_i = 1.02$). We calculate the corresponding KP exact solution at $t = 41.05$ (recall here that the relations (3.8) gives $\tilde{x} - c_0\tilde{t} = h_0x$ and $c_0\tilde{t} = \frac{3h_0}{2}t$). The amplification factor α is still growing along the propagation direction, and the values obtained from the exact solutions are in good agreement with the measurements. We note here that near the critical case (i.e. $\kappa = 1$) the growth of the stem amplitude is very slow and at $x = 71.1$ ($\tilde{x} = 4.27$ m) the amplification factor is only achieved about 65%. Also for the cases with small oblique angle, i.e. $\Psi_0 = 20^\circ$ in Table 1, the amplification factor α grows slower when the incidence wave amplitude is smaller, that is, at $x = 71.1$, α is almost constant (slightly decreases) as κ increases. However the asymptotic value of α for large x increases as κ increases. This means that the observed waves are still in the transient stage, and a longer tank is necessary to observe further growth of the amplification factor (see [47] for the details). In Figure 8.3, we show the image of the wave-profile at $x = 71.1$ for the case when the incident wave amplitude have $A_0 = 0.212$ and $\Psi_0 = 30^\circ$. The

corresponding exact solution with those parameters is of (3142)-type (i.e. $\kappa = 0.887 < 1$). The upper panels show two views in different angles of the temporal variation of the wave profile of the experiment at $x = 71.1$, which is made from 250 slices of the spatial profiles (100 slices per second) with approximately 3000 pixel resolution in the y -direction. As expected from the (3142)-type exact solution, the stem-wave formation is realized, in which the incident and reflected waves separate away from the wall by the stem-wave. The lower panels show the corresponding (3142)-type exact solution at $t = 41.05$ (the x -coordinate is converted to the t -coordinate, using (3.8)). Here the k -parameters are $(k_1, k_2, k_3, k_4) = (-0.614, -0.037, 0.037, 0.614)$ from $A_0 = 0.212$ and $\Psi_0 = 30^\circ$. Then we calculate the A -matrix using (6.9) with $s = 1$, and take

$$A = \begin{pmatrix} 1 & 8.797 & 0 & -1.128 \\ 0 & 0 & 1 & 0.530 \end{pmatrix}.$$

This choice of the A -matrix places the incidence wave crossing at the origin at $t = 0$, i.e. $\theta_{[1,3]}^+ = \theta_{[2,4]}^+ = 0$ in (6.9). We see a good agreement between the experiment and the KP theory. At $x = 71.1$, the wave-profile observed in the experiment is close to the corresponding exact solution of (3142)-type, that is, the radiations generated at the beginning stage dispersed and well separated from the main part of the wave-profile as predicted in the numerical simulation (see subsection 7.2).

8.2.2. T -type interaction. Figure 8.4 shows a preliminary result for T -type interaction pattern generated in the same tank by Yeh and his collaborators. The T -type solution is the most complex and interesting soliton solution associated with the τ -function on $\text{Gr}^+(2, 4)$. The initial wave has the V-shape (half of the X-shape), then other half of the X-shape is generated by the line-soliton with opposite angle. The upper panels of Figure 8.4 show the evolution of the wave pattern with $A_0 = 0.431$ and $\Psi_0 = 25^\circ$. Behind the crossing wave form (the right side in the figure), the large wakes are generated at the early stage of the evolution, but they eventually separate from the main pattern of the T -type interaction, as we observed in the numerical simulation. The figures clearly show the formation of a box pattern as expected by the KP theory. The lower panels show the corresponding T -type exact soliton solution whose parameters are $(k_1, k_2, k_3, k_4) = (-0.697, -0.231, 0.231, 0.697)$ and the A -matrix given by (6.12) and (6.13) with $\theta_{[1,3]}^+ = \theta_{[2,4]}^+ = 0$, $s = 40$ and $r = 1$, i.e.

$$A = \begin{pmatrix} 1 & 0 & -40.34 & -24.07 \\ 0 & 1 & 24.07 & 13.37 \end{pmatrix}$$

The large value of the s -parameter indicates large phase shift of the incident line-solitons (see Figure 6.6), that is, the parts of line-solitons in the right side (i.e. behind the interaction point) were created with some delayed time. In finding those parameter values, we did not make a precise minimization of certain error function, like the one given in (7.3). In a future communication, we hope we will be able to develop a method to determine the exact solution from the experimental data, that is, the inverse problem of the KP equation.

Acknowledgements

I would like to thank Harry Yeh for letting me to use his excellent and important experimental data before publication and for making extremely fruitful collaboration on the Mach reflection problem. I am grateful to Sarbarish Chakravarty for his many excellent suggestions which made a tremendous improvement on the paper and for many valuable discussions throughout our intensive but very pleasant collaboration. I would also like to thank my colleagues, Chiu-Yen Kao, Masayuki Oikawa and Hidekazu Tsuji for many useful discussions related to the subjects presented in this paper. Special thanks to Mark J. Ablowitz who provides his excellent photos in Figure 5.9. My research is partially supported by NSF grant DMS-0806219.

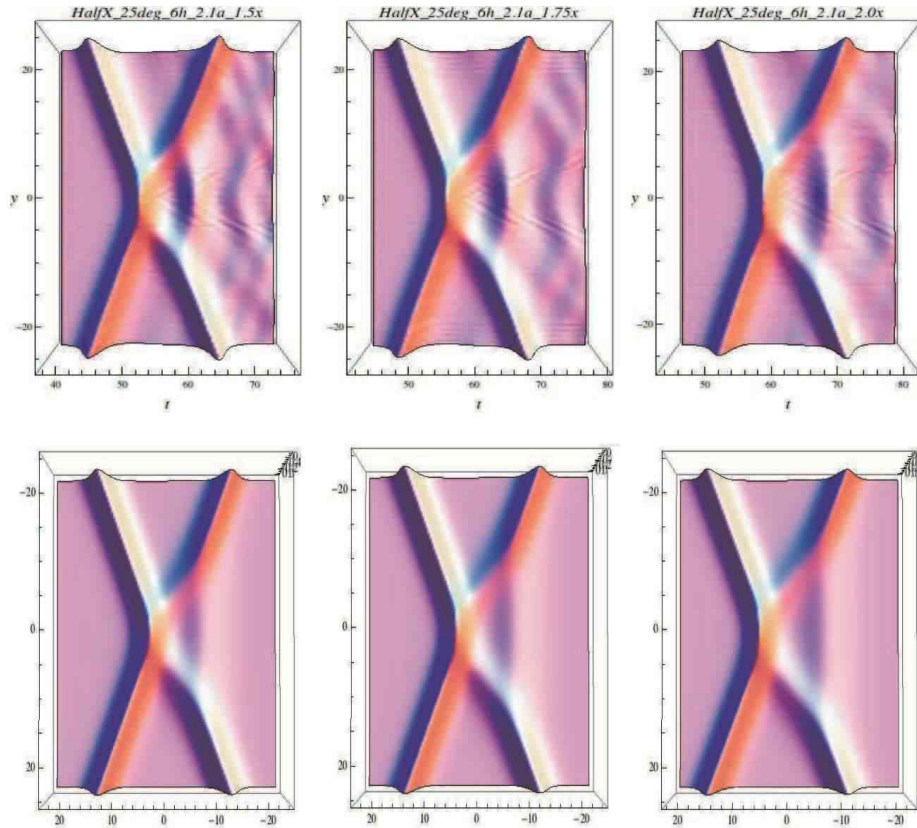


FIGURE 8.4. T-type solutions generated in the water tank [46]. The experimental results are shown in the upper panels. Those figures are made by combining the real image of the wave profiles with their mirror images of the wall at $y = 0$ (the center horizontal line). The lower panels show the corresponding T-type exact solution of the KP equation. The initial wave has $a_i = 2.1$ cm ($A_0 = 0.43$) and $\Psi_0 = 25^\circ$ (i.e. $\kappa = 0.503$). The exact solution is plotted in the xy -plane, and the solitons are propagating to the left. (The experimental figures by courtesy of Harry Yeh.)

REFERENCES

- [1] M. J. Ablowitz and H. Segur, *Solitons and the inverse scattering transform*, SIAM Studies in Applied Mathematics, (SIAM, Philadelphia/ 1981).
- [2] J. Benney and J. C. Luke, Interactions of permanent waves of finite amplitude, *J. Math. Phys.*, **43** (1964) 309-313.
- [3] G. Biondini and S. Chakravarty, Soliton solutions of the Kadomtsev-Petviashvili II equation, *J. Math. Phys.*, **47** (2006) 033514 (26pp).
- [4] G. Biondini and Y. Kodama, On a family of solutions of the Kadomtsev-Petviashvili equation which also satisfy the Toda lattice hierarchy, *J. Phys. A: Math. Gen.* **36** (2003) 10519-10536.
- [5] M. Boiti, F. Pempinelli, A. K. Pogrebkov and B. Prinari, Towards an inverse scattering theory for non-decaying potentials of the heat equation, *Inverse Problems*, **17** (2001) 937-957.
- [6] S. Chakravarty and Y. Kodama, Classification of the line-solitons of KP II, *J. Phys. A: Math. Theor.*, **41** (2008) 275209 (33pp).
- [7] S. Chakravarty and Y. Kodama, A generating function for the N -soliton solutions of the Kadomtsev-Petviashvili II equation, *Contemp. Math.*, **471** (2008) 47-67.
- [8] S. Chakravarty and Y. Kodama, Soliton solutions of the KP equation and application to shallow water waves, *Stud. Appl. Math.*, **123** (2009) 83-151.
- [9] S. Chakravarty and Y. Kodama, Line-soliton solutions of the KP equation, *AIP Conf. Proc.* **1212** (2010) 312-341.
- [10] S. Corteel, Crossing and alignments of permutations, *Adv. Appl. Math.* **38** (2007) 149-163.

- [11] R. Courant and K. O. Friedrichs, *Supersonic flow and shock waves*, (Intersciences Publ., New York, 1948).
- [12] W-S. Duan, Y-R. Shi and X-R. Hong, Theoretical study of resonance of the Kadomtsev-Petviashvili equation, *Phys. Lett. A*, **323** (2004) 89-94.
- [13] P. A. Folkes, H. Ikezi and R. Davis, Two-dimensional interaction of ion-acoustic solitons, *Phys. Rev. Lett.* **45** (1980) 902-904
- [14] N. C. Freeman and J. J. C. Nimmo, Soliton-solutions of the Korteweg-deVries and Kadomtsev-Petviashvili equations: the Wronskian technique *Phys. Lett. A* **95** (1983) 1-3.
- [15] M. Funakoshi, Reflection of obliquely incident solitary waves, *J. Phys. Soc. Jpn*, **49**, (1980) 2371-2379.
- [16] R Hirota, *The Direct Method in Soliton Theory* (Cambridge University Press, Cambridge, 2004)
- [17] B. B. Kadomtsev and V. I. Petviashvili, On the stability of solitary waves in weakly dispersive media, *Sov. Phys. - Dokl.* **15** (1970) 539-541.
- [18] F. Kako and N. Yajima, Interaction of Ion-acoustic solitons in two-dimensional space, *J. Phys. Soc. Jpn*, **49** (1980) 2063-2071.
- [19] F. Kako and N. Yajima, Interaction of ion-acoustic solitons in multi-dimensional space. II, *J. Phys. Soc. Jpn*, **51** (1982) 311-322.
- [20] C.-Y. Kao, and Y. Kodama, Numerical study on the KP equation for non-periodic waves, submitted (arXiv:1004.0407).
- [21] S. Kato, T. Takagi and M. Kawahara, A finite element analysis of Mach reflection by using the Boussinesq equation, *Int. J. Numer. Meth. Fluids*, **28** (1998) 617-631.
- [22] Y. Kodama, Young diagrams and N -soliton solutions of the KP equation, *J. Phys. A: Math. Gen.*, **37** (2004) 11169-11190.
- [23] Y. Kodama, M. Oikawa and H. Tsuji, Soliton solutions of the KP equation with V-shape initial waves, *J. Phys. A: Math. Theor.*, **42** (2009) 312001 (9pp).
- [24] Y. Kodama and B. Shipman, The finite non-periodic Toda lattice: A geometric and topological viewpoint, Preprint - (2008), [arXiv:0805.1389].
- [25] V. B. Matveev, Darboux transformation and explicit solutions of the Kadomtsev-Petviashvili equation, depending on functional parameters, *Lett. Math. Phys.*, **3** (1979) 213-216.
- [26] E. Medina, An N soliton resonance for the KP equation: interaction with change of form and velocity, *Lett. Math. Phys.* **62** (2002) 91-99.
- [27] W. K. Melville, On the Mach reflexion of a solitary wave, *J. Fluid Mech.*, **98** (1980) 285-297.
- [28] J. W. Miles, Resonantly interacting solitary waves, *J. Fluid Mech.*, **79** (1977) 171-179.
- [29] P. A. Millewski and J. B. Keller, Three dimensional surface waves, *Stud. Appl. Math.*, **37** (1996) 149-166.
- [30] T. Miwa and M. Jimbo and E. Date, *Solitons: differential equations, symmetries and infinite-dimensional algebras* (Cambridge University Press, Cambridge, 2000)
- [31] A. C. Newell, *Solitons in Mathematics and Physics*, CBMS-NSF **48**, (SIAM, Philadelphia/ 1985).
- [32] A. C. Newell and L. G. Redekopp, Breakdown of Zakharov-Shabat theory and soliton creation, *Phys. Rev. Lett.* **38** (1977) 377-380.
- [33] T. Nagasawa and Y. Nishida, Virtual states in strong interactions of plane ion-acoustic solitons, *Phys. Rev. A*, **28** (1983) 3043-3050.
- [34] S. Novikov, S. V. Manakov, L. P. Pitaevskii and V. E. Zakharov, *Theory of Solitons: The Inverse Scattering Method*, Contemporary Soviet Mathematics, (Consultants Bureau, New York and London, 1984).
- [35] M. Oikawa and H. Tsuji, Oblique interactions of weakly nonlinear long waves in dispersive systems, *Fluid Dyn. Res.*, **38** (2006) 868-898.
- [36] P. H. Perroud, The solitary wave reflection along a straight vertical wall at oblique incidence, Institute of Engineering Research, Wave Research Laboratory, Tech. Rep. 99/3, University of California, Berkeley (1957) 93pp.
- [37] A. V. Porubov, H. Tsuji, I. L. Lavrenov and M. Oikawa, Formation of the rogue wave due to non-linear two-dimensional waves interaction, *Wave Motion* **42** (2005) 202-210.
- [38] A. Postnikov, Total positivity, Grassmannians, and networks, (math.CO/0609764).
- [39] M. Sato, Soliton equations as dynamical systems on an infinite dimensional Grassmannian manifold, *RIMS Kokyuroku*, (Kyoto University) **439** (1981) 30-46.
- [40] J. Satsuma, A Wronskian representation of N -soliton solutions of nonlinear evolution equations, *J. Phys. Soc. Japan*, **46** (1979), 359-360.
- [41] M. Tanaka, Mach reflection of a large-amplitude solitary wave, *J. Phys. Mech.*, **248** (1993) 637-661.
- [42] T. Soomere, Interaction of Kadomtsev-Petviashvili solitons with unequal amplitudes, *Phys. Lett. A*, **332** (2004) 74-78.
- [43] H. Tsuji and M. Oikawa, Oblique interaction of solitons in an extended Kadomtsev-Petviashvili equation, *J. Phys. Soc. Japan*, **76** (2007) 84401-84408.
- [44] G. B. Whitham, *Linear and nonlinear waves*, A Wiley-interscience publication (John Wiley & Sons, New York, 1974).
- [45] L. K. Williams, Enumeration of totally positive Grassmann cells, *Adv. Math.* **190** (2005) 319-342.

- [46] H. Yeh, Y. S. Chen and W. Li, Laboratory experiments of resonant interactions of solitary waves in shallow water, (2010) in preparation.
- [47] H. Yeh, W. Li and Y. Kodama, Mach reflection and KP solitons in shallow water, Preprint, (2010) submitted to EPJ. (arXiv:1004.0370)

DEPARTMENT OF MATHEMATICS, OHIO STATE UNIVERSITY, COLUMBUS, OH 43210
E-mail address: `kodama@math.ohio-state.edu`